박 성 순 지도교수

박사학위 청구논문

Preparation of Cellular Delivery System for Protein and Immobilization of Recombinant Lipase

세포 투과성 물질의 개발과 재조합 리파제의 고정화에 관한 연구

2011

성신여자대학교 대학원

화 학 과

정 수 현

Preparation of Cellular Delivery System for Protein and Immobilization Recombinant Lipase

세포 투과성 물질의 개발과
재조합 리파제의 고정화에 관한 연구

박 성 순 지도교수

이 논문을 박사학위 논문으로 제출함

2010년 10월

성신여자대학교 대학원
화 학 과
정 수 현

인 준 서

정 수 현의 박사학위논문을 인준함

심사위원 _____ 인

심사위원 _____ 인

심사위원 _____ 인

심사위원 _____ 인

심사위원 _____ 인

성신여자대학교 대학원

논 문 개 요

본 연구에서는 단백질의 세포 내 전달을 위해 기능기를 도입한 나노입자와 세포 투과성 펩타이드의 응용과 함께 재조합 리파제의 고정화에 대한 연구를 다루었다. 일반적으로 eukaryotic cell의 plasma membrane은 크기가 큰 peptide나 protein을 특별한 transporter 없이 통과 시키지 못한다고 알려져 있다. 세포내로 단백질을 전달시키기 위해서는 liposome이나 cell permeable peptides, polymer 그리고 particles 등을 운반체로 이용한다. 한편, 효소는 높은 선택성과 반응성을 가지며 다양한 반응을 촉매 할 수 있지만 쉽게 비활성화가 된다는 단점을 가지고 있다. 효소의 안정성을 높이기 위해서 화학적 혹은 분자생물학적 방법이나 고정화를 이용한다.

세포 투과성 물질의 개발 연구에서는 나노 입자와 기존에 기능이 알려진 세포투과성 펩타이드를 이용하여 단백질을 세포 안으로 운반시키는 연구를 다루었다. 나노입자의 세포 투과율을 높이기 위해 표면에 glucose를 도입시킨 나노입자를 합성한 후 EGFP를 결합시켰다. 나노입자를 쥐의 배아 줄기세포와 HeLa cell에 처리한 후 전달 효율을 확인한 결과 glucose가 없는 나노입자는 세포내로 전달되지 않았지만 glucose가 도입된 나노입자는 세포 내로 전달되는 결과를 얻었다. 이와 더불어 다양한 조건 하에서 쥐의 배아줄기 세포로 형광단백질인 EGFP를 결합 시킨 3 종의 CPPs들 (pEP I_N, pEP I_C, Buforin II) 의 transfection 효율을 관찰한 결과 transfection 효율은 CPPs의 종류에 의존하였다.

재조합 리파제의 고정화 연구에서는 첫 번째로, CAL-B를 *E. coli* 에 맞는 codon으로 바꿔준 후 CAL-B의 표면에 소수성 아미노산을 친수성 아미노산으로 치환시켜 발현효율을 증가시키는 연구를 진행하였다. 분자 모델링을 통하여 CAL-B의 active site에 영향을 미치지 않는 5개의 아미노산을 선택하여 aspartate로 치환시킨 결과 wild type 보다 약 3배 많은 단백질을 얻었다. 두 번째로는 마그네틱 비드를 이용하여 *E. coli* 에서 발현시킨 BCL을 refolding 시키는 연구를 하였다. Chaperone을 고정화 시킨 마그네틱 폴리스틸렌 입자를 이용하여 *B. cepacia* lipase를 refolding 시킨 결과 free-chaperone과 비슷한 refolding 반응성을 가지며 10회의 재사용에도 95 % 이상의 반응성을 유지하였다. 세 번째 고정화 연구에서는 먼저 마그네틱 PMMA 나노입자에 8 종류의 효소를 고정화 시킨 후 반응성을 비교하였다. 그 결과 free한 효소와 비슷한 반응성을 보였으며 6번 재사용 후에도 반응성이 크게 감소하지 않았다. 그리고, 리간드의 종류에 따라 다양한 기능기를 포함시킬 수 있는 금속유기 구조체 (MOFs)에 EGFP와 CAL-B를 공유결합으로 고정화시키는 연구를 진행하였다. 고정화 시킨 CAL-B를 유기 용매에서 반응성을 비교한 결과 free한 CAL-B 보다 높은 반응성을 가졌다. 단백질 및 효소를 고정화 시킨 후에도 원래의 활성을 유지하였으며, 재사용 후에도 반응성이 크게 감소하지 않은 결과를 얻었다.

CONTENTS

LIST OF TABLES

Chapter 1

Chapter 2.1

Chapter 3.1

Chapter 3.2

Chapter 3.3

Chapter 3.4

LIST OF FIGURES

Chapter 1

Chapter 2.1

Chapter 2.2

Chapter 3.1

Chapter 3.2

Chapter 3.3

Chapter 3.4

Chapter 1. Introduction

The cell specific delivery of various molecules has been a valuable delivery system for biological and medical researches and for the diagnosis and therapy of disease [1]. In protein delivery, use of therapeutic proteins has been limited by their inability by pass the plasma membrane [2]. Cell permeable peptides (CPPs) such as TAT are very useful for efficient protein delivery into cells [3]. In addition, nanoparticles are also being developed as alternative carrier systems to traditional colloidal carriers such as liposome.

Enzymes are very useful biocatalyst, and they can accept a wide range of complex molecules substrate and catalyzing reactions with enantio- and regioselectivitys [4]. However, enzymes are often easily inactivated. There are several stabilization strategies to improve catalytic stability of enzymes, for example, enzyme modification, genetic modification, and enzyme immobilization strategies [5]. Among these methods, immobilization strategy using solid supports has been most extensively researched due to the specific advantages such as reduce costs by enabling the efficient separation and reuse.

The goal of this thesis is preparation of cellular delivery system for protein and immobilization of recombinant lipase. The work in this thesis deals with protein delivery systems such as nanoparticles, and cell permeable peptides and immobilized supporting materials such as magnetic nanoparticles and metal-organic frameworks.

1.1. Intracellular protein delivery

The most widely utilized approach for intracellular delivery of proteins has been to link the cargo protein with carrier that have the ability to penetrate membranes. The delivered protein needs to cross the plasma membrane and to be efficiently released in the cytoplasm. Carrier-based systems have been used to deliver protein and peptide for many years because they have several advantages: (1) increasing the proportion of protein that reaches its site of action; (2) improving the transport of the drug to its site of action; (3) allowing colocalized deposition of protein with other proteins or excipients; (4) improving the stability of the drug *in vivo*; and (5) decreasing the nonspecific delivery of the drug to non-target tissues. Many type of synthetic carrier, including liposome, cell permeable peptide, polymer and particles, were studied to delivery exogenous genetic materials into cells in a cellular specific or nonspecific manner.

1.1.1. Cell Permeable Peptides

The cell-penetrating peptides (CPPs) are short positively charged peptides composed of basic residues (lysine or arginine) of 20 to about 50 amino acids which can cross the cellular plasma membrane and efficiently deliver biologically active proteins to all tissues. CPPs are capable of transducting cargo across the plasma membrane, allowing proteins to accumulate within the cell. CPPs can be internalized in most cell types and allow the cellular delivery of conjugated or fused biomolecules [6]. A wide range of biomolecules, for example antigenic peptides [7], peptide nucleic

acid [8] antisense oligonucleotides [9], full-length proteins [10], nanoparticles [11] and liposomes [12], have been delivered into cell (Fig. 1).

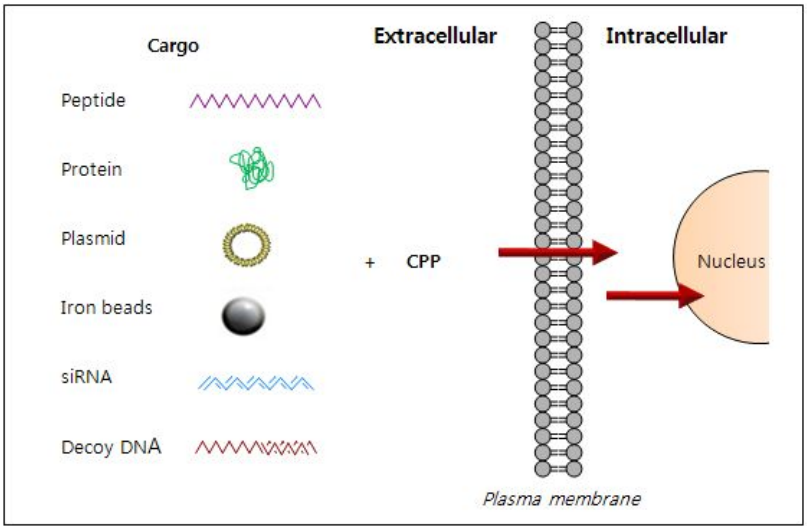

Figure 1. The cell-penetrating peptides (CPPs) are natural peptides identified as cellular membrane-crossing molecules.

During the past decade, several cell-penetrating peptides (CPPs) that enable the intracellular delivery of polar, and biologically active compounds *in vitro* and *in vivo* have been described. The CPPs include synthetic cell-permeable peptides, protein-transduction domains (PTD), and membrane-translocating sequences (MTS), which all have the ability to translocate the cell membrane and gain access to the cellular interior. The first CPP derives from the third helix of the *Antennapedia* protein homeodomain and was originally named *p*Antennapedia (*p*Antp) [13, 14]. This peptide is more commonly referred to as penetrating and, together with peptides such as the HIV protein derived transactivating regulatory protein (TAT) and transportan, is one of the most extensively investigated CPPs.

Examples of sequences of known CPPs are listed in Table 1.

Table 1. Known CPPs

Name	Sequence	Length	Net charge (+)	Isoelectric point	Mw (Da)
Penetratine	RQIKIWFQNRRMKWKK	16	7	12.4	2247
TAT	GRKKRRQRRRPPQ	13	8	12.7	1719
MAP	KLALKLALKALKAALKLA-amide	18	5	11.4	1878
Transportan	GWTLNSAGYLLGKINLKALAALAKKIL-amide	27	5	10.9	2842
Transportan 10	AGYLLGKINLKALAALAKKIL-amide	21	4	10.9	2183
R7 peptide	RRRRRRR	7	7	12.8	1111
pVEC	LLIILRRRIRKQAHAHSK-amide	18	8	12.5	2210
MPG peptide	GALFLGWLGAAGSTMGAPKKKRKV-amide	24	5	11.8	2445
KALA peptide	WEAKLAKALAKALAKHLAKALAKALKACEA	30	6	10.7	3132
Buforin 2	TRSSRAGLQFPVGRVHRLLRK	21	7	12.2	2435

All these peptides possess multiple positive charges and some of them share common features, the ability to interact with lipid membranes and to adopt a significant secondary structure on binding to lipids. Although the mechanism of transduction across a lipid bilayer is unknown, it is clear that transduction does not occur through a classical receptor, transporter, or in an endosome-mediated fashion [15].

1.2. Enzyme

Enzymes are highly efficient catalysts with extraordinary enantio- and regioselectivity, and they can accept a wide range of complex molecules as substrates [16]. Enzymes are widely used in many commercial purpose, such as the dairy, textile, chemical, detergent, food, pharmaceutical, and brewing industries. There are high expectations for processes where enantiomerically enriched intermediates are produced. Lipases, esterases and proteases are usually quite stable enzymes which are enantioselective. The advantages of using enzymes in chemical processes include high substrate and reaction specificity and less side reactions. Enzymes use often more environmentally friendly conditions like lower reaction temperatures, no need for protecting groups, less waste and less energy needed.

1.2.1. Lipase

Lipases are abundant enzymes that have been isolated from a wide variety of mammalian and microbial sources, even several lipases from archaea are known. Generally, there is very little homology among the known sequences, the most conserved feature is the consensus sequence GxSxG found in the substrate binding site. This is common to all lipases and esterases, as is the α/β-hydrolase fold [17].

The interior topology of α/β hydrolase fold proteins is composed largely of parallel β-sheets (at least five in lipases), separated by stretches of α-helix, and forming, overall, a superhelically twisted-pleated sheet. Nearly all lipases have the catalytic triad Ser-Asp(Glu)-His (in some

exceptions like the *Geotrichum candidum* or *Candida rugosa* lipases, the aspartate is replaced by a glutamate).

Lipases catalyze the hydrolysis of acylglycerides and in general of a wide range of low and high molecular weight fatty acid esters, thiol estes, amides, polyol/polyacid esters, diacyglycerol, monoacylglycerol, and glyceol [18]. In addition to the ester hydrolysis, lipases can catalyze the following several reactions in non-aqueous solvents, such as ester synthesis, esterification and transesterification reactions.

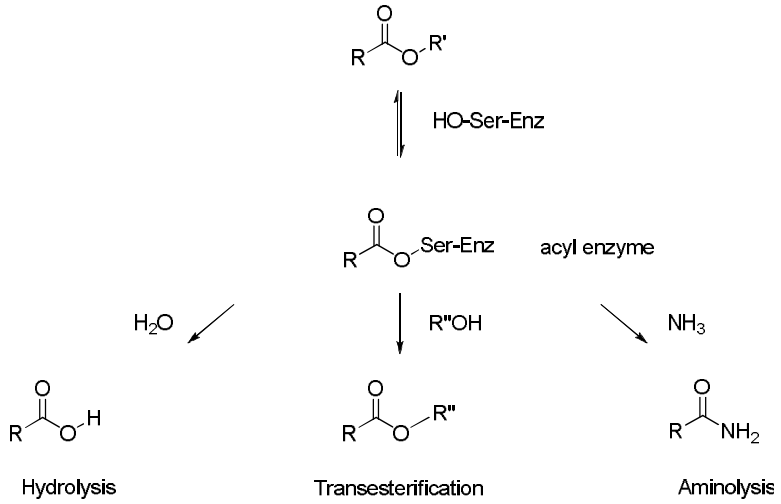

Figure 2. Reactions catalyzed by lipases.

Generally, lipases show almost no activity as long as substrate is in monomeric state. However, when the substrate starts to form an emulsion, there is a sharp increase in enzyme activity, on the other hand, that is not observed for esterase. This phenomenon can be explained by three-dimensional structure. It was found that the active site of a lipase was covered by a lid-like polypeptide chain composed of one or two amphipathic

α-helices. This lid structure rendered the active site inaccessible to substrate molecules, thereby causing the enzyme to be inactive on monomeric substrate molecules [19, 20]. When the substrate and the water-oil phase exist, the lid opens and then lipase becomes active, whereas the lid closed and the enzyme remains inactive without substrate.

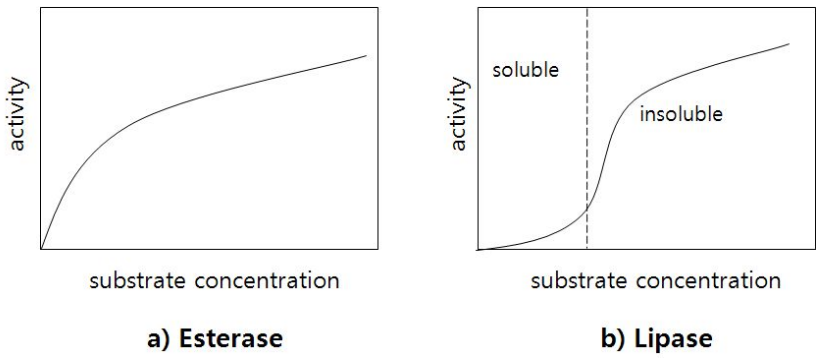

Figure 3. a) Esterase kinetics following normal Michaelis-Menten kinetics [21] and b) Lipase kinetics where interfacial activation [22] is observed.

Lipases are the most common biocatalyst in industrial and academic research. The advantages of lipases are low cost, no cofactors, and showed high activity and stability in water as well as in organic solvents, and converting a broad range of substrates with high steroeselectivity. The most frequently used lipases for organic synthesis are porcine pancreatic lipase (PPL), lipase from *Burkhderia cepacia* (BCL), lipase from *Candida rugosa* (CRL), and lipase B from *Candida antarctica* (CAL-B) [23-25]. In this study, two kinds of lipases, lipase B from *Candida antarctica* (CAL-B) and lipase from *Burkhderia cepacia* (BCL) were used.

1.2.1.1. *Candida antarctica* lipase B

One of the most effective lipases is *Candida antarctica* lipase B (CAL-B). CAL-B has high regio- and stereoselectivity, activity towards a broad range of substrates, and stability at high temperature and in many organic solvents. In 1994, the structure of CAL-B was determined by X-ray crystallography (Fig. 4) [26]. It is consisted of 317 amino acids and has a molecular weight of 33 kDa and an α/β hydrolase fold. The active site is composed of Ser105 - His224 - Asp187, as the catalytic triad.

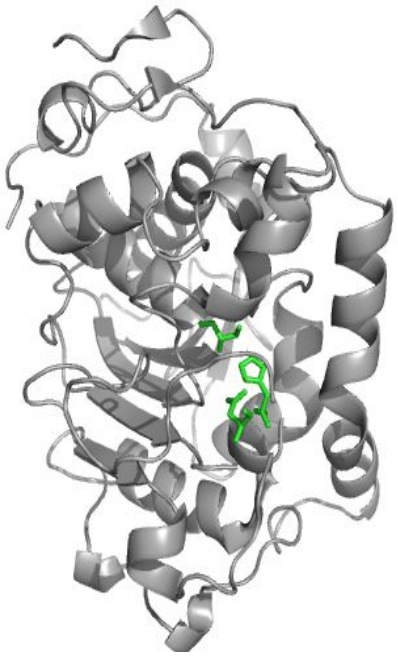

Figure 4. Structure of *Candida antarctica* lipase B (1TCA). The catalytic triad consists of Ser105, Asp187, and His224. They are displayed in stick representation.

A catalytic triad is responsible for the catalytic action with the bi-bi mechanism (Fig. 5). It is a two-step mechanism with an acylation step and a deacylation step separated by a covalent acyl-enzyme intermediate [27]. The oxyanion hole is consisted of Gln106 and Thr40. A charge relay system involving the catalytic triad of residues (Asp187, His224, and Ser105) forms the basis of the mechanism. First, the serine attacks the ester to generate the first tetrahedral intermediate (T_d1). An acyl enzyme intermediate is formed from the release of the alcohol and then by second substrate to form the second tetrahedral intermediate (T_d2). They release of the second product regenerates the free enzyme.

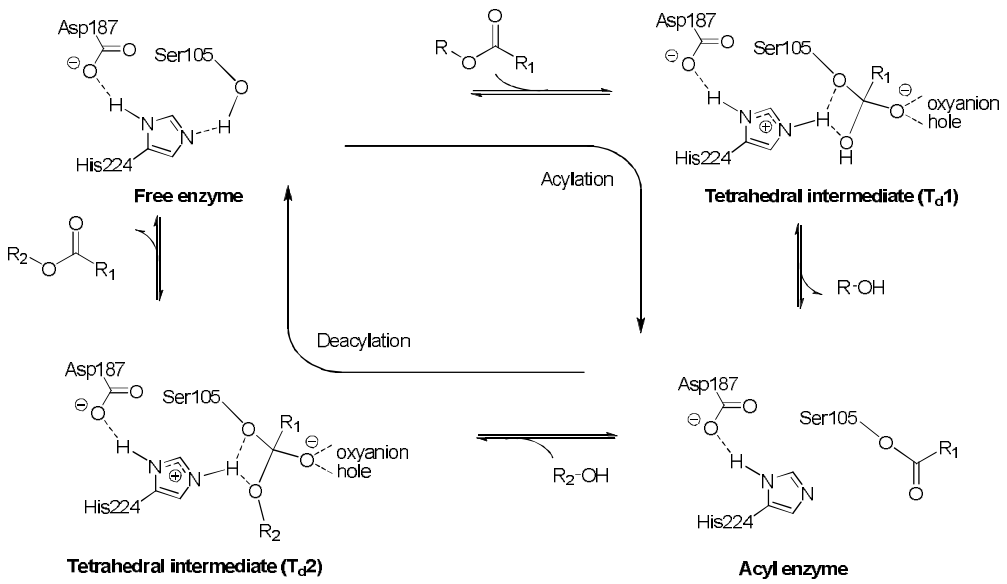

Figure 5. Catalytic mechanism of a *Candida antarctica* lipase B catalyzed hydrolysis (R_2=hydrogen) or transesterification (R_2=alkyl).

1.2.1.2. Lipase from *Burkhderia cepacia* (BCL)

The lipase from *Burkhderia cepacia* is another widely used enzyme for organic synthesis and hydrolysis because of its high enantioselectivity [28]. BCL is a highly selective catalyst for a broad range of substrates, including the kinetic resolution of racemic mixtures of secondary alcohols by hydrolysis in water or esterification in organic solvents [29-31]. It is consisted of 320 amino acid residues with a calculated molecular mass of 33 kDa. The active site is composed of Ser87 - His224 - Asp264, as the catalytic triad. The oxyanion hole is consisted of Glu88 and Leu17.

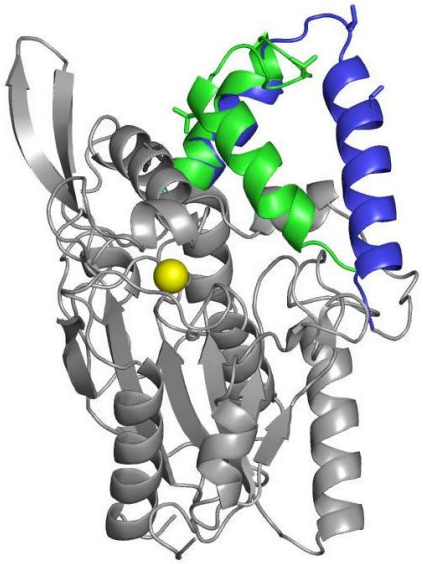

Figure 6. A overlap structure of open and closed BCL. The open and closed conformation of BCL is shown in a cartoon representation. The lid of the open crystal structure of BCL (3LIP) is colored blue and of the closed homology model green, the sphere of the Ca^{2+}-ion is colored yellow.

BCL has a large lid, which covers the active site (Fig. 6) [32]. The lid is opening at a hydrophobic interface, making the active site accessible for substrates and enhancing the activity of the lipases [33, 34]. Because the exterior of the lid is hydrophilic and its interior is hydrophobic, the hydrophobic surface of lipase increases upon lid opening [35].

1.2.2. Protein expression and refolding

Over the past decade the variety of hosts and vector systems for recombinant protein expression has increased dramatically. Typical expression vectors contain promoters that direct the synthesis of large amounts of mRNA corresponding to the gene. They may also include, for example, sequences that allow their autonomous replication within the host organism, sequences that encode genetic traits allowing cells containing the vectors to be selected, and sequences that increase the efficiency with which the mRNA is translated. Researchers now select from among mammalian, insect, yeast, and prokaryotic hosts, and the number of vectors available for use in these organisms continues to grow. Despite the development of eukaryotic systems, *Escherichia coli* remains the most widely used host for recombinant protein expression. *Escherichia coli* is easy to transform, grows quickly in simple media, and requires inexpensive equipment for growth and storage. And in most cases, *Escherichia coli* can be made to produce adequate amounts of protein suitable for the intended application.

Many recombinant proteins expressed in *Escherichia coli* were accumulated inside the cell as inclusion bodies. Especially many of eukaryotic proteins that overexpressed in *Escherichia coli* are apt to form

inclusion bodies because *Escherichia coli* does not perform post-translational modification and formation of disulfide bonds. It is then necessary to extract, solubilize and refold the protein in order to recover activity. A number of strategies are presented that are used to optimize the recovery of functional target protein [36]. Inclusion bodies may be solubilized by exposure to high molarity denaturants, detergents, acidic or alkali buffers, or a combination of reagents. Following solubilization, the target protein may be subjected to any of various strategies for refolding that result in the removal of the solubilizing agent. In general, denaturant removal is performed through the use of dialysis or dilution [37]. In addition, molecular chaperones facilitate protein folding by transiently binding to non-native proteins, which inhibits irreversible protein aggregation and promote folding to native state. Moreover, chaperones also minimize aggregation by mediating the degradation of proteins that cannot be properly folded.

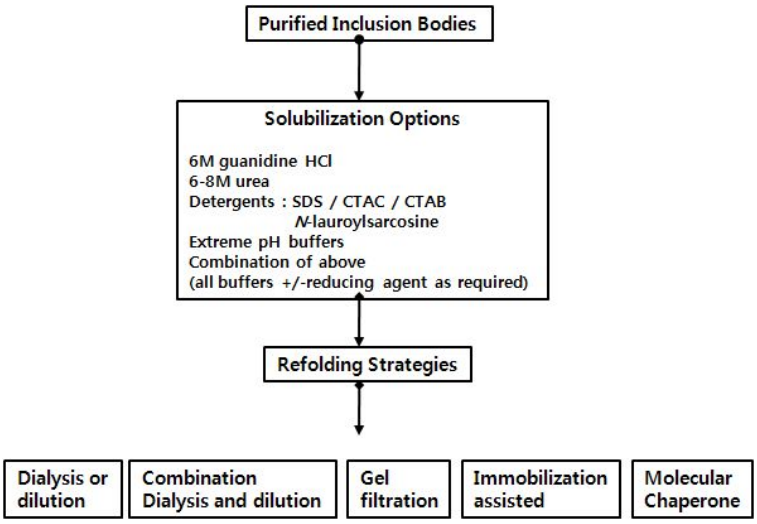

Figure 7. Methods for protein refolding.

1.2.3. Enzyme immobilization

One of the major problems in use of enzymes is their inactivation. There are a large number of stabilization strategies to improve catalytic stability of enzymes; for example, enzyme modification, genetic modification, and enzyme immobilization strategies. Among these methods, immobilization strategy using solid supports has been most extensively studied due to the specific advantages such as cost reduction by enabling the efficient separation and reuse [38, 39]. In addition, improved catalytic features such as activity, stability, and selectivity can be achieved by enzyme immobilization [40].

Enzymes can be immobilized to plenty of different carriers by covalent or ionic binding, entrapment, and adsorption [41]. Among these binding methods, covalent binding possesses several advantages: (1) enzymes do not leak or detach from the support during utilization due to tight binding; (2) the immobilized enzyme can easily make contact with the substrate because it is localized on the support surface; and (3) an increase in heat stability is often observed because of the strong interaction between the enzyme and support material [42, 43].

1.3. Nanoparticles

Nanoparticles are used to refer to a small particle with all three dimensions less than 100 nanometres [44]. The use of nanoparticles has shown great promises due to their unique properties, such as size-tunable luminescent properties and functionalizability to couple biomolecules or drugs

[45]. The nanoparticles, made up of various biodegradable polymers, polycyanoacrylate, polylactides (PLAs), and natural polymers gelatine, chitosan, sodium alginate and albumin can be used effectively for efficient delivery system.

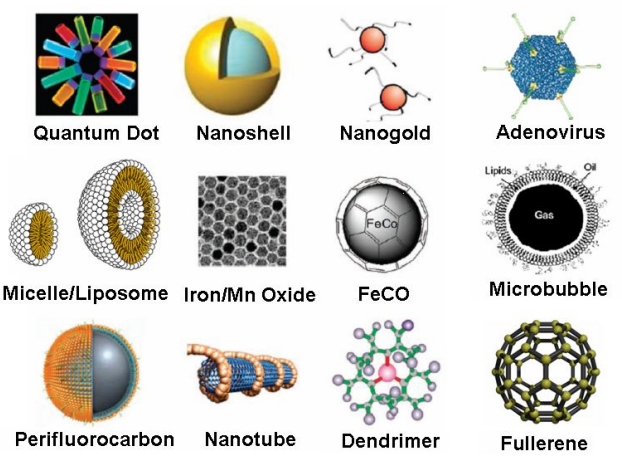

Figure 8. Examples of nanoparticles [46, 47]

1.3.1. Polymer nanoparticles

Polymer nanoparticles with spherical shape have been widely used in the various fields of industry because they have many advantages such as low impact resistance, fair strength and stiffness, high chemical resistance, transparency, afford-ability, and easiness of processing. They have many useful characteristics, which can be manipulated by controlling diameter, degree of cross-linking, surface chemistry, and porosity.

The main benefits are due to easiness of physical separation of the polymer particles and their bound components from the reaction mixture,

and easiness of recycling expensive catalysts and ligands. Immobilization of reactants on polymer particles enables the use of high concentrations of reagents to drive reactions to completion, as byproducts or excess reagents can be easily removed by filtration, and decreases the purification time than chromatography, distillation or crystallization methods. Another advantage is due to the unique environment created for the reactants within the polymer supports. They improve stability of catalysts within polymer matrixes, increase selectivity for intramolecular reaction, and enhanced regioselectivity due to steric hindrance and the activity of some supported chiral catalysts by site cooperation. [48, 49]

Polymeric nanoparticles can be easily prepared by heterogeneous methods. Heterogeneous polymerization processes are based on two-phase systems in which the starting monomers and the resulting polymers are in the form of a fine dispersion in immiscible liquid. The heterogeneous polymerization systems includes 'suspension', 'emulsion', 'dispersion', and 'precipitation' . They are clearly distinguished on the basis of the following four basis for comparison: (1) Initial state of the polymerization mixture; (2) Kinetics of polymerization; (3) Mechanism of particle formation; and (4) Shape and size of the final polymer particles. Kinetic feature and the size range of polymer particles produced by different heterogeneous polymerization process (Fig. 9).

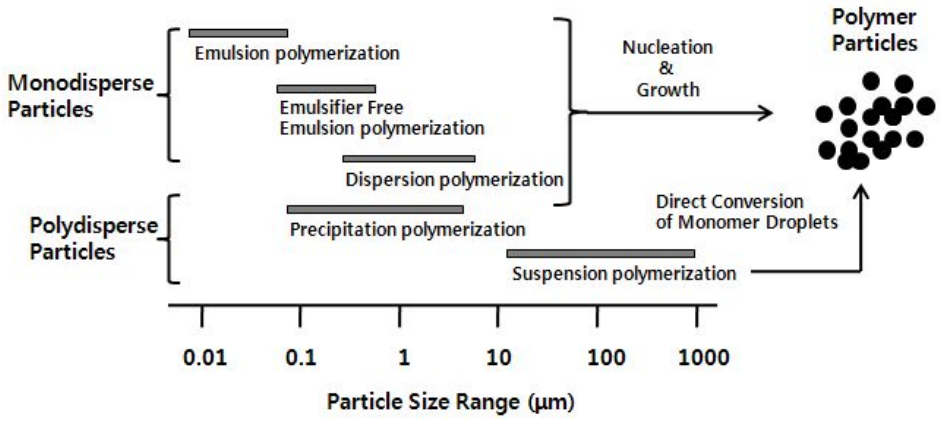

Figure 9. General kinetic features and particle size ranges of heterogeneous polymerization processes [50].

1.3.2. Magnetic polymer nanoparticles

Magnetic polymer nanoparticles are another important material in bioapplications due to their interesting magnetic properties. Because magnetic polymer particles sensitively react in the magnetic field, they are used in the fields of sell separation [51, 52], drug delivery system [53, 54], and magnetic resonance image contrast agents [55].

Magnetic polymer nanoparticles have recently have gained much attention to immobilize enzymes due to their several advantages, such as low mass transfer limitation and high surface-to-volume ratio [56]. In addition they provide a simple procedure of separating reacted enzyme from other reaction mixture using a simple centrifugation or an external magnet.

1.4. Metal-Organic Frameworks (MOFs)

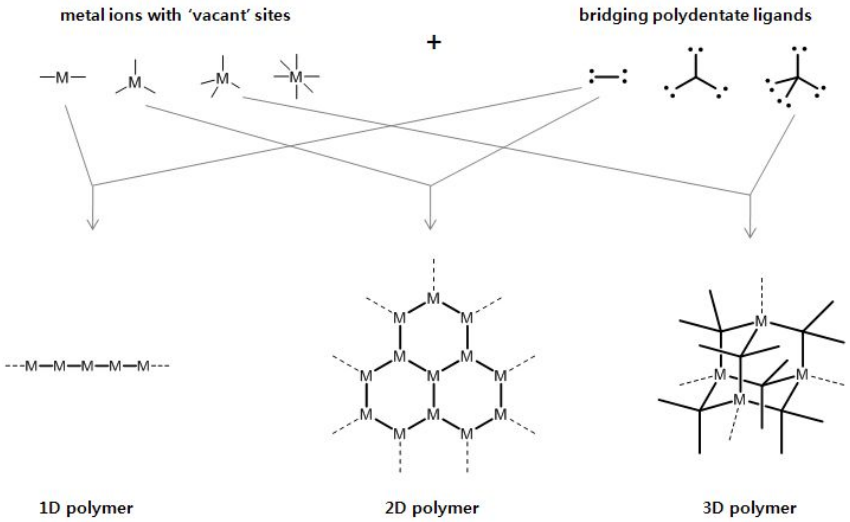

Figure 10. The building block, or 'modular', principle behind coordination polymers

MOFs are a class of coordination polymers with backbones constructed from metal ions and ligands, which form infinite network of one-, two- and three-dimensional structures that can be porous (Fig. 10). The important characteristics of nodes and linkers are their coordination numbers and coordination geometies. These features will affect the overall structure of the framework.

MOFs have attracted the attention of industrial and academic research because of their high surface area and tailorable selectivity, which makes them suitable for a wide range of applications. There is also commercial interest in their applications, such as gas separation, storage, and usage as heterogeneous catalysts [57].

MOFs have been a focus of intense as novel nanoporous materials.

Compared with nanotubes, activated carbon, and zeolites, MOFs have some unique features due to their structural flexibility. These unique features include high porosity and surface area, open structures with almost no inaccessible void space, flexible cavities shape and size, and tunable functionality of pore.

For synthesizing MOFs using precursors including metal precursors and corresponding organic spacing ligands, numerous methods have been developed. First, solvothermal and hydrothermal synthesis methods using these precursors have conventionally been employed to form MOF crystals. Solvothermal synthesis is a method where precursors for MOF crystal formation are heated in a solvent other than water [58]. In hydrothermal synthesis, precursors for MOF crystal are heated in water. Hydrothermal synthesis is suitable when the ligand precursor is water soluble [59]. Solvothermal and hydrothermal synthesis methods are typically slow, often taking hours and even days. Second, sonochemical methods can lead to homogeneous nucleation and a substantial reduction in crystallization time compared with conventional solovothermal methods [60, 61]. Third, Microwave assisted MOF synthesis yields high quality MOF crystals in a reaction time ranging from seconds to minutes. In addition, microwave methods provide MOF materials with a uniform crystal size and well defined shape [62].

1.5. Outline of this thesis

This thesis deals with two studies which are cellular delivery system for protein and immobilization of recombinant lipase. Chapter 2 describes a delivery system using biofuctionalized nanoparticles and cell permeable peptides. The glucose-coated beads and known cell permeable peptides delivered the EGFP as model protein inside the cells. In chapter 3, the recombinant lipases were immobilized on magnetic nanoparticles or metal-organic frameworks. Chapter 3.1 showed the mutational effect on expression yield of *Candida antarctica* lipase B in *E. coli.* The mutant increased expression yield three times compared to the wild type without change of the catalytic machinery of CAL-B. Chapter 3.2 deals with the chaperone conjugated polymeric magnetic beads for refolding of *B. cepacia* lipase. The beads showed comparable refolding activity to the soluble chaperone, and retained more than 95% of activity after ten-times recycling. In the chapter 3.3 and 3.4, magnetic nanoparticles and metal-organic frameworks were investigated for covalent-immobilization of lipase. The lipase-conjugated magnetic beads were showed similar hydrolytic activity to the free enzyme and retained activity after six times recycling. And the immobilized enzyme with MOFs has higher specific activity compared free enzyme in organic solvent. These results clearly indicate that functional proteins can be decorated on MOFs without losing their functions and recyclable without significant loss of the activity.

References

1. Ohno, K.; Levin, B.; Meruelo, D. *Biochem. Mol. Med.* **1996**, *58*, 227-233.
2. Naoya, K.; Takuya, S.; Masaru, M. Tsutomu, T.; Chiaki, O.; Hideki, F.; Akihiko, K. *J. Biochem.* **2008**, *144*, 707-707.
3. Senatus, P.B.; Li, Y.; Mandigo, C.; Nichols, G.; Moise, G.; Mao, Y.; Brown, M.D.; Anderson, R.C.; Parsa, A.T.; Brandt-Rauf, P.W.; Bruce, J.N.; Fine, R.L. *Mol. Cancer Ther.* **2006**, *5*, 20-28
4. Jaeger, K. *Curr. Opin. Biotech.* **2004**, *15*, 269-271.
5. Johannes, T.; Simurdiak, M. R.; Zhao, H. Encyclo. *Chem. Proces.* **2005**, *30*, 101-110.
6. Lindgren, M.; Hallbrink, M.; Prochiantz, A.; Langel, U.; *Trends Pharmacol. Sci*. **2003**, *21*, 99–103.
7. Shibagaki, N.; Udey, M. C. *Immunol.* **2002**, *168,* 2393–2401.
8. Pooga, M.; Soomets, U.; Hallbrink, M.; Valkna, A.; Saar, K.; Rezaei, K.; Kahl, U.; Hao, J. X.; Xu, X. J.; Wiesenfeld-Hallin, Z.; Hokfelt, T.; Bartfai, T.; Langel, U. *Nat. Biotechnol.* **1998**, *16*, 857–861.
9. Astriab-Fischer, A.; Sergueev, D.; Fischer, M.; Shaw, B. R.; Juliano, R. L. *Pharm. Res.* (*N. Y.*) **2002**, *19*, 744–754.
10. Schwarze, S. R.; Ho, A.; Vocero-Akbani, A.; Dowdy, S. F. *Science* **1999**, *285*, 1569–1572.
11. Lewin, M.; Carlesso, N.; Tung, C. H.; Tang, X. W.; Cory, D.; Scadden, D. T.; Weissleder, R. *Nat. Biotechnol.* **2000**, *18*, 410–414.
12. Torchilin, V. P.; Rammohan, R.; Weissig, V.; Levchenko, T. S. *Proc.*

Natl. Acad. Sci. U. S. A. **2001**, *98*, 8786–8791.

13. Green, M.; Loewenstein, P.M. *Cell* **1998,** *55*, 1179–1188.
14. Frankel, A.D.; Pabo, C.O. *Cell* **1998**, *55*, 1189-1194.
15. Schwarze, S.; Dowdy, S. 2000, Trands Pharmocol. Sci. 21, 45-48.
16. Dordick, J.S.; Khosla, C.*Biotec. Bioeng*. **2002**, *79*, 490-495.
17. Ollis, D. L.; Miroslaw, Cheah, E.; Cygler, M.; Dijkstra, B.; Frolow, F.; Franken, S. M.; Harel, M.; Remington, S. J.; Silman, I.; Schrag, J.; Sussman, J. L.; Verschueren, K. H. G.; Goldman, A. *Protein Engineering* **1992**, *5*, 197-211.
18. Faberk. Biotransformation in Oragnic Chemistry, 4th ed.; Springer-Verlag: Berlin, Germany, 2000.
19. Winkler, F.; D'Arcy, A.; Hunziker, W. *Nature* **1990**, *343*, 771-774.
20. Brady, L.; Brzozowski, A. M.; Derewenda, Z. S.; Dodson, E. G.; Tolley, S.; Turkenburg, J. P.; Christiansen, L.; Huge-Jansen, B.; Norskov, L.; Thim, L.; Menge, U. *Nature* **1990**, *343*, 767-770.
21. Fersht, A. Enzyme structure and Mechanism, 2nd ed.; W. H. Freeman and Co.; New York, 1985, pp. 98-103.
22. Verger, R. *Trands Biotechnol*. **1997**, *15*, 32-38.
23. Gotor, V. *Bioorg. Med. Chem*., **1999**, *7*, 2189-2197.
24. Roberts, S. M. *J. Chem. Soc. Perkin Trans.* **2000**, *1*, 611-633.
25. Theil, F. *Chem. Rev.* **1995**, *95*, 2203-2227.
26. Rotticci-Mulder, J. C. Expression and mutagenesis studies of *Candida antarctica* lipase B. Ph. D. Thesis, KTH, Sweden, 2003.
27. Mugnusson, A. Rational redesign of *Candida antarctica* lipase B. Ph. D. Thesis, KTH, Sweden, 2005.
28. Kazlauskas, R.J.; Weber, H.K. *Curr. Opin. Chem. Biol.* **1998**, *2*,

121-126.

29. Bornscheuer, U.T.; Kazlauskas, R.J.; Hydrolases in organic synthesis: regioand stereolelective biotransformations Weinheim: Wiley-VCH; 1999.
30. Schmid, R.D.; Verger, R. *Angew. Chem. Int. Ed.* **1998**, *37*, 1609-1633.
31. Jaeger, K.E.; Eggert, T. *Curr. Opin. Biotechnol.* **2002**, *13*, 390-397.
32. Brady, L.; Brzozowski, A.M.; Derewenda, Z.S.; Dodson, E.; Dodson, G.; Tolley, S.; Turkenburg, J.P.; Christiansen, L.; Hugejensen, B.; Norskov, L. *Nature* **1990**, *343,* 767-770.
33. Sarda, L.; Desnuelle, P. *Biochim. Biophys. Acta.* **1958**, *30*, 513-521.
34. Verger, R. *Methods Enzymol.* **1980**, *64,* 340-392.
35. Vantilbeurgh, H.; Egloff, M.P.; Martinez, C.; Rugani, N.; Verger, R.; ambillau, C. *Nature* **1993**, *362,* 814-820.
36. Marstone, F. A. O. *Biochem. J.* **1986**, *240*, 1-12.
37. Cliana, B. C.; Georgiou, G. *Protein refolding.* **1991**, 1-20.
38. Bayramoglu, G.; Kiralp, S.; Yilmaz, M.; Toppare, L.; Arica, M.Y. *Biochem. Eng. J.* **2008**, *38*,180-188.
39. Libertino, S.; Giannazzo, F.; Aiello, V.; Scandurra, A.; Sinatra, F.; Renis, M.; Fichera, M. *Langmuir* **2008**, *24*, 1965-1972.
40. Clark, D.S. *Trends. Biotechnol.* **1994**, *12*, 439-443.
41. Christensen, M.W.; Andersen, L.; Kirk, O.; Holm, H. C. *Eur. J. Lipid Sci. Technol.* **2003***, 105,* 318–321.
42. He, J.; Li, X.; Evans, DG.; Duan, X.; Li, C. *J. Mol. Catal. B: Enzym.* **2000**, *11*, 45-53.
43. Wong, M.S.; Jeng, E.S.; Ying, J.Y. *Nano Lett.* **2001**, *1*, 637-642.
44. Whitby, K. T. *Atmospheric Environment* **1978**, *12*, 135 -159.
45. Mosbach, K. *Methods Enzymol.* **1976**, *44*, 335-353.

46. Cai, W.; Chen, X. *Small.* **2007**, *3*, 1840-1854.

47. Cai, W.; Chen, X. *J. Nucl. Med*. **2008**, *49*, 113-128.

48. Goldstein, L.; Levin, Y.; Pecht, M.; Katchalski, E. *Biochemistry* 1964, 3, 1914–1919.

49. Itoyama, K.; Tokura, S.; Hayashi, T. *Biotechnol. Prog.* 1994, 10, 225–229.

50. Arshady, R. Suspension, emulsion, and dispersion polymerization: A methodological survey. Colloid and Polymer Science, Vol. 270, pp 717-732, 1992.

51. Sugibayashi, K.; Morimoto, Y.; Nadai, T.; Kato, Y. *Chem. Pharm. bull.* **1997**, *24*, 3433-3434.

52. Haik, Y.; Pai, V.; Chen, C. J. *J. Maga. Mater.* **1999**, *194*, 254-261.

53. Lubbe, A. S.; Bergemann, C.; Huhnt, W.; Fricke, T.; Riess, H.; Brock, J. W.; Huhn, D. *Cancer Res.* **1996**, *56*, 4694-4701.

54. Viroonchatapan, E.; Ueno, M.; Satp, H.; Adachi, I.; Nagae, H.; Tazawa, K.; Horikoshi, I. *Pharmaceut. Res.* **1995**, *12*, 1176-1183.

55. Martin, C. R.; Mitchell, D.T. *Anal. Chem.* 1998, 70, 322-327.

56. Jia, H.; Zhu, G.; Vugrinovich, B.; Kataphinan, W.; Reneker, DH.; Wang, P. *Biothenol. Prog*. **2002**, *18*, 1027-1032.

57. Rowsell, J. L.; Spencer, E. C.; Eclert, J.; Howard, J. A. K.; Yaghi, O. M. *Science* **2005**, *309*, 1350-1354.

58. Chui, S. S. Y.; Lo, S. M. F.; Charmant, J. P. H.; Orpen, A. G.; Williams, I. D. *Science* **1999**, *283*, 1148-1150.

59. Lin, W.; Wang, Z.; Ma, L. *J. Am. Chem. Soc*. **1999**, *121*, 11249-11250.

60. Kenneth, S. S.; Choe, S. B.; Cichowlas, A.; Grinstaff, M. W. *Nature* **1991**, *353*, 414-416.

61. Gedanken, A. *Ultrason. Sonochem*. **2004**, *11*, 47-55.

62. Qiu, L. J.; Li, Z. Q.; Wu, Y.; Wang, W.; Xu, T.; Jiang, X.*Chem. Commun*. **2008**, *31*, 3642-3644.

Chapter 2. Intracellular Protein Delivery for Protein

In this chapter, I investigated protein delivery systems based on the delivery carriers such as nanoparticles and several known cell permeable peptides (CPPs). The EGFP (enhanced green fluorescent protein) as a model protein was translocated into mouse embryonic stem cells and HeLa cells. The glucose-coated beads delivered the EGFP inside the cells. In addition, I examined the transfection efficiency of several known cell permeable peptides (CPPs) into mouse embryonic stem cells under various conditions. The efficiency of transfection of CPPs-EGFP depends on the sequence of CPPs.

2.1. Intracellular Protein Delivery by Glucose-Coated Polymeric Beads*

Abstract: Macromolecules, such as DNAs and proteins, can be internalized into cells by carriers. The intracellular delivery of proteins is garnering more interest because proteins can be used as therapeutic agents and as a research tool for studying intracellular protein-protein, protein-lipid, and protein-DNA interactions. Development of a protein delivery system requires an appended signal or tag molecule that interacts with cell membranes and thus facilitates protein uptake into the cell. For example, cationic lipids are drawn to the cell surface via attraction to negatively charged cell membrane molecules. Finding molecules that suitably mediate such interactions represents a key step in the development of protein delivery systems. Glucose is an excellent candidate molecule because cells have various mechanisms for the uptake of glucose and glycated proteins. Thus, glucose-coated materials could be translocated inside cells, providing a potentially important general system for protein delivery. This idea was evaluated in this study by preparing glucose-coated polymeric nanobeads by dispersion polymerization. The average size of the beads was determined to be about 150 nm by scanning electron microscopy. The EGFP (enhanced green fluorescent protein) as a model protein for protein delivery was attached to the prepared beads by a simple chemical treatment and translocated into mouse embryonic stem cells and HeLa cells. Confocal

---

Jung, S.; Huh, S.; Cheon, Y.-P.; Park, S. "Intracellular protein delivery by glucose-coated polymeric beads," *Chem. Commun.* **2009**, 5003-5005.

image analysis indicated that the glucose-coated beads delivered the EGFP inside the cells whereas non-glucose-coated beads or the EGFP alone did not. This study therefore demonstrates the potential utility of glucose-coated nanobeads for cellular protein delivery.

Introduction

The intracellular delivery of proteins is garnering more interest because proteins can be used as therapeutic agents [1] and research tools for studying intracellular protein–protein, protein–lipid, and protein–DNA interactions [2, 3]. Moreover, the development of a protein delivery system may benefit researchers in a variety of applications including drug delivery [4, 5], and the control of cell differentiation using signaling peptides or functional proteins [6].

However, proteins are generally unable to cross the membrane barrier of eukaryotic cells without using protein-specific transport systems [7]. For intracellular protein delivery, researchers have used recognition molecules that can interact with cell membrane molecules. One example is cationic lipids. The cationic head group of cationic lipids [8] is able to interact with negatively charged cell membrane molecules through electrostatic attractions. Another approach for protein delivery is the usage of cell-permeable peptides or proteins that can interact with cell membranes and penetrate into cells [9, 10]

The development of protein carriers requires the usage of a recognition molecule to establish interactions with the cell membrane.

Glucose is a good candidate for such a molecule because it is an important monosaccharide in living systems, and most cells utilize it for energy and for other metabolic processes. Many mechanisms for the uptake of glucose into cells have recently been described [11], although the detailed mechanisms are still a matter of debate [12].

Results and Discussion

Preparation and identification of polymeric nanobeads. The mono-dispersed polymeric nanobeads were prepared by dispersion polymerization. Dispersion polymerization is an appropriate method in attaining small-sized monodispersed beads in a single step. In this procedure, various functional groups can be introduced to the beads by using proper monomers [13]. Glucose-coated nanobeads were prepared using 6-*O*-glucosyl methacrylate, styrene, and acrylic acid. Acrylic acid provided the functional group with which to conjugate proteins. Glucose was ligated to methacrylate by CAL-B (*Candida antarctica* lipase B, Novozyme 435) to form 6-*O*-glucosyl methacrylate (1 in Fig. 1). Although CAL-B has high regioselectivity toward the primary alcohol of glucose, the product may be a mixture of mono- or diacylated compounds, but we did not attempt to separate them because both products can be used for polymerization. The 6-*O*-methacryl glucose was polymerized with styrene and acrylic acid in aqueous methanol to form nanosized beads (2 in Fig. 1) [14].

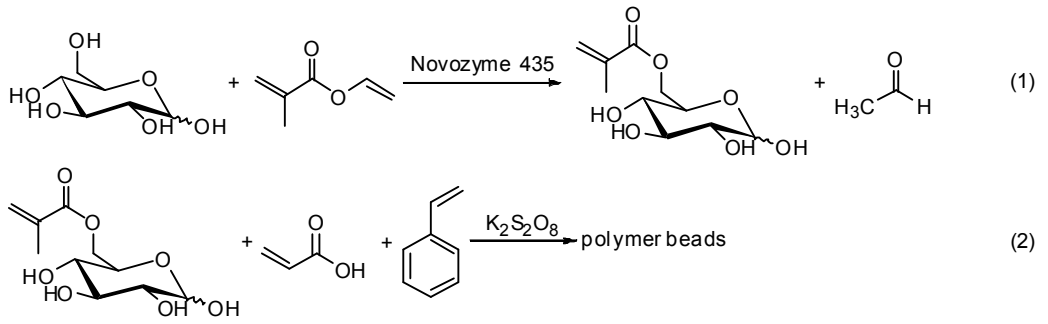

Figure 1. Synthesis of 6-*O*-methacryl glucose and mono-dispersed polymeric beads.

The amount of glucose units on the beads was limited to 5-10% molar ratio compared to the amount of styrene used. Preparation of glucose-free acrylic acid beads for the control experiment was attempted by polymerization of styrene and acrylic acid without the addition of 6-*O*-glucosyl methacrylate.

Scanning electron microscopy (SEM) (Fig. 2) was used to show that the glucose-coated beads were uniformly of an average diameter of about 150 nm (Fig. 2a). However, the acrylic acid beads were larger than glucose-coated beads, having an average diameter of about 300 nm (Fig. 2b). Because we were unable to prepare acrylic acid beads with the same diameter of the glucose-coated beads (~100 nm), and transduction efficiency may vary with size, an alternative approach was employed. Thus, similar-sized non-glucose-coated nanobeads (0%-glucose-coated beads) for the control experiment were prepared by removing glucose units from the glucose-coated beads via acid hydrolysis.

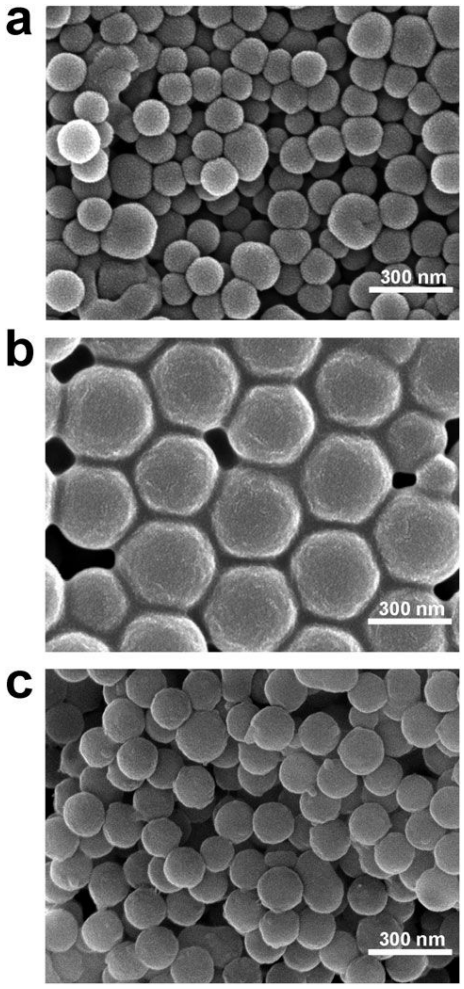

Figure 2. The scanning electron micrographs of the prepared polymeric beads. (a) Glucose-coated beads (10%-glucose content) with diameters of about 150 nm. (b) Acrylic acid beads prepared from polystyrene and acrylic acid only have diameters of about 300 nm. (c) Non-glucose-coated beads (0%-glucose-coated beads) prepared by removing glucose units from the glucose-coated beads via acid hydrolysis. Scale bar = 300 nm.

.

Conjugation of polymeric nanoparticles with EGFP. EGFP (enhanced green fluorescent protein) was chosen as a model protein because it can easily be tracked in cells and its folding status may easily be recognized by fluorescence. The fluorescent protein EGFP was covalently attached to the beads by a simple chemical treatment. The carboxylic acid groups on the beads were utilized tobind proteins after activation with EDC (1-ethyl-3-(3-dimethylaminopropyl) carbodiimide) (Fig. 3). The free amino groups of EGFP react with the activate dcarboxylic acid groups of the beads to form amide bonds at pH 7.3. The amount of bound EGFP was determined to be 1.4 mg/g of beads.

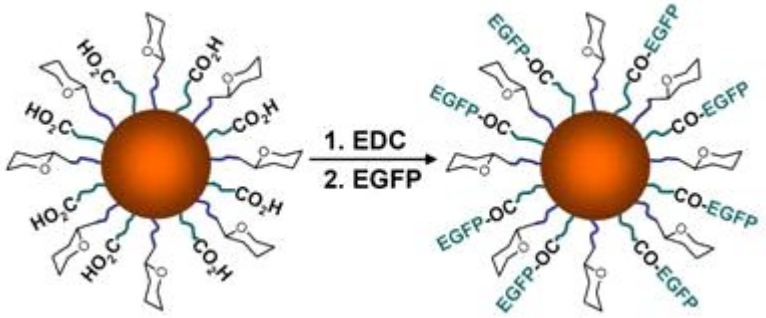

Figure 3. Conjugation of glucose-coated polymeric nanobeads with the EGFP. EDC = 1-ethyl-3-(3-dimethylaminopropyl) carbodiimide, EGFP = enhanced green fluorescent protein.

Turbidity measurements of the beads with concanavalin A. A turbidity measurement using concanavalin A was carried out to confirm whether the glucose units are present on the surface of the beads and can function to interact with protein. Concanavalin A specifically binds glucose or mannose and then aggregates [15]. Thus, if glucose units are present on the surface of the beads, they can interact with concanavalin A and aggregation occurs, which may be detected by a turbidity measurement at 600 nm. Fig. 4 shows the aggregation behavior of concanavalin A after addition to the bead suspension. The turbidity is significantly correlated with the amount of glucose units on the beads. Addition of concanavalin A to the non-glucose-coated beads (the acrylic-acid beads and the 0%-glucose-coated beads) does not increase turbidity, while addition to the glucose-coated beads does. Higher turbidity was observed in 10%-glucose-coated beads than in 5%-glucose-coated beads.

The process of conjugating proteins on to the beads provides a convenient alternative to genetic hybridization of protein transduction domains to the target protein because additional optimization of the recombinant protein expression is not required. However, a potential problem involves the small size of glucose relative to the conjugated target protein. For instance, the larger target protein might shield glucose from the membrane and there by interrupt the key interaction for delivery. To address this problem, we tested whether the glucose unit of the EGFP-conjugated beads can interact with the concanavalin A protein. Indeed, the turbidity increased upon mixing concanavalin A with the EGFP-conjugated glucose-coated beads, although the turbidity was lower than for non-EGFP-conjugated glucose-coated beads (Fig. 4). This result

indicated that some shielding does occur, but the glucose units can still interact with concanavalin A and thereby may establish an interaction with the cell membrane to facilitate transduction.

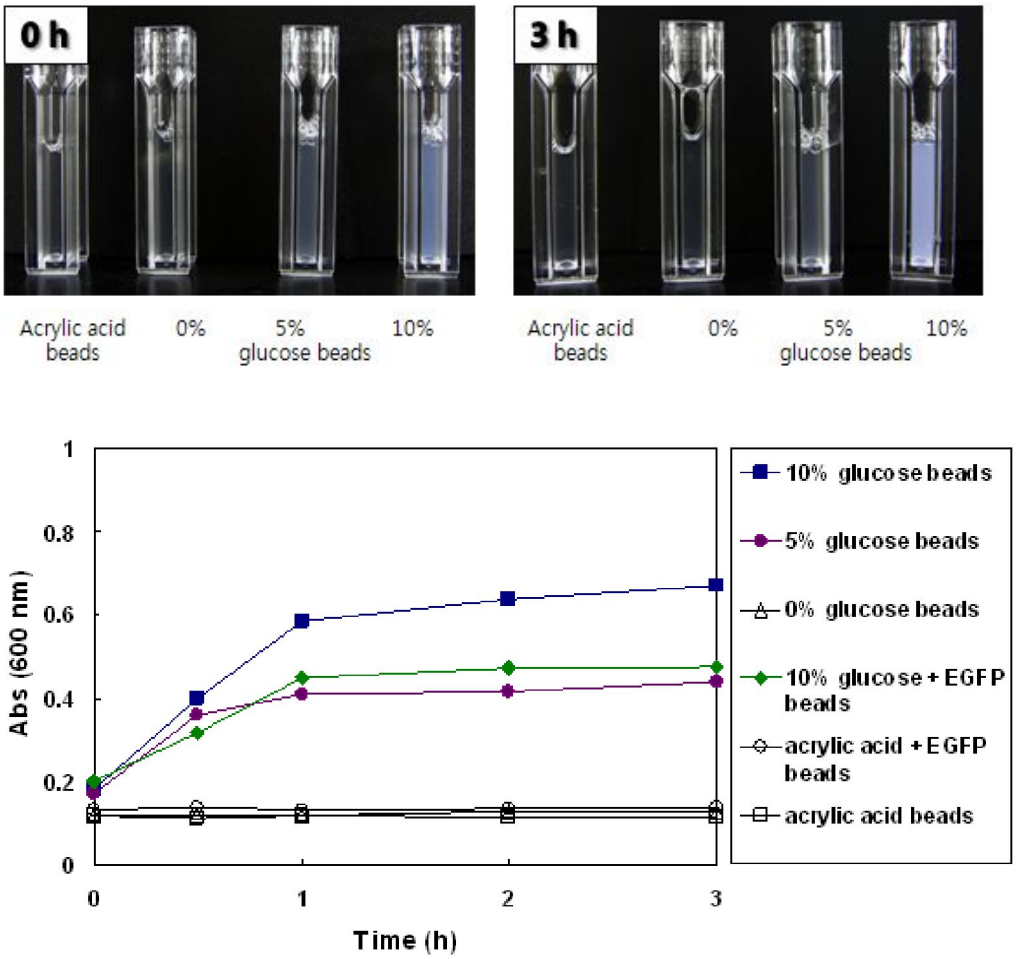

Figure 4. Turbidity measurements for a mixture of beads and concanavalin A. Glucose-coated beads aggregated concanavalin A and lead to a turbidity increase, but non-glucose-coated beads did not cause concanavalin A to aggregate. The 0%-glucose beads were prepared by removing glucose units via acid hydrolysis while the acrylic-acid beads were synthesized from a mixture of styrene and acrylic acid without glucose.

Transduction of the glucose-coated nanobeads into mouse embryonic stem cells and HeLa cells. Mouse embryonic stem cells (mES cells) were chosen to test the transduction activity of the glucose-coated nanobeads for protein delivery. The development of protein delivery system into stem cells is potentially important in clinical therapy using stem cells because protein transduction can be applied to directing stem cell differentiation [16, 17]. Therefore the development of a novel protein-delivery system into stem cells, therefore, has tremendous potential.

EGFP does not cross the membrane of mES cells and thus the confocal image of the mES cells treated with EGFP alone does not show fluorescence inside the cells (1-a in Fig. 5). Presumably the cell membrane does not contain any specific acceptor proteins for EGFP. The EGFP-conjugated non-glucose-coated beads were also not found inside the mES cells (2-a in Fig. 5). This result clearly indicates that the EGFP-conjugated non-glucose-coated beads cannot penetrate into mES cells. However, the EGFP-conjugated glucose-coated beads were internalized and showed fluorescence in the cells (3-a and 4-a in Fig. 5). The merged images (3-b and 4-b in Fig. 5) show that the cells are placed on the fluorescent regions. The glucose units on the glucose-coated nanobeads are therefore likely responsible for mediating transduction. The relative fluorescence intensities for both glucose-coated beads (5% and 10%-glucose content) were similar within the error range (b in Fig. 5). The amount of glucose units does not seem critical in the range used.

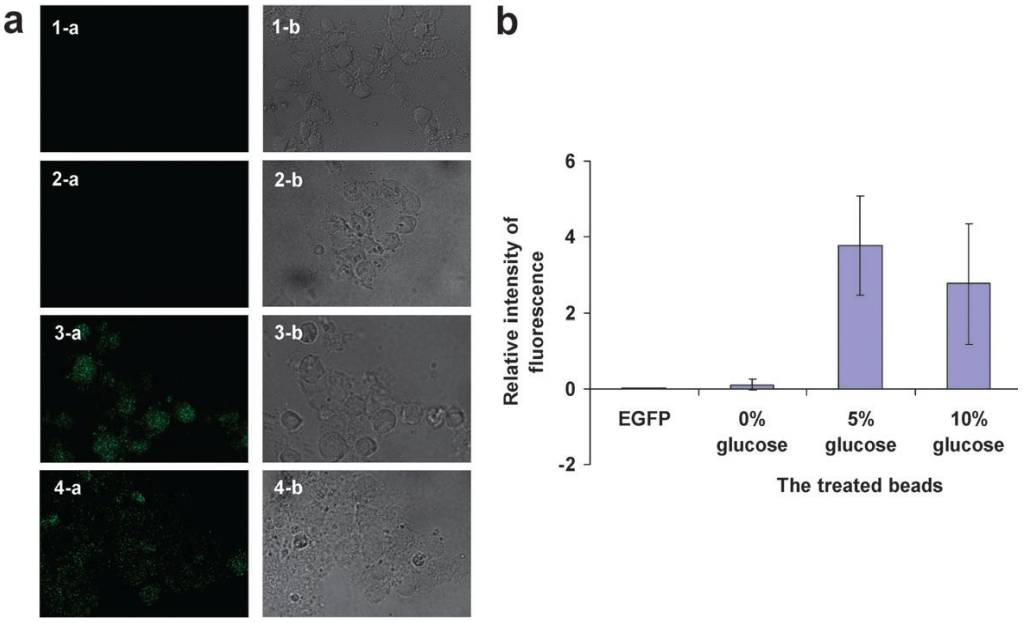

Figure 5. Translocation experiments of the EGFP-ligated beads into R1 mouse embryonic stem cells. (a) The confocal microscopic images. 1-a and 1-b, cells treated with EGFP alone; 2-a and 2-b, cells treated with non-glucose-coated beads; 3-a and 3-b, cells treated with 5%-glucose-coated beads; 4-a and 4-b, cells treated with 10%-glucose-coated beads; 1-a, 2-a, 3-a and 4-a are dark field images; 1-b, 2-b,3-b and 4-b are bright field images. The fluorescent regions are identical to the area of cells located. (b) The relative intensities of the translocated EGFP. The intensities in a single cell were measured using a confocal microscope. Errors are the standard deviations for at least seven measurements.

Analysis by transmission electron microscopy (TEM) of translocation experiments. Transmission electron micrographs also provided direct evidence that the glucose coated polymeric beads were internalized. The TEM image for R1 mES cells untreated (Fig. 6a) and treated with non-glucose-coated beads (Fig. 6b) did not show any particles with diameters of about 150 nm inside a cell. In contrast, the polymeric beads were detected inside a cell in the TEM images for a cell treated with 5%-glucose-coated beads (Fig. 6c, 6d). The size of the particles is same to that of the polymeric beads

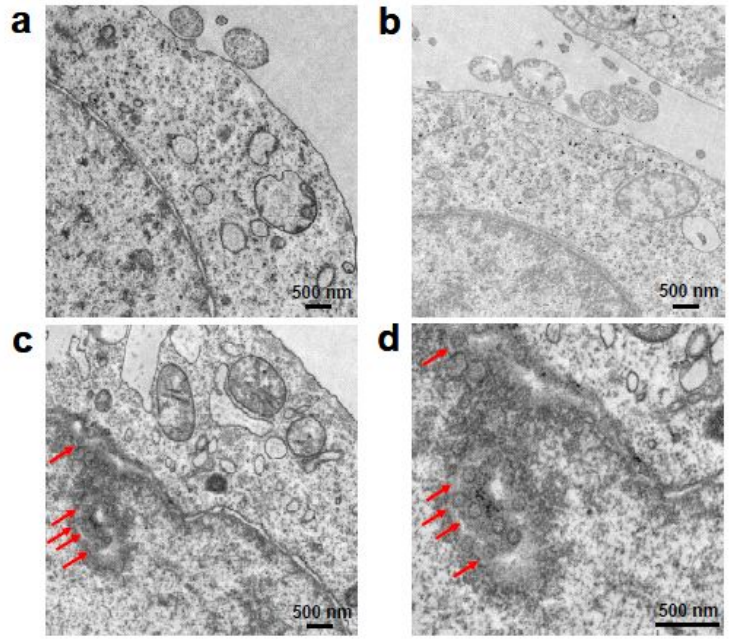

Figure 6. Analysis by transmission electron microscopy (TEM) of translocation experiments of the beads into R1 mES cells. a) a cell untreated. b) a cell treated with non-glucose-coated beads. c) a cell treated with 5%-glucose-coated beads d) the amplified image of c. The arrows indicate the polymeric beads.

Transduction of the beads into HeLa cells at 37 ºC and mouse embryonic stem cells at 4 ºC. Hella cells were tested to evaluate further applicability of our delivery system. Similar results were observed in the transduction experiment with HeLa cells (Fig. 7). The confocal images for HeLa cells treated with EGFP alone or non-glucose-coated beads did not show fluorescence in the cells (1-a, 1-b, 2-a, and 2-b in Fig. 7). However, the cells treated with 5%-glucose-coated beads clearly showed fluorescence (3-a in Fig. 7) and the overlap image indicates that fluorescence is present in the cells (3-b in Fig. 7). It can therefore be concluded that glucose plays the key role in enabling protein-conjugated beads to cross membranes.

We also performed the transduction experiment at 4 ºC because the experiment could provide a clue for the uptake mechanism. In general, inhibition of the uptake at 4 °C indicates that the internalization process presumably involves an endocytic pathway [18,19]. The mES cells were cultured for 8 hr at 4 °C before being incubated with the beads. Incubation at 4 °C for 8 hr did not cause internalization of EGFP or any lucose-coated beads in the cells (4-a, 5, 6, and 7 in Fig. 7). Again a repeated xperiment of incubation at 37 °C resulted in internalization of the glucose-coated beads (8 in Fig. 7). Although the detailed mechanism of the cellular uptake of the protein-conjugated glucose-coated beads is unclear at this time, the result indicates that the glucose-coated beads are presumably internalized by endocytic machinery.

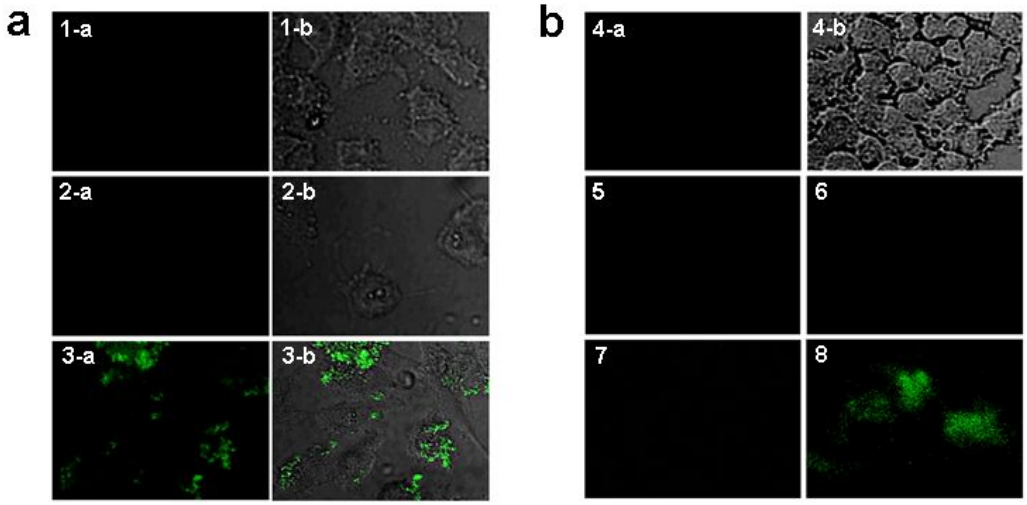

Figure 7. Translocation experiments of the EGFP-ligated beads into HeLa cells at 37 °C, and into R1 mouse embryonic stem cells at 4 °C (4, 5, 6, and 7) and at 37 °C (8). (a) The confocal microscopic images of HeLa cells. 1-a and 1-b, cells treated with EGFP alone; 2-a and 2-b, cells treated with non-glucose-coated beads; 3-a and 3-b, cells treated with 5%-glucose-coated beads. 1-a, 2-a, and 3-a are dark field images. 1-b, 2-b, and 3-b are merged images (dark-bright fields). (b) The confocal microscopic images of R1 mouse embryonic stem cells. 4-a and 4-b, cells treated with EGFP alone (4-a is a dark field image and 4-b is a merged image.) at 4 °C; 5, cells treated with non-glucose-coated beads at 4 °C; 6, cells were treated with 5%-glucose-coated beads at 4 °C; 7, cells were treated with 10%-glucosecoated beads at 4 °C; 8, cells treated with 5%-glucose-coated beads at 37 °C. 5, 6, 7, and 8 are dark field images.

Cytotoxicity of glucose-coated beads on the mES cells. We have measured degeneration rate (death rate) of the mES cells after treatment of 5%-glucose-coated beads (Fig. 8). The rate was dependent on the amount of beads used. Addition of below 0.25 μL, that is the experimental condition in this study, did not show considerable death rate compared to the control experiment. However, adding above 0.5 μL showed significant toxicity on the cells.

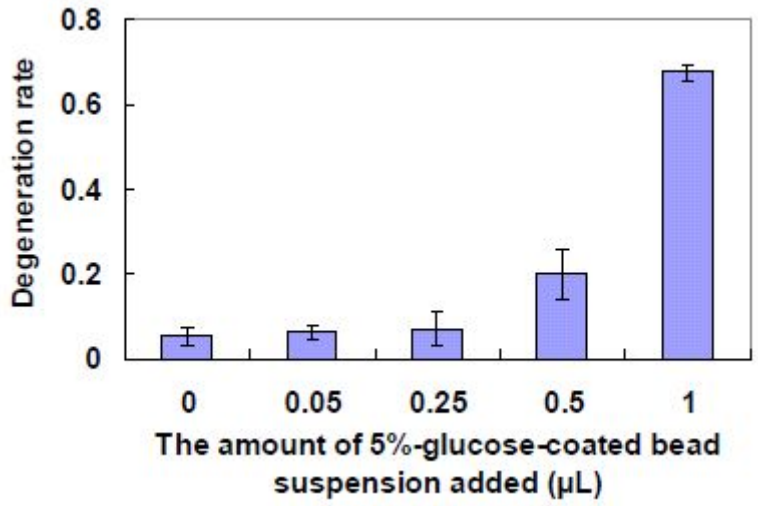

Figure 8. Cytotoxicity of 5%-glucose-coated beads on the mES cells. Toxicity was measured by degeneration rate (death rate). The number of dead cells was counted using a hemocytometer after being stained with 0.4% trypan blue.

Macromolecule-delivery systems often utilize a cationic moiety to interact with the negatively charged cell membrane and there by facilitate cell uptake. Non-charged glucose offers an attractive alternative to cationic molecules by reducing the cytoxicity associated with charged molecules present in cationic-lipid-mediated delivery systems.

Conclusion

We demonstrated that glucose can be utilized for developing a novel protein delivery system. Our experimental results clearly showed that glucose mediated delivery of EGFP into mouse embryonic stem cells and HeLa cells although the detailed transduction mechanism is unclear at this

time. The discovery of glucose-coated-bead-mediated delivery may have many biological applications. For example, EGFP can be substituted by numerous macromolecules such as peptide-based drugs and functional proteins. In addition, biotin-binding proteins may be employed to deliver biotinated DNAs and si-RNAs. In summary, our glucose-coated nanobeads may provide a universal system for the delivery of a wide variety of macromolecules

Experimental Section

General Methods. Chemicals, buffers, lysozyme, and concanavalin A were purchased from Sigma-Aldrich. *Pfu* DNA polymerase and restriction enzymes (*Xho* I and *Bam* HI) were purchased from Enzynomics (Daejeon, Korea). DNA oligomers were obtained from Sigma-Proligo (Singapore). The vector (pET-15b) was purchased from Merck biosciences. DNA sequencing was performed by Solgent Co. (Daejeon, Korea).The Ni-NTA agarose resin was purchased from QIAGEN. ^{1}H-NMR spectrum was recorded from D_2O solutions on a Varian 500 MHz spectrometer. The SEM images were obtained by a Nano-SEM at KIST (Seoul, Korea).

Synthesis of 6-*O*-methacryl glucose. The monomer (6-*O*-methacrylglucose) was prepared similarly to the literature method [20-21]. Novozyme 435 (3 g) was added to a mixture of D-(+)-glucose(6 g, 33 mmol) and vinyl methacrylate (11 g, 100 mmol) in *t*-butyl alcohol (100 ml), and the reaction mixture was stirred at 50 °C for 12 hours. After Novozyme 435 was removed by filtration, 6-*O*-methacryl glucose (4.7 g, 55%) was obtained by

evaporation of the solvent. The product was used for polymerization without further purification. The NMR data were obtained as a mixture of the α- and β-forms of 6-*O*-methacryl glucose.

^{1}H-NMR (500 MHz, D_2O) δ 6.02 (d, 2H), 5.59 (s, 2H), 5.08 (d, 1H), 4.52(d, 1H), 4.33-4.25 (m, 4H), 3.92 (m, 1H), 3.58 (m, 2H), 3.41-3.37 (m, 4H), 3.12(t, 1H), 1.80 (s, 6H); ^{13}C-NMR (125 MHz, D_2O): δ 169.6,135.8, 127.2, 96.1, 92.3, 75.6, 74.2, 73.6, 72.7, 71.6, 69.8, 69.7, 69.4, 63.7,17.5

Synthesis of polymeric nanoparticles. Styrene (5 ml, 44 mmol) washed with a sodium hydroxide solution (0.1 M), acrylic acid (274 μl, 3 mmol), and 6-*O*-methacryl glucose (1.1 or 0.55 g, 4 or 2 mmol, repectively) were added to preheated methanol (50 ml) containing water (10%) and hexane (5%) at 70 °C. The reaction mixture was stirred at 70 °C for 20 hours after potassium persulfate (125 mg, 0.43 mmol) was added. The solvent was removed by decanting after centrifugation at 10,000 rpm. The prepared beads (1.2 g) were washed three times with distilled water (25 ml) and dried under vacuum. The acrylic acid beads were prepared similarly without addition of 6-*O*-methacryl glucose.

Removing glucose from nanobeads. The beads (10% glucose-coated beads, 1 g) were added to an HCl solution (6 M, 100 ml) and refluxed for 16 hours. After washing three times with distilled water (25 ml), the beads were dried under vacuum.

Expression and purification of the EGFP. The EGFP gene was subcloned from EGFP-C2 (Clontech) into the pET-15b (Merckbiosciences). Gene specific primers used were as follows:

EGFP-XhoI-F1(5'-GCAAACTCGAGGTGAGCAAGGGCGAGGAGCTG-3'), EGFP-BamHI-R1(5'-CAGCCGGATCCTTACTTGTACAGCTCGTCCATGCCG-3'). The primers containing restriction sites for *Xho* I and *Bam* HI were used to introduce these two sites into the genes and to clone the genes into the pET-15b vector. The plasmid containing the EGFP gene was transformed into BL21(DE3).

An overnight culture of BL21(DE3) (1 ml) containing the EGFP gene was added to LB medium (100 ml; ampicillin,100 μg/ml) and incubated at 37 °C and 200rpm to an OD_{600} of 0.5. Protein expression was induced by adding an IPTG solution (1 ml; 2% w/v) and the expression culture was incubated for 6 h at 25 °C and 200 rpm, at which point the OD_{600} was ~1.5. The cells were harvested by centrifugation (10 min, 3,800 g, 4 °C) and the supernatant was discarded. The cell pellet (~0.8 g) was resuspended in the lysis buffer (5 ml/g wet weight; NaH_2PO_4, 50 mM; NaCl, 300 mM; imidazole, 10 mM; adjusted to pH 8.0 with NaOH), and lysozyme was added to 1 mg/ml. Incubation on ice for 45 min was followed by a freeze-thaw cycle at -20 °C and room temperature. The viscous lysate was passed several times through a sterile 20-gauge syringe needle and centrifuged (10 min, 10,000 g, 4 °C). The supernatant was separated from the cell debris. Ni-NTA agarose resin (1 ml of 50% slurry) was added to the supernatant (4 ml) and the mixture was shaken at 25 °C for 1 h. The lysate-Ni-NTA mixture was loaded on a Poly-Prepcolumn (Bio-Rad), drained, and then washed three times with the wash buffer (4ml; NaH_2PO_4, 50 mM;

NaCl, 300 mM; imidazole, 20 mM; adjusted to pH 8.0 with NaOH). The His_6-EGFP was eluted from the column with four volumes of the elution buffer (0.5 ml; NaH_2PO_4,50 mM; NaCl, 300 mM; imidazole, 250 mM; adjusted to pH 8.0 with NaOH).

Eluate (2 ml) containing the purified EGFP from the Ni-NTA column was exchanged from the elution buffer to PBS buffer (0.1 M, pH7.3) using a centrifugal device (Amicon Ultra-15, Millipore). The protein amount was estimated from the absorption at 280 nm (molar absorptivity = 22,015 M^{-1} cm^{-1}, calculated with tools at Swiss Prot Expasy, http://ca.expasy.org/tools /protparam.html)

Conjugation of polymeric nanoparticles with the EGFP. The EGFP was conjugated to the polymeric beads similarly to the method in the literature [22]. The polymeric beads (100 mg) were resuspended in MES buffer (5 ml, 0.1 M, pH5.0) and EDC (1-ethyl-3-(3-dimethylaminopropyl) carbodiimide, 100 mg) was added. The mixture was stirred for 20 min and centrifuged to remove the buffer. The activated beads were washed three times with PBS buffer (5 ml, 0.1 M, pH 7.3) and resuspended in PBS buffer (1 ml). The resuspended beads in PBS buffer (100 μl) and EGFP solution (100 μl, 15 mg/ml) were mixed and incubated overnight at 4 °C. The EGFP-bound beads were washed three times with PBS buffer (1 ml) and resuspended in PBS buffer (100 μl).

Turbidity measurement of aggregation of concanavalin A by the prepared beads. The prepared beads (1 mg) were suspended in PBS buffer (1 ml)

by sonication. The suspension of beads (50 μl) was added to PBS buffer (750 μl) in a cuvette (1 ml). The absorbance change at 600 nm was monitored for 3 hours after adding a concanavalin A solution (200 μl, 2 mg/ml of PBS buffer).

mES cell culture and transduction of beads into mES cells. Undifferentiated R1 mouse embryonic stem (mES) cells were grown on gelatin-coated tissue culture plates in the mES medium (5 ml, Dulbecco's modified eagles medium supplemented with 0.1 mM nonessential amino acids, 0.1 mM β-mercaptoethanol, and 10% fetal calf serum). The mES medium contained the 1000 U/ml leukemia inhibitory factor (LIF, Chemicon). The mES cells were passed every 3 or 4 days onto freshly prepared gelatin-coated plates, and fed every day with the mES medium (5 ml) at 37 °C with 5% CO_2 and > 95% humidity. The mES cells were plated on gelatin-coated cover glasses for the test of the transduction activity of the prepared beads. The cover glasses were placed in each well of a 24-well culture plate and the mES medium (0.5 ml) was added. After the mES cells were grown for 2 or 3 days to 80% confluency, the mES medium was replaced with the mES medium (0.5 ml) containing the EGFP solution (0.25 μL, 15 mg/ml) or the above EGFP conjugated bead suspension (0.25 μL, 100 mg/ml). The mES cells were additionally incubated for 8 hr at 37 °C. The confocal-microscopy images were obtained under the unfixed condition after washing three times with PBS buffer.

To evaluate temperature dependency of the transduction of the beads, a transduction experiment at 4 °C was performed. The mES cells were preincubated for 8 hr at 4 °C maintaining 5% CO_2 in air before

adding the beads. After addition of the beads, the mES cells were additionally incubated for 8 hr at 4 °C and then analyzed with a confocal microscope.

Fluorescent intensity analysis. The intensity of intracellular EGFP was analyzed using a confocal microscope operated by FluoView (Ver1.26). After XYX scanning, the images were accumulated and analyzed for measuring the intensity from a single mES cell. Experiments were repeated 6 times and the measurements were repeated 10 times at each experiment.

HeLa cell culture and transduction of beads into HeLa cells. HeLa cells (CRL-1658, ATCC) were cultured under the standard condition with Dulbecco's modified Eagle medium (DMEM; Invitrogen) containing 10% fetal bovine serum (FBS; GIBCO), 100 μg/ml penicillin, and 100 U/ml streptomycin. HeLa cells were plated on a culture slide glass (Nalgene, Rochester, NY) and grown for 2 or 3 days until 80% confluency at 37 °C with 5% CO_2 in the culture medium supplemented with 10% fetal bovine serum. The cells were treated with the beads and analyzed in the same manner as the mES cells.

Cytotoxicity of the glucose-coated beads in mES cells. The mES cells were cultured on the 24-well culture plate in the mES medium containing LIF (1000 iu/ml). When the cells reached 80-90% confluency, the mES medium was replaced with the medium containing various amount of 5% glucose

bead suspension. After incubation for 8 hr, the cells were treated with trypsin-EDTA (Gibco BRL), and harvested and washed with DMEM. The trypan-blue-viability test was performed in order to analyze cytotoxicity. Briefly, 0.4% trypan blue (Sigma) was added into the cell suspension and the cell suspension was incubated for 15 min. The number of dead cells was counted using a hemocytometer. The test was repeated 3 times.

References

1. Pavlou, A. K.; Reichert, J. M. *Nat. Biotechnol.*, **2004**, *22*, 1513-1519.
2. Hawiger, J. *Curr. Opin. Immunol.*, **1997**, *9*, 189-194.
3. An, S.; Kumar, R.; Sheets, E.D.; Benkovic, S.J. *Science*, **2008**, *320*, 103-106.
4. Sinha, V.R.; Trehan, A. *J. Controlled Release*, **2003**, *90*, 261-280.
5. Koo, A.N.; Lee, H.J.; Kim, S.E.; Chang, J.H.; Park, C.; Kim, C.; Park, J.H.; Lee, S.C. *Chem. Commun.*, **2008**, 6570-6572.
6. Noda, T.; Kawamura, R.; Funabashi, H.; Mie, M.; Kobatake, E.; *J. Biotechnol.,* **2006,** *126,* 230-236.
7. Hawiger, J. *Curr. Opin. Chem. Biol.*, **1999**, *3*, 189-194.
8. Zelphati, O.; Wang, Y.; Kitada, S.; Reed, J.C.; Felgner, P.L.; Corbeil, J. *J. Biol. Chem.*, **2001**, *276*, 35103-35110.
9. Vives, E.; Brodin, P.; Lebleu, B. *J. Biol. Chem.,* **1997**, *272*, 16010-16017.
10. Schwarze, S.R.; Hruska, K.A.; Dowdy, S.F. *Trends Cell Biol.*, **2000**, *10*, 290-295.
11. Gould, G.W.; Holman, G.D. *Biochem. J.*, **1993**, *295*, 329-341.
12. Dugani, C.; Klip, A. *EMBO Rep.*, **2005**, *6*, 1137-1142.

13. Stoica, F.; Alexander, C.; Tirelli, N.; M. A. F.; Saiani, A. *Chem. Commun*., **2008**, 4433-4435.
14. Horak, D.; Svec, F.; Frechet, J.M.J. *J. Pol. Sci. A,* **1995**, *33*, 2961-2968.
15. Sharon, N.; Lis, H. *Science*, **1972**, *177*, 949-959.
16. Heng, B.C.; Cao, T. *Biomed. Pharmacother.*, **2005**, *59*, 132-134.
17. Heng, B.C.; Cao, T.; Haider, H.K.; Wang, D.Z.M.; Sim, E. K.-W.; Ng, S.C. *Cell Tissue Res.*, **2004**, *315*, 291-303.
18. Vivès, E.; Brodin, P.; Lebleu, B. *J. Biol. Chem*. **1997**, *272*, 16010-16017.
19. Wender, P. A.; Mitchell, D. J.; Pattabiraman, K.; Pelkey, E. T.; Steinman, L.; Rothbard, J. B. *Proc. Natl. Acad. Sci. U.S.A*. **2000**, *97*, 13003-13008.
20. Kim, J.; Haam, S.; Park, D.-W.; Ahn, I.-S.; Lee, T. G.; Kim, H.-S.; Kim, W.-S. *Chem. Eng. J.* **2004**, *99*, 15-22.
21. Jeong, G.-T.; Byun, K.-Y.; Lee, W.-T.; Ryu, H.-W.; Sunwoo, C.; Kim, H.-S.; Park, D.-H. *Biochem. Eng. J*. **2006**, *29*, 69-74.
22. Zheng, W.; Gao, F.; Gu, H. *J. Magn. Magn. Mater*. **2005**, *293*, 199-205.

2.2. Mouse Embryonic Stem Cell Uptakes of Buforin 2 and pEP-1 Conjugated with EGFP*

Abstract: Differentiation of cells can be induced through modulation of endogenous regulators using exogenous factors. Useful transfection systems to transport such a specific exogenous regulator into cells have been tried but still there are many obstacles to overcome. In this study, we examined the transfection efficiency of several known cell permeable peptides (CPPs) into mouse embryonic stem cells under various conditions. To identify the CPP-mediated translocation of a protein, we employed recombinant CPP-enhanced green fluorescent protein (EGFP). Viability of R1 cells was varied according to experimental groups depending on the kinds of CPPs and the concentration employed of CPP-EGFP. Translocation of CPP-EGFPs into the R1 cells was not detected until 30 min after CPP-EGFPs treatment in all groups. After 1 hr, translocation of pEP-1-EGFP-N was detected, but it could not be detected in the other group. Transfection of pEP-1EGFP-N was independent on its concentration. The time course did not show saturation even after 24 hr in pEP-1-EGFP-N. These results showed that the permeability depended on the kinds of CPPs and the location of His-tag in the case of examined CPPs, and did not need biological energy. In summary, the efficiency of transfection of CPP-EGFP depends on the CPP sequences but the culturing time is not a key factor in transfection for the mouse embryonic stem cell.

Jung, S.; Park, S.; Lim, H.; Cheon. Y. " Mouse Embryonic Stem Cell Uptakes of Buforin 2 and pEP-1 Conjugated with EGFP," *Dev. Reprod.* **2007**, *11,* 111-119.

Introduction

In recent years, embryonic stem cells (ES cells) are widely used as a model system to explore the mammalian embryonic development and applied to the cell therapy. Stem cells possess the capability of transforming into many cell types and are good candidates for cell-based therapies in regenerative medicine for diseases [1, 2]. So far, stem cell biology has been focused on identifying novel pathways such as maintaining the pluripotency, and inducing specific cell types. However, it is not easy to use as medicine or to study about the differential induction to a specific cell type. To get a specific cell type, it is essential to know the interactions of multiple genes and the associated factors which are involved in differentiation and de-differentiation of ES cells. To meet these requirements, many experimental conditions and gene delivery systems like high performance microinjection [3], various vector system [4], nucleofection [5], lipofectants and calcium phosphate were used. However, stem cells are resistant to most common transfection methods. The developments of effective strategies for genetic modification of ES cells have been progressed and have been resulting in improvement the differentiation of the ES cells to a specific cell type. One of the useful methods to modulate the gene expression is transgene delivery. Transgene delivery is a powerful strategy for induction of specific cell types from ES cells since several transcription factors have been demonstrated to regulate stem cell differentiation [6, 7, 8]. Among the existing approaches for delivery a gene, viral systems is suspected of their potential life-threatening effects of immunogenicity and carcinogenicity whereas non-viral ones possess

significant limitation in terms of efficacy as previously mentioned. Besides, genetic modulation has also problem because it should be change the genetic structure of the mammals. In addition, an essential prerequisite for application of ES cells in regenerative medicine is the development of efficient protocols to direct stem cell differentiation into well-defined lineage [9]. So we need various ways to modulate the gene expression, nucleic acids, proteins, chemicals. However, protein delivery or chemical delivery has also limits. Development of a safe as well as an efficient carrier is, therefore, an urgent requirement for effective implementation of stem cells in regenerative medicine or gene therapy. One of the best candidates is the cell permeable peptides (CPP; protein transduction domains, membrane translocating sequences); it is known as small peptides that are able to ferry much larger molecules, nucleic acids, protein, chemical, into living cells. However, it is know that the efficiency is controversy and that the permeability depends on the kinds of CPPs and cell types. In this study therefore to get a good vehicle for transfection of proteins, chemicals or nucleic acids to the differentiating mES cell, we designed two synthetic CPPs, expressed CPP-EGFPs and analyzed the transfection modulating factors.

Results

Toxicity of CPPs on Mouse Embryonic Stem Cell. To know the effects of CPP-EGFPs on viability of R1 stem cell, R1 cells were exposed to CPP-EGFPs for 12 hr with various concentrations. The viability was analyzed using trypan blue import assay. The toxicity was detected and it was dependent on the kind of CPPs. pEP 1-EGFP-N and pEP 1-EGFP-C showed cytotoxicity at 500 μg/ml dose. In the case of pEP-EGFPs, that cytotoxicity was correlated with concentration. However Buforin-2 was not much toxic to R1 cells compared with pEP-1-EGFPs (Fig. 1).

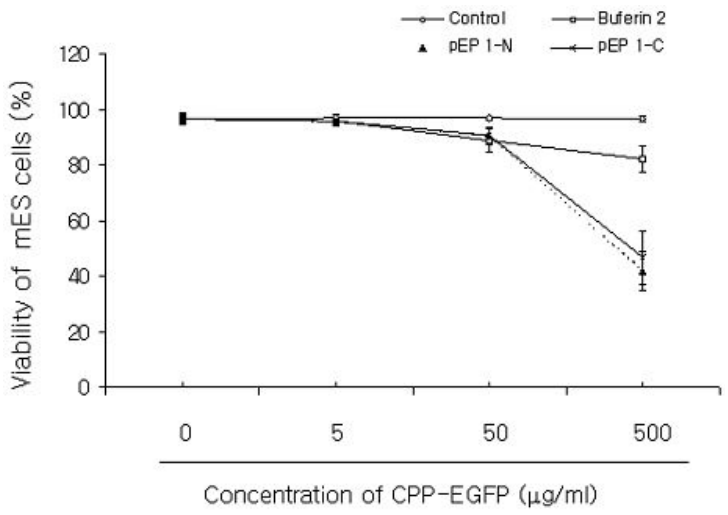

Figure 1. Cytotoxicity of CPP-EGFPs on the R1 mouse embryonic stem cell. Cells were treated with CPP-EGFPs for 12 hr and checked viability using trypan blue dye exclusionmentioned in Materials and Methods.

Concentration Effects on Transfection. To analyze the concentration effects on CPP-EGFPs transfection, CPP-EGFPs were treated as mentioned in Materials and Methods. R1 was treated with CPP-EGFPs, 5 μg/ml, 50 μg/ml and 500 μg/ml for 12 hr, and observed using confocal microscope. The permeability of CPP-EGFPs depended on the kinds of CPPs but not on their doses. Transfection of EGFP and Bufroin 2-EGFP was not detected after 12 hr (Fig. 2). Buforin 2 could not translocate EGFP into the cytoplasm, even in 500 μg/ml (Fig. 2C). In the case of pEP-1, however, it could translocate the EGFP-N in to the cytoplasm of R1 cells throw plasma membrane. Efficiency in transfection of pEP-1 was not correlated with the concentration (Fig. 2D). However, if His-tag was moved to the C-terminal of EGFP, pEP-1 could not translocate the EGFP through the plasma membrane. pEP-1-EGFP-C was mainly localized around the plasma membrane of R1 cells (Fig. 2E).

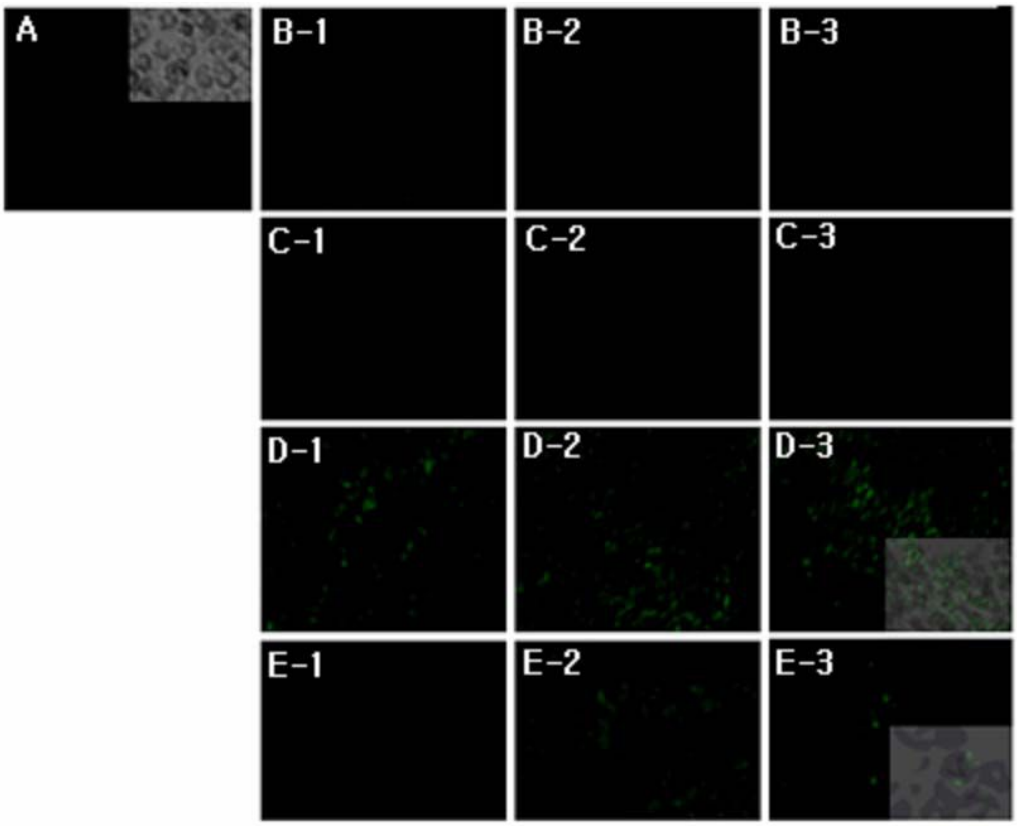

Figure 2. Efficiency of transfection depends on the CPP. CPP-EGFPs were treated with various concentration (-1; 5 μg/ml, -2; 50 μg/ml, -3; 500 μg/ml) and observed after 12 hr. Vehicle (A), EGFP (B), Buforin 2-EGFP (C), pEP-1-EGFP-N (D), pEP-1-EGFP-C (E) were exposed to R1 embryonic stem cell and transfection was detected using confocal microscope. Confocal images illustrate clear intracellular localization of pEP-1-EGFP-N (D-1, D-2, and D-3). In the case of pEP-1-EGFP-C it was mainly localized around the cells. Overlays show where localization of EGFP (D-3, E-3). Magnification = 200×(box: 400×).

Treatment Time on the Transfection Efficiency. In order to explore the treatment-time efficiency on CPPs-facilitate-delivery, we examined cellular uptake of the recombinant CPP-EGFPs, after 5 min, 30 min, 1 hr and 24 hr incubation of mES cells with EGFP, Buforin 2-EGFP, pEP-1-EGFP-N and pEP-1-EGFP-C. After treatment the R1 cells were observed without fixation under the confocal microscope. Until 30 min, translocation of recombinant CPP-EGFPs was not detect in all groups (Fig. 3, 4).

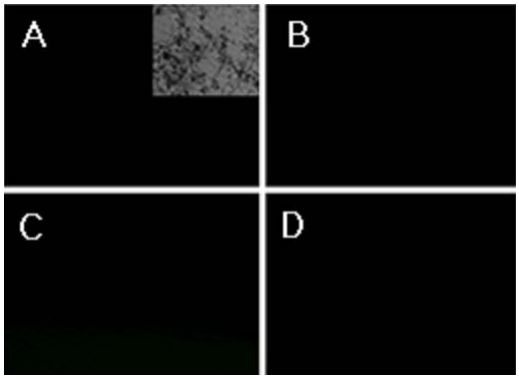

Figure 3. Transfection of EGFP (A), Buforin 2-EGFP (B), pEP-1-EGFP-N (C) and pEP-1-EGFP-C (D) into R1 mES cells at 5 min after treatment. 50 μg/ml CPP-EGFPs overlaid on the R1 cells for 5 min and washed with PBS three times. Evidence of transfection could not detect inall group (Large box figure; fluorescence field, small box; overlapped image with bright field). Magnification = 200×.

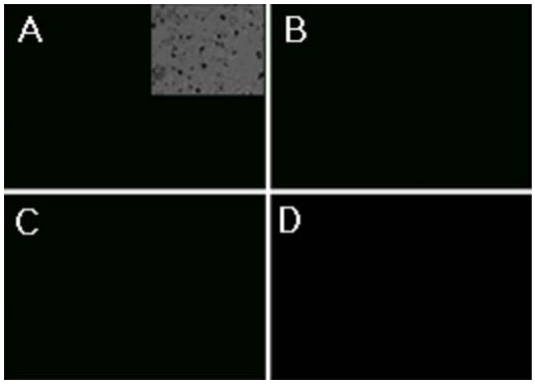

Figure 4. Transfection of EGFP (A), Buforin 2-EGFP (B), pEP-1-EGFP-N (C) and pEP-1-EGFP-C (D) into R1 mES cells at 30 min after treatment. 50 μg/ml CPP-EGFPs overlaid on the R1 cells for 30 min and washed with PBS three times. Evidence of transfection could not detect in all group (Large box figure; fluorescence field, small box; overlapped image with bright field).Magnification = 200×.

pEP-1-EGFP-N was detected in the cytoplasm of R1 cell at 1 hr post treatment (Fig. 5). However, translocalization of Buforin 2-EGFP and pEP-1-EGFP-C through plasma membrane or nuclear membrane was not observed in R1 cells at 1 hr post treatment. Besides the signals was not detected even after 24 hr treatment (Fig. 6). pEP-1-EGFP-C could not be transfected into the R1 cell but localized mainly around the R1 plasma membrane (Fig. 6).

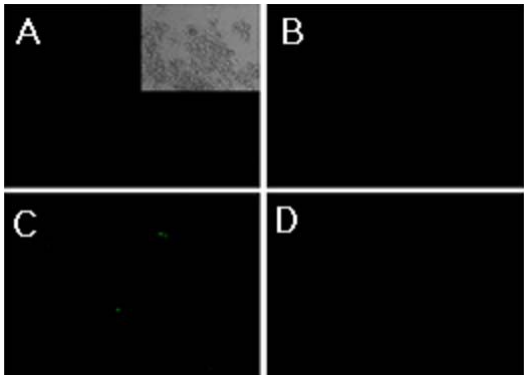

Figure 5. Transfection of EGFP (A), Buforin 2-EGFP (B), pEP-1-EGFP-N (C) and pEP-1-EGFP-C (D) into R1 mES cells at 1 hr after treatment. 50 μg/ml CPPEGFPs overlaid on the R1 cells for 1 hr and washed with PBS three times. Evidence of transfection could detect in pEP-1-EGFP-N but signal was weak (C). Large box figure is fluorescence field and small box is overlapped image with bright field. Magnification = 200×.

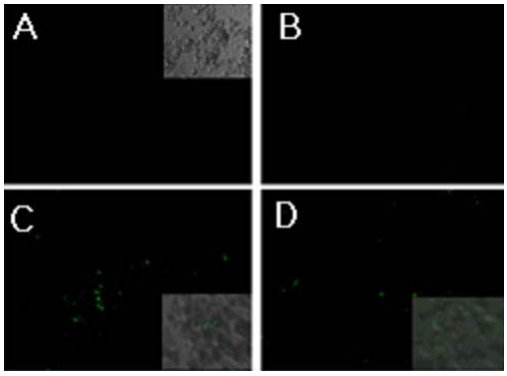

Figure 6. Transfection of EGFP (A), Buforin 2-EGFP (B), pEP-1-EGFP-N (C) and pEP-1-EGFP-C (D) into R1 mES cells at 24 hr after treatment. 50 μg/ml CPPEGFPs overlaid on the R1 cells for 24 hr and washed with PBS three times. Evidence of transfection could detect both in pEP-1-EGFP-N and pEP-1-EGFP-C. Signal was mainly detected inner cell area in pEP- 1-EGFP-N but it was mainly observed around the cells in pEP-1-EGFP-C. Large box figure is fluorescence field and small box is overlapped image with bright field. Magnification = 200× (box: A; 200×, C & D; 400×)

Discussion

Genetic manipulation of ES cells is essential to elucidate gene function. Through genetic manipulation, we can direct the differentiation of ES cells to specific lineages, use the differentiated cell types from mixed populations of ES cell derivatives, use the differentiated derivatives of ES cells as a vehicle for gene therapy, and modulated immune response to transplanted ES cell derivatives. For therapeutic application in transplantation medicine, controlled modification of specific genes could be useful for purifying specific ES cell-derived and differentiated cell type from a mixed population, and for giving cells new properties to combat specific diseases.

To manipulate the genes, homologous recombination and electrophoration protocols have been used with mouse ES cells and human ES cells. Nanoparticles are also used as a mediator to transfection the gene constructs or proteins into the eukaryotic cell. However it is needed help of the component of target cell to quick transport such as fibronectin or E-cadherin in stem cells [13]. To use as a medicine, there are overwhelming safety concerns with regards to the application of genetic manipulation in human clinical therapy, uncontrolled expression or suppression, cellular viability, and unpredictable physiological consequences [14. 15]. Therefore it has been asked to develop a methodology which is non-genomic modulation.

A novel alterative would be look at the possibility of incorporating CPP within transcription factors. Recent reports show that the usefulness of the cell permeable proteins as a delivery mediator. Recently using a recombinant cell permeable Cre protein successfully conditional knockin

efficiently was induced recombination at defined stages of neural differentiation. Cre treatment has no overt side effects on proliferation and neural differentiation [16]. In HeLa cell, Buforin-2 and GFP fused Buforin-2 could enter into the cytoplasm. Syn B1 could effectively transfect peptide through blood-brain barrier and into the nervous system [17]. In human ES cells import efficacy of PDX1 is very poor compared with TAT-PDX1 in the human ES cells [18, 19]. In addition, from this study we know that Buforin-2 is a poor transfection mediator in R1 embryonic stem cells. However, pEP-1 is a good candidate as a mediator for protein transfection into the embryonic stem cells. Based on them, it is clear that the composition of CPP is a key factor for the high efficiency of transfection and the cell types in effect of the transfection mediated with CPP. It is suggested that translocation of CPP is partially under the control by the composition of target membrane.

So far the mechanism of CPP mediated transport is controversy. Because in the previous studies, CPP-mediated translocation occurred even at low temperatures, and does not have strong cellular specificity, it is likely to be independent of endocytotic mechanisms, transmembrane protein channels, and protein receptor binding [20]. On the other hand, the other groups suggested that any effects of CPP were due to an enhanced physical chemical interaction but not uptake of the fusion peptide [21, 22]. pEP-1-EGFP-N binding to the cell membrane in R1 cells was not observed at 5 min or 30 min after treatment. From 1 hr after treatment, cell-membrane-binding pEP-1-EGFP-N was observed and translocalized pEP-1-EGFP-N was detected in the cytoplasm. Besides the translocalization of pEP-1EGFP-N was not depend on the concentration. This transfection

pattern is similar with the Buforin peptide in the HeLa cells [23]. Put together it is suggested that pEP-1-EGFP transfection follows the concentration-independent passive mechanism.

It is also known that there is dependence of translocation of CPP on the dose, time, temperature, and energy [23]. The Buforin-2 peptide is moved into the cytoplasm within 10 min by a temperature-independent and less concentration-dependent passive mechanism, and the magainin peptide show cooperative concentration dependence of uptake [16, 18, 23, 24]. CPPs used in this study, Buforin 2 and pEP-1 also were not showed dependence on the time and dose. It is suggested that the transfer of CPP is dependent on their chemical characteristics in embryonic stem cells.

Recently the techniques for protein transfection has been developed and used in studies such as nanoparticle [25]. Until, however, it is limited to apply them on various cell types same as other techniques such as DNA or RNA transfection [13]. It has been suspected that CPP mediate transfection of protein, and it can be supported from our results. On summary, translocation of CPPs is under the control through the composition of target membrane and through on their chemical characteristics. pEP-1-EGFP transfection is follow the concentration-independent passive mechanism. In conclusion our data provide an asking other CPP for apply to the embryonic stem cells. Our data showed a possible application to protein transfection into the ES cells. For the future studies, modified CPP or mediator based on this study is needed to develop a better construct for translocation of target protein in embryonic stem cell.

Experimental Section

General methods. All used buffer and chemicals were purchased from Aldrich-Sigma, and restriction enzymes (*Bam* HI and *Nde* I) were got from New England Biolab.

Expression and Purification of CPP fusion EGFP. CCP genes were synthesized as 60~70mer oligonucleotide based on the amino acid sequences (Table 1) and got full length sequence using overlap PCR. For getting CCP- EGFP proteins, we used pET15b and pET20b(+) (Merck) and linked to a EGFP construct, and then transformation into *E. coli* DH5 α or BL21 (DE3).

Table 1. Cell permeable protein transduction domains

CPP	Amino acid sequence	Net charge(+)
Buforin 2	TRSSRAGLQFTPVGRVHRLLRK	7
pEP-1	KETWWETWWTEWSQPKKKRKV	6

pET15b has sequences for His-tag in N terminal (depicted as -N) and pET20b in C terminal (depicted as -C) (Fig. 7). DNA sequencing was done in Solgent In. C. (Korea). Recombinant CCP-EGFPs were purified using Ni-NTA agarose resin (Quagen) according to the manual of manufacture. Protein concentration was measured using SDS-PAGE and standard protein.

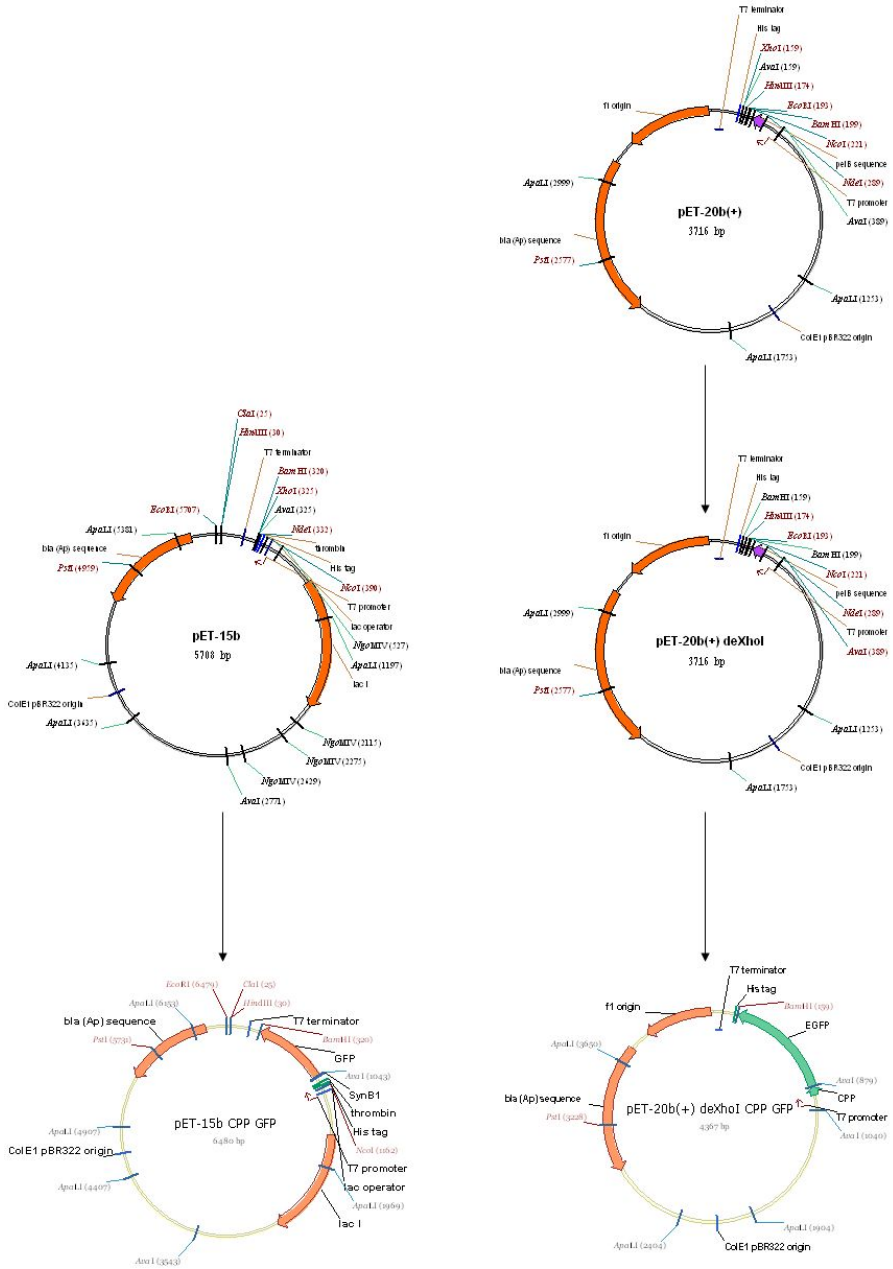

Figure 7. Vector map of constructed. pEP20b (+) was modified to make the pEP20b-de*Xho* I. CPP and EGFP were arranged as depicted in the panel.

ES Cell Culture. Undifferentiated mouse ES cells (mES cells, R1) were maintained as described previously [10, 11]. Briefly, undifferentiated mES cells were grown on gelatin-coated tissue culture plates in the mES medium, Dulbecco's modified eagles medium (DMEM) supplemented with 0.1 mM nonessential amino acids, 0.1 mM β-mercaptoethanol, and 10% fetal calf serum. mES medium contained the 1,000 U/ml leukemia inhibitory factor (LIF; Chemicon, Temecula, CA). The ES cells were passed every 3 or 4 days onto freshly prepared gelatin-coated plates, and fed every day with mES medium.

Import Assay. mES cells were plated on the gelatin-coated slide glass (Nalgene, Rochester, NY) and grown to 2 or 3 days until 70~80% confluency at 37℃ with 5% CO_2 in mES medium supplemented with 10% fetal bovine serum (FBS) and 1000 U/ml LIF. To asses the concentration effects of CPP-EGFP fusion proteins, R1 was treated with CPP-EGFP with 5 μg/ml, 50 μg/ml and 500 μg/ml for 12 hr. To know whether is there time dependent procedure, R1 mouse embryonic stem cells were overlaid with preformed CPP-EGFP fusion proteins (50 μg/ml) in mES medium and the cells were cultured for 5 min, 30 min, 60 min, or 24 hr. Confocal microscopy was performed on unfixed condition after 3 times washing with PBS as described in detail elsewhere [12].

Dye-exclusion Assay

To assay the viability of the CPP-EGFPs, R1 cells were washed with PBS, and incubated with 0.4% trypan blue (Sigma-Aldrich, Stl Louis, MO) for 3 min. The dye was thereafter rinsed off with PBS and observed viability was

analyzed under the inverted microscope (IX 70, Olympus).

Reference

1. Mathur, A.; Martin, J.F. *Lancet.* **2004**, *364*, 183-192.
2. Webber, D.J.; Minger, S. L. *Curr. Opin. Investig. Drugs* **2004**, *5*, 714-719.
3. Matsuoka, H.; Shimoda, S.; Ozaki, M.; Mizukami, H.; Shibusawa, M.;Yamada, Y.; Saito, M. *Biotechnol. Lett.* **2007**, *29*, 341-350.
4. Gropp, M.; Reubinoff, B. *Methods Enzymol*. **2006**, *420*, 64-81.
5. Zaragosi, L.E.; Billon, N.; Ailhaud, G.; Dani, C. *Stem Cells* **2007**, *25*, 790-797.
6. Ishizaka, S.; Shiroi, A.; Kanda, S.; Yoshikawa, M.; Tsujinoue, H.;Kuriyama, S.; Hasuma, T.; Nakatani, K.; Takahashi, K. *FASEB J.* **2002**, *16*, 1444-1446.
7. Kim, S. K.; Hebrok, M. *Genes Dev*. **2001**, *15*, 111-127..
8. Xian, H. Q.; Gottlieb, D. I. *Trends Neurosci*. **2001**, *24*, 685-686.
9. Heng, B. C.; Cao, T.; Haider, H. K.; Wang, D. Z.;Sim, E. K.; Ng, S. C. *Cell Tissue Res*. **2004**, *315*, 291-303.
10. Lee, S. H.; Lumelsky, N.; Studer, L.; Auerbvach, J. M.; McKay, R. D. *Nat. Biotechnol*. **2000**, *18*, 675-679.
11. Schoonjans, L.; Kreemers, V.; Danloy, S.; Moreadith, R. W.; Laroche, Y.; Collen, D. *Stem Cells* **2006**, *21*, 90-97.
12. Lundberg, M.; Wikstrom, S.; Johansson, M. Mol. Ther. **2003**, 8,143-150.
13. Kutsuzawa, K.; Chowdhury, E. H.; Nagaoka, M.; Maruyama, K.; Akiyama, Y.; Akaike, T. *Biochem. Biophys. Res. Commun.* **2006**, *350*,

514-520.

14. Chou, T. H.; Biswas, S.; Lu, S. *Methods Mol. Biol.* **2004**, *245*, 147-166.
15. Dunbar, C. E.; Emmons, R. V. *Stem Cells* **1994**, *12*, 563-576.
16. Haupt, S.; Edenhofer, F.; Peitz, M.; Leinhaas, A.; Brustle, O. *Stem Cells* **2007**, *25*, 181-188.
17. Rousselle, C.; Clair, P.; Smirnova, M.; Kolesnikov, Y.; Pasternak, G. W.;Gac-Breton, S.; Rees, A. R.; Scherrmann, J. M.; Temsamani, J. *J. Pharmacol. Exp. Ther.* **2003**, *306*, 371-376.
18. Kwon, Y.D.; Oh, S. K.; Kim, H. S.; Ku, S. Y.;Kim, S. H.; Choi, Y. M.; Moon, S. Y. *Mol. Ther.* **2005**, *12*, 28-32.
19. Noguchi, H.; Kaneto, H.; Weir, G. C.; Bonner-Weir, S. *Diabetes* **2003**, *52*, 1732-1737.
20. Vives, E.; Brodin, P.; Lebleu, B. *J. Biol. Chem*. **1997**, *272*, 16010-16017.
21. Holm, T.; Hohansson, H.; Lundberg, P.; Pooga, M.; Lindgren, M.; Langel, U. *Nat. Protoc.* **2006**, *1*, 1001-1005.
22. Falnes, P. O.; Wesche, J.; Olsnes, S. *Biochemistry (Moscow)* **2001**, *40*, 4349-4358.
23. Takeshima, K.; Chikushi, A.; Lee, K. K.; Yonehara, S.; Matsuzaki, K. *J Biol. Chem*. **2003**, *278*, 1310-1315.
24. Morris, J. B. *Fundam. Appl. Toxicol*. **1997**, *35*, 91-100.
25. Tran, D. N.; Ota, L. C.; Jacobson, J. D.;Patton, W. C.; Chang, P. J. *Fertil. Steril.* **2007**, *87*, 965-970.

Chapter 2. Appendix

BMC Biotechnology

BioMed Central

Research article

Open Access

Transduction of the MPG-tagged fusion protein into mammalian cells and oocytes depends on amiloride-sensitive endocytic pathway

So-Jung Kwon[1], Kyuyong Han[1], Suhyun Jung[2], Jong-Eun Lee[1], Seongsoon Park[2], Yong-Pil Cheon[3] and Hyunjung Jade Lim*[1]

Address: [1]Department of Biomedical Science & Technology IBST Konkuk University 1 Hwayang-dong, Kwangjin-gu, Seoul 143-701, Korea, [2]Department of Chemistry, Center for NanoBio Applied Technology, Institute of Basic Sciences, Sungshin Women's University, Seoul 136-742, Korea and [3]School of Biological Sciences and Chemistry, Sungshin Women's University 136-742 Korea

Email: So-Jung Kwon - ksjpo47@hanmail.net; Kyuyong Han - hankyuyong@gmail.com; Suhyun Jung - sswu98@hanmail.net; Jong-Eun Lee - eunjongyi@hanmail.net; Seongsoon Park - spark@sungshin.ac.kr; Yong-Pil Cheon - ypcheon@sungshin.ac.kr; Hyunjung Jade Lim* - hlim@konkuk.ac.kr

* Corresponding author

Published: 26 August 2009

BMC Biotechnology 2009, **9**:73 doi:10.1186/1472-6750-9-73

Received: 14 May 2009
Accepted: 26 August 2009

This article is available from: http://www.biomedcentral.com/1472-6750/9/73

Abstract

Background: MPG is a cell-permeable peptide with proven efficiency to deliver macromolecular cargoes into cells. In this work, we examined the efficacy of MPG as an N-terminal tag in a fusion protein to deliver a protein cargo and its mechanism of transduction.

Results: We examined transduction of MPG-EGFP fusion protein by live imaging, flow cytometry, along with combination of cell biological and pharmacological methods. We show that MPG-EGFP fusion proteins efficiently enter various mammalian cells within a few minutes and are co-localized with FM4-64, a general marker of endosomes. The transduction of MPG-EGFP occurs rapidly and is inhibited at a low temperature. The entry of MPG-EGFP is inhibited by amiloride, but cytochalasin D and methyl-β-cyclodextrin did not inhibit the entry, suggesting that macropinocytosis is not involved in the transduction. Overexpression of a mutant form of dynamin partially reduced the transduction of MPG-EGFP. The partial blockade of MPG-EGFP transduction by a dynamin mutant is abolished by the treatment of amiloride. MPG-EGFP transduction is also observed in the mammalian oocytes.

Conclusion: The results show that the transduction of MPG fusion protein utilizes endocytic pathway(s) which is amiloride-sensitive and partially dynamin-dependent. Collectively, the MPG fusion protein could be further developed as a novel tool of "protein therapeutics", with potentials to be used in various cell systems including mammalian oocytes.

Background

Cell-permeable or cell-penetrating peptides (CPPs) are considered a promising method to deliver macromolecular cargoes into live cells across lipid bilayers. These peptides commonly bear stretches of basic amino acids. Many CPPs have been shown to deliver oligonucleotides or siRNA efficiently across cell membrane with or without covalent conjugation [1]. As for the delivery of proteins, expression and purification of CPP-fusion protein in a single step produces more stable form of cargo for in vitro and in vivo uses. The Protein Transduction Domain (PTD) from TAT protein of the human immunodeficiency

virus (HIV), is known to deliver large proteins up to ~120 kDa into cells in the form of fusion protein [2,3]. Thus, it has been in the forefront of protein delivery and is being widely used to deliver various proteins for functional experiments [4]. Other CPPs have been tested for their efficiency for protein delivery by cross-linking, by simple mixing, or as a fusion protein form [5-7].

While the list of applicable CPPs is expanding, recent works have been focused on identifying the mechanisms of cellular uptake of CPPs. These studies generally utilize arrays of endocytosis inhibitors to identify specific endocytic pathway involved in the uptake [8-11]. These works provided evidence that the uptake of TAT PTD, polyarginine, and other peptides is dependent on the lipid rafts-mediated macropinocytosis, "the cell-drinking" process.

MPG is a designed CPP comprised of two independent domains [12]. The first 17 amino acids of the N-terminus is derived from glycine-rich region of the viral gp41 [13] and the hydrophilic C-terminus from nuclear localization signal (NLS) of the SV40 large T antigen [14]. The original MPG peptide is acetylated at the N-terminus and synthesized with a cysteamide group at the C-terminus. This form was used to deliver siRNA or oligonucleotide and the effectiveness was proven in several cell systems [12,15]. A recent report showed that the initial interaction of MPG peptide with the cell surface uses negatively charged glycosaminoglycans. Furthermore, the mechanism of MPG peptide-mediated delivery of nucleic acids seems to involve Rac1-dependent remodeling of actin network within the cell [16]. However, the potential for MPG as a carrier of protein cargoes has not been investigated.

The present investigation was initiated to identify CPPs which can be effectively used for the protein delivery in the form of CPP-fusion proteins. We chose 8 known CPP sequences and prepared CPP-EGFP fusion proteins [5,6,12,17-20]. Our initial screening unveiled the efficient transduction of modified MPG-EGFP fusion proteins into various cell lines and thus we focused on identifying the mechanism of cellular uptake of MPG-EGFP. We report herein that the uptake of MPG-fusion proteins utilizes specific endocytic pathway which is sensitive to amiloride and partially dependent on dynamins.

Results

High transduction efficiency of MPG-EGFP fusion protein in mammalian cells

We initially chose 8 CPPs that have not been used to deliver protein cargoes in the form of fusion proteins (Table 1), and prepared CPP-EGFP fusion proteins. These CPPs, in peptide forms, had all been shown effective in delivering oligonucleotides or nucleic acids into cells when used as a mixture. As N-terminal tags of EGFP recombinant proteins, however, most of these CPPs did not seem to enter cells efficiently (data not shown). Among the tested CPPs, MPG-EGFP entered the cells and exhibited a punctate vesicular pattern of EGFP fluorescence (Figure 1A). Efficient transduction of MPG-EGFP was confirmed in various cell lines, including AN3CA, 293T, NIH3T3, F9, BV2, and HT29. Treatment of MPG-EGFP at 40, 80, or 120 μg/ml for more than 24 hr did not cause any significant cytotoxicity (all above 93% survival rate).

Representative figures are shown in Figure 1A. Intracellular localization of MGP-EGFP was mostly cytoplasmic vesicular patterns reminiscent of endosomal vesicles. Since the fixation of cells reportedly affects the subcellular localization of CPPs [21], we compared the subcellular localization of MPG-EGFP in live and fixed cells. As shown in Figure 1A, no significant redistribution of MPG-EGFP signal in the cells was noted. To examine if MPG-EGFP proteins are present within endosomal vesicles, we stained the MPG-EGFP-treated HeLa cells with a general fluorescence marker of endocytosis FM4-64 [10]. As shown in Figure 1B, most of the MPG-EGFP overlaps with the endosomal staining of FM4-64 (red). Localization of MPG-EGFP in intracellular vesicles was further confirmed by the vesicle fractionation procedure. By using the differential centrifugation, the vesicle fractionation procedure separates the particulate fractions containing most of the subcellular vesicles from the cytosolic supernatant. As shown in Figure 1C, the vesicle fraction of the MPG-EGFP treated cells showed a clear immunoreactive EGFP, confirming the vesicular localization of MPG-EGFP. The immunoreactive EGFP was detected in the cytosolic fraction at a low intensity. The result shows that MPG-EGFP proteins are mainly localized in endosomes. The confocal live imaging clearly demonstrated that MPG-EGFP signals are present within multiple endosomes. These vesicles dynamically move around and a small number of them fuses or disappears during several minutes of observation (see Additional file 1).

In our work, two different MPG sequences were adapted from published works [12] and are shown in Table 1 as MPG1 and MPG2. These MPG sequences do not contain the linker region and thus are modified from the original sequence. The seventh amino acid is tryptophan in MPG1 and phenylalanine in MPG2. This modification of W to F at the seventh position was reported to enhance nuclear localization of the mixed cargo [22]. Both forms, without significant difference, showed effective transduction and exhibited similar cellular distribution and signal intensity (data not shown). Therefore, we used MPG1-EGFP in all the subsequent experiments (indicated as MPG-EGFP thereafter).

Table 1: CPPs tested herein as EGFP fusion forms (reviewed in [1])

CPP	Sequence	Reference
Buforin 2	TRSSRAGLQFTPVGRVHRLLRK	[17]
Transportan	GWTLNSAGYLLGKINLKALAALAKKIL	[5]
Transportan 10	AGYLLGKINLKALAALAKKIL	[18]
MPG1	GALFLGWLGAAGSTMGAPKKKRKV	[12]
MPG2	GALFLGELGAAGSTMGAPKKKRKV	[12]
KALA	WEAKLAKALAKALAKHLAKALAKALKACEA	[19]
Pep-1	KETWWETWWTEWSQPKKKRKV	[6]
SynB1	RGGRLSYSRRRFSTSTGR	[20]

Rapid internalization of MPG-EGFP depends on endocytosis

Internalization of MPG-EGFP occurs within 1 min and the signal gradually intensifies until about 30 min of incubation (Figure 2A). To eliminate the possibility that MPG-EGFP adheres to the cell surface, we washed MPG-EGFP-treated cells with the acid buffer for 30 sec before observing under a fluorescence microscope in all experiments. The acid wash did not significantly reduce the fluorescence signals of MPG-EGFP, suggesting that the observed signal is not an artifact produced by MPG-EGFP adhering to the cell surface.

To address if the entry of MPG fusion protein depends on endocytosis, we examined the entry of MPG-EGFP at 4°C when general endocytosis is blocked. MPG-EGFP was added to BV2 cells or HeLa cells at 40 μg/ml. BV2 cells were co-treated with FM4-64. As shown in Figure 2B, the uptake of MPG-EGFP was significantly reduced in both cell lines at 4°C, showing only a weak surface binding in some cells. FM4-64 staining was also absent at 4°C in BV2 cells, suggesting efficient blockade of endocytosis in our experimental condition. This result suggests that an energy-dependent endocytic pathway is responsible for the transduction of MPG-EGFP. In the next series of experiments, we investigated which pathway of endocytosis is associated with the uptake of the MPG fusion protein.

Effects of endocytosis inhibitors on the entry of MPG-EGFP

Endocytosis occurs in cells using multiple pathways, such as clathrin-mediated, caveolae-mediated, lipid rafts-mediated endocytosis, and macropinocytosis [23]. By using various inhibitors of endocytosis, we determined which endocytic pathway is associated with MPG-EGFP uptake. Cytochalasin D, an inhibitor of actin polymerization, blocks actin-dependent macropinocytosis. Amiloride is a sodium channel blocker and is known to block macropinocytosis [24]. Inhibitors were added to the cells 30 min prior to the addition of MPG-EGFP and were maintained at the same concentrations for the duration of the experiments (Figure 3B). When cytochalasin D was added prior to MPG-EGFP treatment, most of cells became round due to the depolymerization of actin filaments but the distinct vesicular pattern of MPG-EGFP remained unchanged. In contrast, 4 mM amiloride treatment effectively reduced MPG-EGFP uptake as shown in Figure 3A. Methyl-β-cyclodextrin (MβCD) depletes cholesterol from the plasma membrane, and is used as an inhibitor of the caveolae-mediated endocytosis and macropinocytosis [25]. Both of these pathways are known to be dependent on cholesterol-rich lipid rafts. Surprisingly, MβCD treatment significantly increased the fluorescence intensity of MPG-EGFP (Figure 3B). Collectively, these results show that the uptake of MPG-EGFP seems to utilize amiloride-sensitive endocytic pathway, but is not dependent on the organization of actin filaments or cholesterol. These experiments were repeated several times with similar results (Figure 3C).

MPG-EGFP uptake is independent of caveolins but partly dependent on the GTPase activity of dynamins

To examine if caveolin-mediated endocytosis is involved in the transduction of MPG-EGFP, we used the human T lymphocyte Jurkat cells which is known to lack caveolin-1 [26]. EGFP or MPG-EGFP was added to the cells at 40 μg/ml for 1 hr and cells were processed for FACS analysis after the acid wash. As shown in Figure 4A, the transduction efficiency of MPG-EGFP in Jurkat cells was above 60%. Although the overall efficiency of MPG-EGFP transduction in Jurkat cells was not as high as in adherent cells, the successful entry of MPG-EGFP shows that this transduction was not dependent on the caveolin-mediated endocytosis.

Dynamin GTPase is required for several types of endocytosis including clathrin-mediated endocytosis [23]. Transferrin is a marker of dynamin-dependent endocytosis. Thus, we first examined if transferrin is co-localized with MPG-EGFP within cells. As shown in Figure 4B, the vesicles containing MPG-EGFP partially overlapped with those of transferrin-Alex Fluor 546, showing a yellow fluorescence. Amiloride treatment did not seem to affect the endocytosis of transferrin but most of MPG-containing vesicles disappeared by this treatment. Some vesicles with both transferrin and MPG were noted.

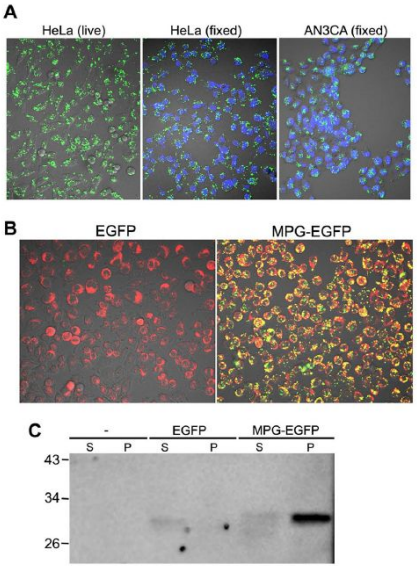

Figure 1
Efficient transduction of the MPG-EGFP fusion protein into various cell lines. A. 40 μg/ml MPG-EGFP was added to AN3CA or HeLa cells. NIH3T3, BV2, 293T, and HT29 were also tested (data not shown). MPG-EGFP exhibits a punctate vesicular pattern in the cytoplasm in cells. Fixation of the cells with 4% PFA (fixed) did not alter the subcellular distribution of MPG-EGFP. Cells were all observed under a confocal microscope. Fixed cells were counterstained with TO-PRO-3 iodide (shown in blue, 1:500). B. MPG-EGFP is mostly present in the endosomes. Cells were stained with 5 μg/ml FM4-64, a general marker of endocytosis (shown in red), and visualized under a confocal microscope without fixation. Overlapping of MPG-EGFP signal and FM4-64 staining generates a yellow fluorescence. C. Vesicle fractionation was performed using HeLa cells treated with EGFP or MPG-EGFP for 1 hr. -, no treatment; EGFP, 40 μg/ml EGFP; MPG-EGFP, 40 μg/ml MPG-EGFP; S, supernatant containing the cytosolic fraction; P, pellet containing the intracellular vesicles. Western blotting was performed with anti-GFP antibody.

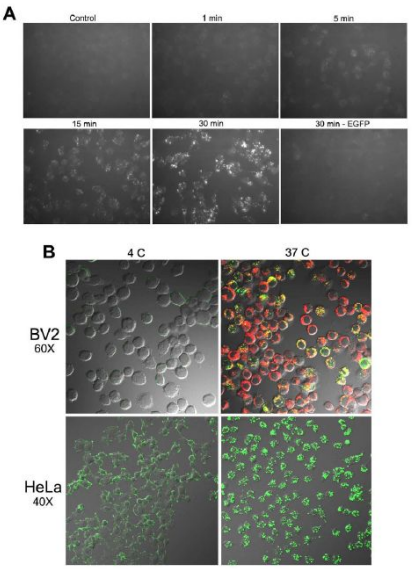

Figure 2
Internalization of MPG-EGFP occurs rapidly and is inhibited at 4°C. A. EGFP or MPG-EGFP was added to HeLa cells at 40 μg/ml and cells were fixed with 4% PFA at indicated times after the acid wash. Fixed cells were visualized under an inverted fluorescence microscope. B. 40 μg/ml MPG-EGFP was added to BV2 or HeLa cells in 2-well slide chambers for 30 min, with (BV2) or without (HeLa) 5 μg/ml FM4-64. To maintain 4°C, cells and all reagents were precooled for 20 min on ice. Cells were fixed with 4% PFA for 20 min, mounted, and visualized under a confocal microscope.

The observation suggests that dynamins may be partly involved in the transduction of MPG-EGFP. Thus, we tested this hypothesis by using the dominant-negative form of dynamin-1, Dyn^{K44A}. Dyn^{K44A}, a dominant-negative form blocking the GTPase activity of dynamin I, has been widely used to elucidate the involvement of these proteins in endocytosis [10,27,28]. This form is capable of blocking the GTPase activity of both dynamin-1 and dynamin-2 [29]. Dynamin-1 is a neuron-specific form, while dynamin-2 is ubiquitously expressed [30,31]. We overexpressed Dyn^{K44A} in HeLa cells and added 40 μg/ml MPG-EGFP and 50 μg/ml transferrin (Figure 5A). Expression of Dyn^{K44A} was detected by an antibody specific to dynamin-1 [28]. As shown in Figure 5A, overexpression of Dyn^{K44A} in HeLa cells blocks the entry of transferrin effectively. While MPG-EGFP entry is shown in Dyn^{K44A}-expressing HeLa cells, the number of vesicular structures in these cells was notably reduced (arrowheads). Furthermore, amiloride treatment in Dyn^{K44A}-expressing HeLa cells almost completely abolished MGP-EGFP uptake,

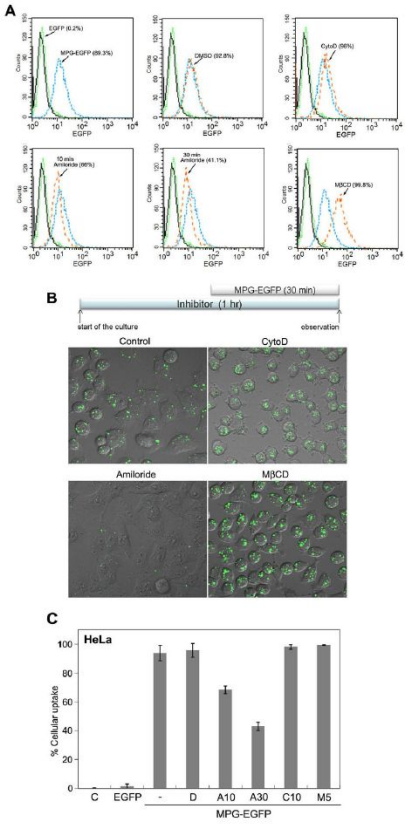

Figure 3

Transduction of MPG-EGFP is dependent on an amiloride-sensitive endocytic pathway. A. Flow cytometric analysis of the MPG-EGFP uptake in the presence of various endocytosis inhibitors. The following concentrations were used: 10 μM cytochalasin D, 4 mM amiloride, and 5 mM MβCD. An inhibitor or DMSO (vehicle, 0.2%) was added to HeLa cells 30 min prior to the addition of MPG-EGFP, except for amiloride, which was added 10 min or 30 min prior to the addition of MPG-EGFP. MPG-EGFP at 40 μg/ml was treated to cells for 30 min in the presence of an inhibitor (see the diagram in B.). All cells were washed with the acid buffer before the analysis. Note the decreased MPG-EGFP signal in the amiloride-treated cells. MβCD treatment increased the intensity of EGFP signal significantly. These experiments were repeated at least three times with similar results and one representative set of data is shown. B. Confocal live images of HeLa cells treated with an endocytosis inhibitor as indicated. Photomicrographs were taken at 40X and zoomed in 2X. C. A barogram showing the averaged transduction efficiencies in the presence of various inhibitors. Errors bars represent the standard deviations. C, no protein added; EGFP, 40 μg/ml EGFP protein; MPG-EGFP, 40 μg/ml MPG-EGFP; -, no drug added; D, 0.2% DMSO (vehicle); A10, 4 mM amiloride for 10 min; A30, 4 mM amiloride for 30 min; C10, 10 μM cytochalasin D; M5, 5 mM MβCD.

suggesting that the transduction of the MPG fusion protein utilizes unique pathway(s) which is amiloride-sensitive and dynamin-dependent.

Blockade of a lysosomal pathway intensifies the accumulation of MPG-EGFP in endosomes

Chloroquine is an inhibitor which blocks the lysosomal pathway of protein degradation [32]. We co-treated chloroquine and MPG-EGFP to HeLa cells for 17 hr to examine if the blockade of the endolysosomal pathway leads to the accumulation of the transduced MPG fusion protein. As shown in Figure 6A, chloroquine-treated cells show enlarged endosomes containing MPG-EGFP. Number of MPG-EGFP-containing vesicles seems to have increased as well. This observation was further explored by the vesicle fractionation experiment. Prolonged treatment of MPG-EGFP showed a lower band representing degradation products. Chloroquine treatment increased the intensity of MPG-EGFP band in the particulate fraction and, notably, the supernatant fraction in 100 μM chloroquine-treated cells contains a much higher level of MPG-EGFP than that in control cells. Collectively, the result shows that the blockade of the lysosomal pathway would increase the transduction efficiency and also lead to the increased release of MPG fusion proteins into the cytosol from the endosomes.

Uptake of MPG-EGFP in mouse eggs

CPP is an excellent tool for a short-term regulation of protein expression. As we showed herein, MPG fusion protein may be a useful tool to deliver proteins to achieve short-term regulation of protein expression. We tested if MPG fusion protein can be used in mammalian eggs for this purpose. So far, the transduction efficiency of any CPP-fusion protein has not been tested in mammalian oocytes. We obtained mouse eggs by the ovary puncture and removed zona pellucidae with the acid Tyrode solution (pH 2). Denuded eggs were treated with control EGFP or MPG-EGFP recombinant protein at 40 μg/ml. As shown in Figure 7, the treatment of EGFP did not give any fluorescence signal, while MPG-EGFP-treated eggs showed strong signal around the ooplasmic periphery. As in the cultured mammalian cells, 4 mM amiloride treatment disturbed the uptake of MPG-EGFP, suggesting that similar endocytic pathway is operative in the mouse egg. Whether MPG fusion protein can be used to deliver proteins to eggs without adverse effects requires further investigation.

Discussion

In a peptide form, MPG is highly effective in delivering oligonucleotides, plasmid DNA, siRNAs, and peptides via a non-covalent complex formation [12,15,33]. Unlike other CPPs, the uptake of MPG-nucleic acid complex was not inhibited by the treatment of cytochalasin B [34], and this result suggests that the transduction of MPG peptide is independent of macropinocytosis. CPP tag at the N-terminal of a full-length protein would pose an entirely different conformation in the solution. Thus, we aimed to investigate if a similar or distinct cellular pathway of transduction is used for the uptake of the MPG-fusion protein. The macropinocytosis is an actin-dependent endocytic pathway which takes up solutes and fluid by the membrane ruffling and fusion [23]. Several arginine-rich CPPs, such as HIV TAT, Antp, Rev, and VP22 are shown to be dependent on the lipid rafts-mediated macropinocytosis, as their uptake is inhibited by cytochalasin D, MβCD, and amiloride [9,10,35]. TAT-CRE, in a fusion protein form, also used a similar endocytic pathway, and the release of this fusion protein from macropinosomes can be improved by the addition of TAT peptides conjugated with the influenza virus hemagglutinin fusogenic motif [10].

We found that, unlike TAT-fusion protein and arginine-rich CPPs, MPG-EGFP is likely to use a specific endosomal pathway which is sensitive only to amiloride among other endocytosis inhibitors we used. Since the uptake of MPG-EGFP is resistant to actin depolymerization, the macropinocytosis is ruled out. Likewise, caveolae and cholesterol both are not required for the transduction of MPG-EGFP, suggesting that lipid rafts are not associated with the uptake. Notably, the overexpression of the mutant form of dynamin could partially reduce MPG-EGFP uptake in HeLa cells, suggesting that the GTPase activity of dynamins may be involved in the transduction. A recent report showed that the transduction of VP22-EGFP fusion protein was similarly dependent on dynamins, but the uptake of VP22-EGFP is sensitive to MβCD and CytoD [36]. Thus, the transduction pathway is seemingly distinct. Collectively, our results indicate that the transduction of MPG-EGFP seems to utilize a less well-characterized endocytic pathway [23] and suggest that the transduction of MPG-EGFP is dependent on more than singular endocytic pathway, as amiloride and dynamin mutant are both able to reduce the transduction efficiency.

One unique feature of MPG-EGFP transduction is that the sequestration of plasma membrane cholesterol increased cytosolic labeling of this fusion protein (Figure 3). As the cholesterol depletion has a negative effect on the transduction of many CPPs including TAT-fusion protein, this observation further supports that MPG-fusion protein utilizes a distinct endocytic pathway. Enhanced labeling of a fluorescence-tagged octaarginine peptide in the presence of MβCD has been reported and it was suggested that the entry of this peptide depends on more fluidic region of the plasma membrane with less cholesterol [11]. Whether this interpretation can be applied to the case of MPG-fusion protein requires further investigation.

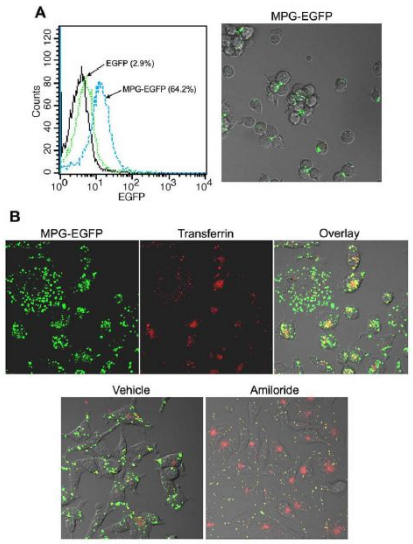

Figure 4
Transduction of MPG-EGFP is independent on caveolae but may share a pathway with transferrin. A. Jurkat cells were treated with 40 μg/ml MPG-EGFP for 1 hr. Cells were processed for flow cytometry after the acid wash. In Jurkat cells which lack caveolae, the transduction of MPG-EGFP still occurs. Confocal live image of MPG-EGFP-treated Jurkat cells is shown at 80X. B. Live confocal images showing partial co-localization of transferrin (red) and MPG-EGFP (green) in HeLa cells, generating a yellow fluorescence. Transferrin was added at 50 μg/ml for 30 min along with 40 μg/ml MPG-EGFP. Pre-treatment of amiloride (4 mM for 30 min) significantly reduced MPG-EGFP transduction while transferrin uptake proceeds.

The mechanisms of endocytosis are diverse and new information is continuously being added. The amiloride-sensitive pathway that MPG-EGFP depends on may be somewhat associated with clathrin- and caveolin-independent endocytosis. However, the mechanisms of this pathway mostly remain unknown [37,38]. One novel CPP, namely C105Y, has been reported to use a clathrin- and caveolin-independent endocytosis [39]. The amiloride-sensitive uptake of MPG-EGFP seems to be reminiscent of what was previously described as one type of the endocytic uptake of Chlamydiae [40]. This intracellular bacterium utilizes multiple endocytic pathways, one pathway being the cytochalasin D-resistant and amiloride-sensitive pathway. This is very similar to what we observed herein with the MPG-fusion protein. No other information regarding this pathway is available to delineate the molecular characteristics. A recent report evaluating the entry of the human papillomavirus type 16 showed that this virus utilizes tetraspanin-enriched microdomains, another example of clathrin- and caveolin-independent endocytosis [41]. More elaborate follow-up to dissect the endocytic pathway of MPG-EGFP could serve as a tool to characterize this pathway.

The GTPase dynamin is involved in multiple forms of endocytosis, including caveolae-mediated, clathrin-mediated, and some clathrin- and caveolae-independent endocytic pathway [23]. Therefore, our result showing a partial reduction of MPG-EGFP transduction after the overexpression of the Dyn^{K44A} mutant cannot pinpoint which pathway is utilized by the transduction of this fusion protein. Since the intracellular localization of MPG-EGFP to some extent overlaps with that of transferrin, clathrin-mediated endocytosis may be involved. However, clear dissection on the role for dynamins in CPP transduction warrants further investigation. As in the case of MPG peptide [16], whether the initial interaction of MPG-fusion protein with the cell surface also utilizes negatively charged glycosaminoglycans needs further work. Likewise, studies on the interaction of MPG-fusion protein with lipid membrane will address if MPG-fusion protein bears a similar affinity towards lipids as MPG peptide [22].

We previously showed that MPG-EGFP is effectively transduced into the human amnion-derived mesenchymal stem cells [42]. This system may also be applicable to the oocyte system as a short-term manipulation of protein expression, as we show herein.

Conclusion

In this work, we show that MPG fusion protein utilizes an endocytic pathway(s) which is amiloride-sensitive and partially dynamin-dependent, which is entirely different from other widely used CPPs. Thus, we suggest that the MPG fusion protein could be further developed as a novel tool of "protein therapeutics", with potentials to be used in various cell systems including mammalian oocytes. Furthermore, the MPG fusion protein system can be used to target and deliver cargos to certain subcellular compartments. And it also may be a useful tool to explore the mechanism of previously uncharacterized type of endocytosis.

Methods

Cell culture

AN_3CA human uterine adenocarcinoma cells, HeLa, 293T, NIH3T3, and BV2 cells were purchased from American Type Culture Collection (Rockville, MD, USA) and

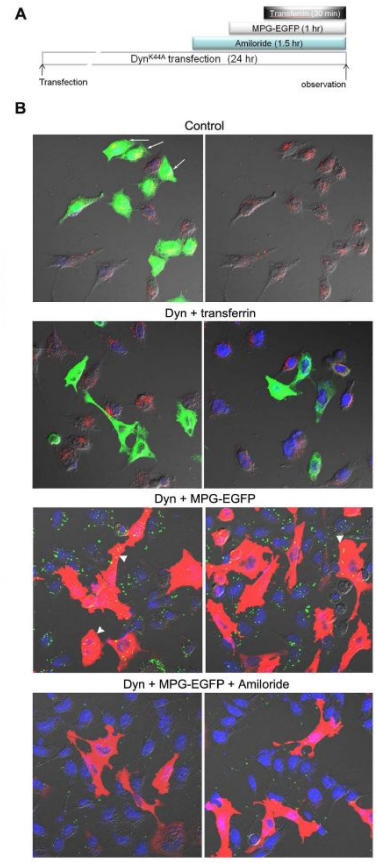

Figure 5
MPG-EGFP uptake partially depends on the GTPase activity of dynamins. A. A diagram depicting the experimental scheme of B. B. A mutant form of dynamin I which lacks the GTPase activity (Dyn^{K44A}, 1 μg) was transfected into HeLa cells and MPG-EGFP was added at 40 μg/ml for 1 hr. Transferrin was added to cells as a marker of dynamin-dependent endocytic pathway. After washing, cells were fixed and subjected to the immunofluorescence staining with anti-dynamin I antibody. Control, control transfection of 1 μg pEGFP-N1 plasmid showing a high efficiency of transfection. Arrows indicate that transfected cells show normal transferrin localization. Dyn + transferrin, transferrin cannot enter Dyn^{K44A}-expressing cells (shown in green), showing efficient blockade of clathrin-mediated endocytosis by overexpression of this mutant form. Dyn + MPG-EGFP, MPG-EGFP was added at 40 μg/ml for 1 hr to Dyn^{K44A}-transfected cells. Note the reduced MPG-EGFP localization (arrowheads) in Dyn^{K44A}-expressing cells (shown in red). Dyn + MPG-EGFP + amiloride, 30 min pre-treatment of amiloride effectively blocked overall MPG-EGFP uptake. Photomicrographs are shown at 80X.

using anti-GFP antibody (Young-In Frontier, Seoul, Korea).

Inhibition of endocytosis

To block general endocytosis at 4°C, cells were plated onto a 2-well slide chamber and precooled on ice for 20 min. All reagents were also precooled on ice. MPG-EGFP at 40 μg/ml was added to the cells and incubated for 30 min on ice. After 30 min, cells were briefly fixed with 4% PFA in PBS and slides were mounted using Profade Gold antifade reagent (Invitrogen) to be visualized under an inverted microscope. Chloroquine, cytochalasin D, amiloride, and methyl-β-cyclodextrin were purchased from Sigma-Aldrich (St. Louis, MO, USA) and used at indicated concentrations.

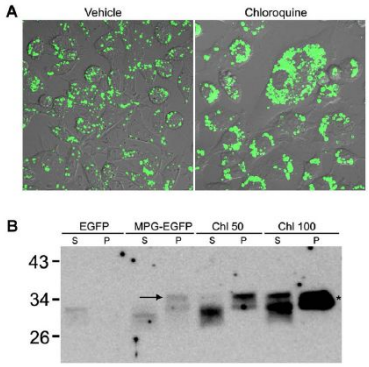

Figure 6
Chloroquine effectively blocks the endolysosomal pathway of transduced MPG-EGFP. A. 100 μM chloroquine was added along with 40 μg/ml MPG-EGFP for 17 hr. Note the increased intensity of MPG-EGFP signal and enlarged vesicle. Confocal live images are shown at 80X. B. Vesicle fractionation was performed using HeLa cells treated with MPG-EGFP and chloroquine for 17 hr. Note that the vesicular uptake of MPG-EGFP intensified in the presence of chloroquine, and that the cytosolic fraction also contains a significant amount of MPG-EGFP. EGFP, 40 μg/ml EGFP; MPG-EGFP, 40 μg/ml MPG-EGFP; Chl 50, MPG-EGFP plus 50 μM chloroquine; Chl 100, MPG-EGFP plus 100 μM chloroquine; S, supernatant containing the cytosolic fraction; P, pellet containing the intracellular vesicles. The asterisk indicates that the band is a merged doublet due to the prolonged exposure, and the arrow points the expected size of MPG-EGFP. Western blotting was performed with anti-GFP antibody.

Flow Cytometric Analysis

MPG-EGFP-treated cells were washed with HBSS and the acid wash buffer, and then trypsinized with 0.01% trypsin-EDTA solution for 10 min. Cells were resuspended in DMEM supplemented with 10% FBS, and washed with PBS containing 3% FBS. After washing, cells were analyzed on FACSCalibur flow cytometer (BD Biosciences, Franklin Lakes, NJ, USA) equipped with Cell Quest Pro software (BD Biosciences).

Transfection of Dynamin^{K44A}

For transfection of dynamin-1 K44A mutant cDNA [27], Fugene HD (Roche, Indianapolis, IN, USA) and 1 μg of plasmid DNA were mixed in the serum-free media at 4:1 ratio and incubated for 15 min at RT. The mixture was added to HeLa cells seeded in 2-well slide chambers. Twenty-four hours later, 40 μg/ml MPG-EGFP was treated to cells for 1 hr and processed for the immunofluorescence staining [42]. Transferrin at 50 μg/ml was added to these cells for 30 min prior to the fixation. Cells were fixed with 4% PFA, nonspecific antiserum binding was blocked with 2% BSA/PBS for 60 min. Cells were incubated for 1 hr with anti-dynamin I mouse monoclonal antibody diluted to 1:100 in 2% BSA/PBS. Following three washes with 2% BSA/PBS, a goat anti-mouse secondary antibody conjugated with Alexa 568 or Alex 488 (Invitrogen, 1:250 in 2% BSA/PBS) was applied for 30 min. Subsequently slides were washed with 2% BSA/PBS and nuclei were

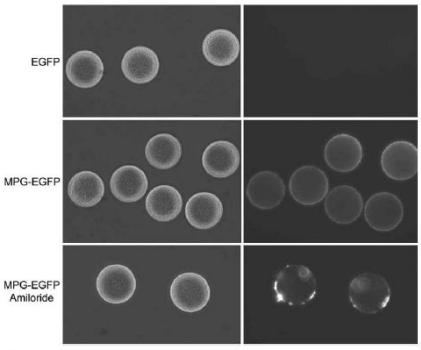

Figure 7
Successful transduction of MPG-EGFP into the mouse oocytes. Mature oocytes were obtained from 4-week mouse ovaries, and zona pellucidae were removed by the acid Tyrode solution. EGFP or MPG-EGFP was added to M16 media for 1 hr. Note the strong peripheral EGFP signal in MPG-EGFP treated oocytes. Amiloride, as in HeLa cells, effectively blocked the transduction of MPG-EGFP.

stained with TO-PRO-3-iodide (Invitrogen, 1:500) for 20 min. After a final wash with PBS, coverslips were mounted using ProLong Gold antifade reagent (Invitrogen). Specimens were examined by using Olympus Fluoview™ FV1000 confocal microscope (Olympus, Japan) and analyzed using the software Fluoview version 1.5, a platform associated with the confocal microscope. The primary antibody used is specific for the neuron-specific dynamin-1 (BD Biosciences, San Jose, CA, USA) as the epitope at the C-terminal region is variable in Dynamin-2 [30].

Confocal laser scanning microscopy

Cells were split and seeded on the poly-*L*-lysine coated cover slips placed in a 6-well plate a day before the experiment. Cells were treated with CPP-EGFP or EGFP for one hour and intracellular localization of EGFP was observed as follows. Cells were washed twice with PBS and fixed for 10 min in 4% PFA in PBS. Cells were washed with PBS three times, counterstained with TO-PRO-3-iodide in PBS (1:500, Invitrogen) for 20 min, and rinsed three times in PBS. Coverslips were mounted onto sections with ProLong Gold mounting media (Invitrogen) and sealed with nail polish. Images were obtained using the Olympus Fluoview™ FV1000 confocal microscope. For live imaging, unfixed cells on a glass-bottom plate were placed onto a warm plate and images were obtained for 10–20 min at 20 sec interval.

Oocyte handling

Five-week old virgin CD-1 female mice were purchased from Orient-Bio (Gyunggi-do, Korea). Mice were maintained in accordance with the policies of the Institutional Animal Care and Use Committee in Konkuk University. Female mice were injected i.p. with 5 I.U. pregnant mare's serum gonadotropin (PMSG) (Sigma) to stimulate the growth of preovulatory follicles. Forty-eight hrs later, ovaries were taken from these mice and were punctured with fine forceps to release fully grown oocytes. Cumulus cells were removed by repeated pipetting and zona pellucidae were digested with the acid Tyrode solution [45]. Purified EGFP or MPG-EGFP in M16 media was added to the denuded oocytes at the indicated concentration and EGFP signal was visualized under an inverted fluorescence microscope.

Authors' contributions

SJK, KH, SJ, and JEL performed experiments and interpreted data. SJK organized experiments and prepared figures. SP and YPC participated in research design and manuscript writing. HJL supervised the overall experiments and wrote the manuscript. All authors read and approved the final manuscript.

Additional material

Additional file 1

Live images of HeLa cells treated with 40 g/ml MPG-EGFP and 5 g/ml FM4-64. *Cells on a glass-bottom plate were placed onto a warm plate and images were obtained for 50 min at 20 sec interval. Images were obtained using the Olympus Fluoview™ FV1000 confocal microscope.*
Click here for file
[http://www.biomedcentral.com/content/supplementary/1472-6750-9-73-S1.avi]

Acknowledgements

This work was supported by the Korean Science and Engineering Foundation (KOSEF) grants funded by the Korean Government (MOST) (No. R01-2006-000-10501-0 and No. 2009-A002-0012). We thank Dr. S. J. Lee and Ms. E. J. Bae for helpful discussions.

References

1. Jarver P, Langel U: **The use of cell-penetrating peptides as a tool for gene regulation.** *Drug Discov Today* 2004, **9:**395-402.
2. Schwarze SR, Ho A, Vocero-Akbani A, Dowdy SF: **In vivo protein transduction: delivery of a biologically active protein into the mouse.** *Science* 1999, **285:**1569-1572.
3. Wadia JS, Dowdy SF: **Modulation of cellular function by TAT mediated transduction of full length proteins.** *Curr Protein Pept Sci* 2003, **4:**97-104.
4. Wadia JS, Dowdy SF: **Protein transduction technology.** *Curr Opin Biotechnol* 2002, **13:**52-56.
5. Pooga M, Hallbrink M, Zorko M, Langel U: **Cell penetration by transportan.** *FASEB J* 1998, **12:**67-77.
6. Morris MC, Depollier J, Mery J, Heitz F, Divita G: **A peptide carrier for the delivery of biologically active proteins into mammalian cells.** *Nat Biotechnol* 2001, **19:**1173-1176.
7. Peitz M, Pfannkuche K, Rajewsky K, Edenhofer F: **Ability of the hydrophobic FGF and basic TAT peptides to promote cellular uptake of recombinant Cre recombinase: a tool for efficient genetic engineering of mammalian genomes.** *Proc Natl Acad Sci USA* 2002, **99:**4489-4494.
8. Fittipaldi A, Ferrari A, Zoppe M, Arcangeli C, Pellegrini V, Beltram F, Giacca M: **Cell membrane lipid rafts mediate caveolar endocytosis of HIV-1 Tat fusion proteins.** *J Biol Chem* 2003, **278:**34141-34149.
9. Nakase I, Niwa M, Takeuchi T, Sonomura K, Kawabata N, Koike Y, Takehashi M, Tanaka S, Ueda K, Simpson JC, *et al.*: **Cellular uptake of arginine-rich peptides: roles for macropinocytosis and actin rearrangement.** *Mol Ther* 2004, **10:**1011-1022.
10. Wadia JS, Stan RV, Dowdy SF: **Transducible TAT-HA fusogenic peptide enhances escape of TAT-fusion proteins after lipid raft macropinocytosis.** *Nat Med* 2004, **10:**310-315.
11. Fretz MM, Penning NA, Al-Taei S, Futaki S, Takeuchi T, Nakase I, Storm G, Jones AT: **Temperature-, concentration- and cholesterol-dependent translocation of L- and D-octa-arginine across the plasma and nuclear membrane of CD34+ leukaemia cells.** *Biochem J* 2007, **403:**335-342.
12. Morris MC, Vidal P, Chaloin L, Heitz F, Divita G: **A new peptide vector for efficient delivery of oligonucleotides into mammalian cells.** *Nucleic Acids Res* 1997, **25:**2730-2736.
13. Freed EO, Myers DJ, Risser R: **Characterization of the fusion domain of the human immunodeficiency virus type 1 envelope glycoprotein gp41.** *Proc Natl Acad Sci USA* 1990, **87:**4650-4654.
14. Kalderon D, Richardson WD, Markham AF, Smith AE: **Sequence requirements for nuclear location of simian virus 40 large-T antigen.** *Nature* 1984, **311:**33-38.

15. Morris MC, Chaloin L, Mery J, Heitz F, Divita G: **A novel potent strategy for gene delivery using a single peptide vector as a carrier.** *Nucleic Acids Res* 1999, **27:**3510-3517.
16. Gerbal-Chaloin S, Gondeau C, drian-Herrada G, Heitz F, Gauthier-Rouviere C, Divita G: **First step of the cell-penetrating peptide mechanism involves Rac1 GTPase-dependent actin-network remodelling.** *Biol Cell* 2007, **99:**223-238.
17. Takeshima K, Chikushi A, Lee KK, Yonehara S, Matsuzaki K: **Translocation of analogues of the antimicrobial peptides magainin and buforin across human cell membranes.** *J Biol Chem* 2003, **278:**1310-1315.
18. Soomets U, Lindgren M, Gallet X, Hallbrink M, Elmquist A, Balaspiri L, Zorko M, Pooga M, Brasseur R, Langel U: **Deletion analogues of transportan.** *Biochim Biophys Acta* 2000, **1467:**165-176.
19. Wyman TB, Nicol F, Zelphati O, Scaria PV, Plank C, Szoka FC Jr: **Design, synthesis, and characterization of a cationic peptide that binds to nucleic acids and permeabilizes bilayers.** *Biochemistry* 1997, **36:**3008-3017.
20. Rousselle C, Clair P, Lefauconnier JM, Kaczorek M, Scherrmann JM, Temsamani J: **New advances in the transport of doxorubicin through the blood-brain barrier by a peptide vector-mediated strategy.** *Mol Pharmacol* 2000, **57:**679-686.
21. Richard JP, Melikov K, Vives E, Ramos C, Verbeure B, Gait MJ, Chernomordik LV, Lebleu B: **Cell-penetrating peptides. A reevaluation of the mechanism of cellular uptake.** *J Biol Chem* 2003, **278:**585-590.
22. Deshayes S, Morris MC, Divita G, Heitz F: **Interactions of amphipathic CPPs with model membranes.** *Biochim Biophys Acta* 2006, **1758:**328-335.
23. Conner SD, Schmid SL: **Regulated portals of entry into the cell.** *Nature* 2003, **422:**37-44.
24. West MA, Bretscher MS, Watts C: **Distinct endocytotic pathways in epidermal growth factor-stimulated human carcinoma A431 cells.** *J Cell Biol* 1989, **109:**2731-2739.
25. Hao M, Mukherjee S, Sun Y, Maxfield FR: **Effects of cholesterol depletion and increased lipid unsaturation on the properties of endocytic membranes.** *J Biol Chem* 2004, **279:**14171-14178.
26. Razani B, Woodman SE, Lisanti MP: **Caveolae: from cell biology to animal physiology.** *Pharmacol Rev* 2002, **54:**431-467.
27. Zhang J, Ferguson SS, Barak LS, Menard L, Caron MG: **Dynamin and beta-arrestin reveal distinct mechanisms for G protein-coupled receptor internalization.** *J Biol Chem* 1996, **271:**18302-18305.
28. Lee HJ, Suk JE, Bae EJ, Lee JH, Paik SR, Lee SJ: **Assembly-dependent endocytosis and clearance of extracellular alpha-synuclein.** *Int J Biochem Cell Biol* 2008, **40:**1835-1849.
29. Damke H, Baba T, Warnock DE, Schmid SL: **Induction of mutant dynamin specifically blocks endocytic coated vesicle formation.** *J Cell Biol* 1994, **127:**915-934.
30. Sontag JM, Fykse EM, Ushkaryov Y, Liu JP, Robinson PJ, Sudhof TC: **Differential expression and regulation of multiple dynamins.** *J Biol Chem* 1994, **269:**4547-4554.
31. Urrutia R, Henley JR, Cook T, McNiven MA: **The dynamins: redundant or distinct functions for an expanding family of related GTPases?** *Proc Natl Acad Sci USA* 1997, **94:**377-384.
32. Seglen PO, Grinde B, Solheim AE: **Inhibition of the lysosomal pathway of protein degradation in isolated rat hepatocytes by ammonia, methylamine, chloroquine and leupeptin.** *Eur J Biochem* 1979, **95:**215-225.
33. Morris MC, Robert-Hebmann V, Chaloin L, Mery J, Heitz F, Devaux C, Goody RS, Divita G: **A new potent HIV-1 reverse transcriptase inhibitor. A synthetic peptide derived from the interface subunit domains.** *J Biol Chem* 1999, **274:**24941-24946.
34. Simeoni F, Morris MC, Heitz F, Divita G: **Insight into the mechanism of the peptide-based gene delivery system MPG: implications for delivery of siRNA into mammalian cells.** *Nucleic Acids Res* 2003, **31:**2717-2724.
35. Sugita T, Yoshikawa T, Mukai Y, Yamanada N, Imai S, Nagano K, Yoshida Y, Shibata H, Yoshioka Y, Nakagawa S, *et al.*: **Comparative study on transduction and toxicity of protein transduction domains.** *Br J Pharmacol* 2008, **153:**1143-1152.
36. Nishi K, Saigo K: **Cellular internalization of green fluorescent protein fused with herpes simplex virus protein VP22 via a lipid raft-mediated endocytic pathway independent of caveolae and Rho family GTPases but dependent on dynamin and Arf6.** *J Biol Chem* 2007, **282:**27503-27517.
37. Damke H, Baba T, Bliek AM van der, Schmid SL: **Clathrin-independent pinocytosis is induced in cells overexpressing a temperature-sensitive mutant of dynamin.** *J Cell Biol* 1995, **131:**69-80.
38. Lamaze C, Dujeancourt A, Baba T, Lo CG, Benmerah A, utry-Varsat A: **Interleukin 2 receptors and detergent-resistant membrane domains define a clathrin-independent endocytic pathway.** *Mol Cell* 2001, **7:**661-671.
39. Rhee M, Davis P: **Mechanism of uptake of C105Y, a novel cell-penetrating peptide.** *J Biol Chem* 2006, **281:**1233-1240.
40. Reynolds DJ, Pearce JH: **Characterization of the cytochalasin D-resistant (pinocytic) mechanisms of endocytosis utilized by chlamydiae.** *Infect Immun* 1990, **58:**3208-3216.
41. Spoden G, Freitag K, Husmann M, Boller K, Sapp M, Lambert C, Florin L: **Clathrin- and caveolin-independent entry of human papillomavirus type 16 – involvement of tetraspanin-enriched microdomains (TEMs).** *PLoS ONE* 2008, **3:**e3313.
42. Han K, Lee JE, Kwon SJ, Park SY, Shim SH, Kim H, Moon JH, Suh CS, Lim HJ: **Human amnion-derived mesenchymal stem cells are a potential source for uterine stem cell therapy.** *Cell Prolif* 2008, **41:**709-725.
43. Becker-Hapak M, McAllister SS, Dowdy SF: **TAT-mediated protein transduction into mammalian cells.** *Methods* 2001, **24:**247-256.
44. Kameyama S, Horie M, Kikuchi T, Omura T, Tadokoro A, Takeuchi T, Nakase I, Sugiura Y, Futaki S: **Acid wash in determining cellular uptake of Fab/cell-permeating peptide conjugates.** *Biopolymers* 2007, **88:**98-107.
45. Eo J, Han K, Murphy M, Song H, Lim HJ: **Etv5, an ETS transcription factor, is expressed in granulosa and cumulus cells and serves as a transcriptional regulator of the cyclooxygenase-2.** *J Endocrinol* 2008, **198:**281-290.

Chapter 3. Immobilization of recombinant lipase

In this chapter, I investigated immobilization of recombinant lipase. First, I achieved increase of the expression yield of CAL-B (lipase B from *Candida antarctica*). The mutant showed three folds higher expression yield compared to the wild type without change of catalytic activity. Second, the chaperone-conjugated magnetic polystyrene beads were synthesized for refolding *B. cepacia* lipase. The beads showed comparable refolding activity to the soluble chaperone, and retained more than 95% of their refolding activity after ten times recycling. Third, the magnetic nanoparticles and metal-organic frameworks (MOFs) were investigated for covalent-immobilization of lipase. The lipase-conjugated magnetic beads were showed similar hydrolytic activity to the free enzyme. And the immobilized enzyme on MOFs has the higher specific activity compared to the free enzyme in organic solvent.

3.1. Improving the Expression Yield of *Candida antarctica* lipase B in *Escherichia coli* by Mutagenesis*

Abstract: Increasing the expression yield of active *Candida antarctica* lipase B (CAL-B) in *Escherichia coli* was achieved by using a codon-optimized synthetic gene and by mutagenesis to introduce hydrophilic residues on the surface of CAL-B. Five residues (four leucines and one isoleucine) on the surface of CAL-B were selected and changed with aspartate after codon optimization. While the codon optimized synthetic gene of CAL-B did not increase the expression yield, the mutation increased the activity of the enzyme three-fold (3.3 mg/L of culture) compared to the wild type. The mutant enzyme had similar hydrolytic activity toward hydrolysis of *p*-nitrophenyl acetate or *p*-nitrophenyl butyrate and enantioselectivity toward hydrolysis of *rac*-1-phenylethyl acetate compared to the wild-type enzyme.

Introduction

Lipases are industrially and academically important biocatalysts because of their high selectivity, reactivity, and stability [1]. One of the most frequently used lipases is *Candida antarctica* lipase B, which has three

---

Jung, S.; Park, S. "Improving the expression yield of *Candida antarctica* lipase B in *Escherichia coli* by mutagenesis," *Biotechnol. Lett.* **2008**, *30*, 717-722.

disulphide bonds. It has high thermostability, broad substrate-specificity, and high selectivity [2]. Recently it has been cloned and expressed in lower eukaryotes as well as in *E. coli* [3-8]. Although it can be expressed with high yield in yeasts, such as *Pichia pastoris* [4] and *Saccharomyces cerevisiae* [5], expression in *E. coli* is more attractive because of its fast growth and easy handling. Expression of fungal proteins in *E. coli* has potential problems such as glycosylation of proteins and rare codon usages because *E. coli* lacks post-modification machinery and has different codon preferences from those of fungi. The crystal structure of CAL-B shows glycosylation at the Asn74 residue [9] and the sequence of CAL-B gene contains several rare codons that are not normally used in *E. coli.* In addition, hydrophobic proteins, such as lipases, are often expressed poorly in *E. coli* because of the formation of inclusion bodies in the cytoplasm or the translocation being blocked during the secretion of the protein into the periplasm [10].

Functional expression of CAL-B in *E. coli* has been achieved by three groups: Chodorge et al. [6] reported the first functional expression of CAL-B in *E. coli* but did not show the detailed result of the functional expression level; Blank et al. [7] compared expression of CAL-B in *E. coli* and *Aspergillus oryzae* and showed that glycosylation may not be necessary for functional expression; Liu et al. [8] reported that CAL-B can be expressed in *E. coli* and that a cold shock promoter with co-expression of a chaperone provided the highest yield (0.04 mg/l of culture) of the active CAL-B.

In this paper, we describe effects of codon optimized gene and mutagenesis of introducing hydrophilic residues onto the surface of CAL-B

on the yield of functional expression of CAL-B in the *E. coli* periplasm. We show that mutagenesis increased the amount of functional form being produced, although codon-optimized synthetic gene did not provide higher yield of the amount of functional enzyme in the soluble fraction.

Results

Synthesis of a codon-optimized CAL-B gene and expression of the functional CAL-B. The natural CAL-B gene contains several rare codons for *E. coli* such as Arg (AGG and CGA), Leu (CTA), and Pro (CCC). These rare codons often cause low level expression of proteins in *E. coli* because of slow translation, misincorporation of amino acids, and premature translation termination [11]. We designed and synthesized a codon-optimized gene (opt2CAL-B) containing only two or three most frequently used codons in *E. coli* by recursive PCR [12]. The gene was cloned into a periplasmic expression vector (pBAD/gIIIa) containing a 6×His tag at C-terminal. Periplasmic expression may help to form disulfide bonds in the tertiary structure of CAL-B [13] and to reduce proteolysis during cultivation [14]. The culture was incubated at 25 ℃ for 6 h after adding L-arabinose. When incubation was performed at 37 ℃, the amount of CAL-B in the soluble fraction decreased (Fig. 1). Although functional CAL-B was successfully expressed in *E. coli* using a codon-optimized gene, the amount of the purified active CAL-B (about 1 mg/l culture) was similar to that from the natural CAL-B gene.

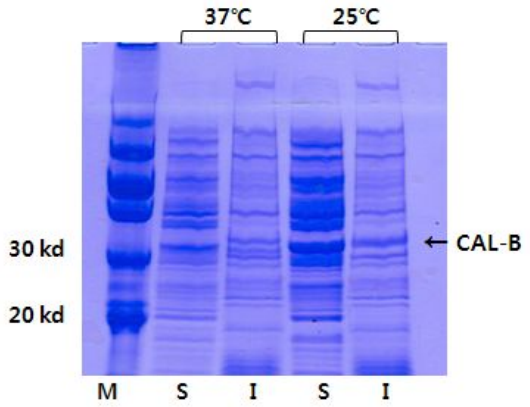

Figure 1. SDS PAGE analysis of recombinant synthetic CAL-B (opt2CAL-B) produced in *E. coli.* at 37 ℃ for 4 h and 25 ℃ for 6 h. SDS-PAGE was performed on a 12% polyacrylamide gel and stained using the Coomassie brilliant blue. M, molecular weight marker; I, insoluble fraction; S, soluble fraction.

Selection of the mutation sites and mutagenesis. The CAL-B enzyme contains many hydrophobic residues, such as leucine, isoleucine, and valine, on its surface. The hydrophobic residues on the surface of CAL-B may increase formation of the inclusion body in the cytoplasm or block translocation during its secretion to the periplasm [10]. Thus, the substitution of the hydrophobic residues with hydrophilic ones may improve solubility of an enzyme and increase the expression yield of the functional enzyme. However, substitution of residues locating near the active site or residues containing side chains oriented toward the interior of the enzyme may cause unwanted influence on the catalytic machinery of the enzyme. However, distant mutation causes less impact on the catalytic machinery of an enzyme [15]. To avoid the unwanted potential influence, we chose the

sites for mutagenesis with the following rules; (1) the residues are hydrophobic (2) the residues are present on the surface (3) the side chains of the residues are oriented toward the outside of CAL-B. Four leucine residues (Leu147, Leu199, Leu219, and Leu261) and one isoleucine (Ile255) were selected (Fig. 2). The side chains of these residues are located at least 17 Å apart from the active center and oriented toward the outside of CAL-B. We chose aspartate for substitution because it is a hydrophilic amino acid and also has similar size to leucine.

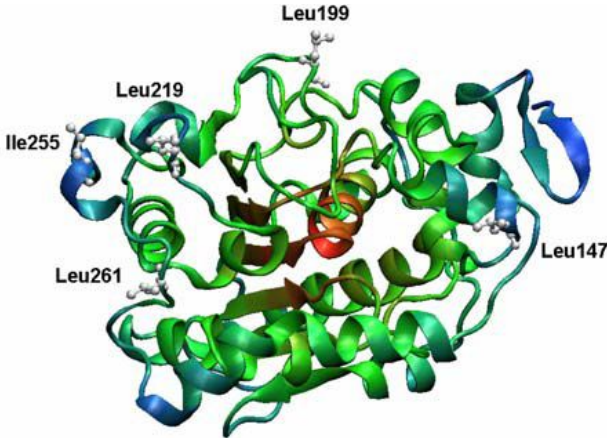

Figure 2. The crystal structure of CAL-B (pdb entry, 1TCA). Four leucine residues and one isoleucine residue (Leu147, Leu199, Leu219, Leu261, and Ile255) for substitution with aspartate were represented by ball-and-stick. The side chains of these residues are located at least 17 Å apart from the active center and oriented toward the outside of CAL-B. The structure was created using PyMOL 0.99 (Delano Scientific, San Carlos, CA).

Expression of the mutant enzyme (5D-CAL-B) and comparison of the expression yield with that of the wild-type enzyme. The mutant enzyme (5D-CAL-B) was expressed same as the wild type enzyme and the yield was determined from the amount of the purified protein. The expression yield of the mutant was higher than that of the wild-type CAL-B. The SDS-PAGE analysis showed stronger band for the mutant enzyme than that for the wild-type enzyme (Fig. 3). The total amount of the active enzyme in the soluble fraction was determined as 0.12 (±0.07) mg for opt2CAL-B (wild-type) and 0.33 (±0.16) mg for 5D-CAL-B (mutant) from 100 ml of culture.

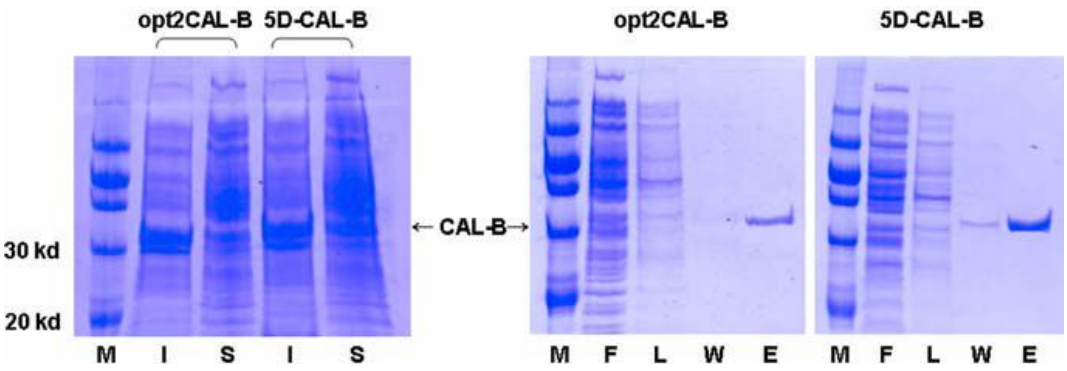

Figure 3. SDS PAGE analysis of recombinant synthetic CAL-B (opt2CAL-B) and the mutant (5D-CAL-B) produced in *E. coli.* SDS-PAGE was performed on a 12% polyacrylamide gel and stained using the Coomassie brilliant blue. The left is unpurified fractions and the right purified ones. M, molecular weight marker; I, insoluble fraction; S, soluble fraction; F, flow-through fraction; L, lysis buffer fraction; W, wash buffer fraction; E, elution buffer fraction (for details see section Materials and methods)

Comparison of the hydrolytic activity and enantioselectivity between the wild-type CAL-B and the mutant enzyme. To determine the effect of the mutation on the catalytic machinery of CAL-B, we compared specific

activity and enantiomeric ratio of the wild-type and mutant enzyme. *p*-Nitrophenyl acetate and *p*-nitrophenyl butyrate were chosen to compare hydrolysis activity (Eq. 1 in Fig. 4). Both enzymes have similar specific activity and specific constant (Table 1). For comparison of enantioselectivity, we measured enantioselectivity toward the hydrolysis of *rac*-1-phenylethyl acetate (Eq. 2 in Fig. 4). The glycosylated CAL-B is highly enantioselective ($E \geq 200$) toward *rac*-1-phenylethanol [16] and the both present enzymes had similar and high enantioselectivity ($E \geq 200$) toward the hydrolysis of *rac*-1-phenylethyl acetate (Table 1).

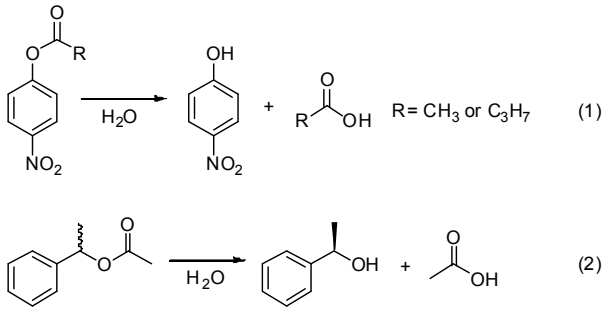

Figure 4. Model reactions to determine hydrolytic activity and selectivity of the mutant and wild-type enzymes.

Table 1. Hydrolytic activity and selectivity of CAL-B and the mutant enzyme[a]

Enzyme	Specific activity for *p*-nitrophenyl acetate (μmol min $^{-1}$ mg^{-1})	Specific activity[b] for p-nitrophenyl acetate (k_{cat}/K_M, s^{-1} M^{-1})	Specific activity for p-nitrophenyl butyrate[c] (μmol min $^{-1}$ mg^{-1})	Enantiomeric ratio (E)[d]
opt2CAL-B (wild type)	1.7 ± 0.46[e]	3.9 (±0.97) ×10^3	5.5 ± 0.34	>200 (*R*)
5D-CAL-B (mutant	1.6 ± 0.29	4.0 (±0.87) ×10^3	5.4 ± 0.25	>200 (*R*)

[a] Reaction condition: see section Materials and methods

[b] Specific constant was obtained from initial rates determined at 0.08-0.8 mM substrate concentrations

[c] The hydrolysis condition is same to the method of Blank *et al.* [7]

[d] Enantiomeric ratio was calculated using the measured enantiomeric excess of the starting material (ee_s) and product (ee_p) at ~40% conversion by the method of Chen *et al.* [22]

[e] Errors are standard deviations for at least three measurements; entries without errors are single measurements

Discussion

There are several potential problems to express fungal proteins in *E. coli* ; (1) glycosylation (2) different codon usages (3) formation of inclusion body. To express CAL-B in *E. coli,* these problems should be solved because CAL-B is also a fungal protein. *E. coli* does not have post-translational machinery for peptide modification such as glycosylation. However, the glycosylation would not be critical for the catalytic machinery of CAL-B because the previous results showed that the deglycosylated CAL-B is still active. To solve the second problem, we have designed a synthetic gene of CAL-B that does not contain any rare codons and used it for expression. However, the amount of active CAL-B from the synthetic gene was similar to that from the natural gene, although the overall amount of proteins expressed from the synthetic gene is higher than that from the natural gene. In the case using the synthetic gene, more amounts of proteins was found in the insoluble fraction. We assumed that introducing hydrophilic amino acids, such as aspartate, onto the surface of CAL-B would increase the protein amount in the soluble fraction by decreasing formation of inclusion bodies during expression. We selected five residues (four leucines and one isoleucine) that are present on the surface of CAL-B and substituted them with aspartate. The substitution decreases the theoretical hydropathicity of CAL-B from -0.016 to -0.127. As we assumed, the substitution resulted in increasing the expression yield of the functional CAL-B by a factor of three. In addition to producing more functional enzyme, it is important to keep the characteristics of CAL-B as a

biocatalyst. To confirm that the mutation does not change the activity and enantioselectivity of CAL-B, we performed the hydrolysis of *p*-nitrophenyl acetate, *p*-nitrophenyl butyrate, and *rac*-1-phenylethyl acetate as model reactions for determining the activity and enantioselectivity. The hydrolysis activity and enantioselectivity of the mutant were similar to those of the wild-type CAL-B. According to the results, it can be concluded that the mutation resulted in producing more functional enzyme without change of the catalytic machinery of CAL-B.

Experimental Section

General Methods. Chemicals, buffers, and lysozyme were purchased from Sigma-Aldrich Korea (Yongin, Korea). *Pfu* DNA polymerase and restriction enzymes (*Nco* I and *Sal* I) were purchased from Enzynomics (Daejeon, Korea). DNA oligomers were obtained from Sigma-Proligo (Singapore). The vector (pBAD/gIIIa) was purchased from Invitrogen Korea (Seoul, Korea). DNA sequencing of the synthetic gene and mutants of CAL-B was performed by Solgent Co. (Daejeon, Korea). The Ni-NTA agarose resin was purchased from QIAGEN Korea Ltd. (Seoul, Korea).

Synthesis of CAL-B gene and cloning the synthetic gene. A codon-optimized sequence for *E. coli* was designed based on the protein sequence of CAL-B (pdb entry, 1TCA) by the Leto backtranslation tool (http://www.entelechon.com/). The optimization was performed by cutting off the codons below 50% theoretical ratio. The optimized CAL-B gene

(opt2-CAL-B) was synthesized using the recursive PCR. Eighteen oligomers were designed to have an overlap of 18–24 nucleotides for the synthesis of the codon optimized gene for CAL-B (Table 2). Gene specific primers (opt2CAL-B_F1_NcoI, 5'-TAGCACCATGGCTCTGCCGTCT-3', and opt2-CAL-B-R1_SalI, 5'-TGATGGTCGACCGGAGTTA CGATG-3') having restriction sites for *Nco* I and *Sal* I were used to introduce these two sites in the gene and to clone the gene into pBAD/gIIIa vector (Invitrogen).

Table 2. Codon-optimized sequences of CAL-B

Sequence 1 (opt1CAL-B)	Sequence 2 (opt2CAL-B)
TTG CCG TCA GGT TCT GAC CCG GCC TTT AGC CAG CCG AAG TCT GTT CTG GAT GCT GGC CTG ACA TGT CAG GGT GCA AGC CCG TCG TCC GTA AGC AAA CCA ATT CTG CTT GTA CCA GGC ACG GGC ACT ACG GGC CCG CAG AGC TTT GAT TCT AAT TGG ATT CCC CTG TCT ACC CAG CTT GGG TAC ACC CCT TGT TGG ATT AGC CCG CCT CCC TTC ATG CTG AAC GAT ACA CAA GTG AAT ACT GAG TAC ATG GTC AAC GCA ATT ACC GCC CTT TAT GCG GGA AGT GGT AAC AAT AAA CTT CCC GTG CTG ACA TGG AGT CAG GGG GGC CTG GTG GCA CAG TGG GGA TTG ACG TTT TTC CCA TCG ATC CGC TCG AAA GTT GAT CGT CTG ATG GCA TTT GCG CCT GAT TAT AAA GGC ACA GTG CTC GCG GGG CCA TTA GAT GCC CTG GCT GTG TCA GCA CCT AGT GTC TGG CAA CAG ACG ACC GGT TCC GCG CTG ACG ACC GCC CTC CGG AAC GCA GGT GGA CTG ACC CAA ATT GTG CCG ACA ACC AAC TTG TAT AGC GCC ACC GAC GAA ATT GTT CAG CCG CAG GTC TCC AAT TCG CCT CTC GAT TCA AGC TAT CTG TTT AAC GGC AAA AAT GTA CAG GCA CAG GCT GTT TGC GGG CCA TTA TTC GTC ATC GAC CAT GCC GGT AGC TTA ACC TCC CAG TTC AGT TAC GTG GTT GGT CGC TCT GCC CTG CGT AGT ACC ACG GGC CAA GCG CGC TCA GCG GAC TAC GGT ATC ACT GAT TGC AAT CCG TTA CCG GCG AAT GAC CTG ACT CCG GAA CAA AAG GTA GCG GCT GCG GCT TTG TTA GCG CCG GCC GCT GCC GCG ATT GTG GCA GGT CCT AAA CAA AAC TGT GAA CCG GAT CTG ATG CCC TAT GCC CGT CCG TTT GCG GTC GGC AAA CGT ACT TGC TCA GGT ATC GTT ACG CCA	CTG CCG TCT GGT TCC GAT CCG GCT TTC TCC CAG CCG AAA TCC GTG CTG GAC GCG GGT CTG ACC TGT CAG GGT GCT TCT CCA AGC AGC GTG TCT AAA CCG ATC CTG CTG GTA CCG GGC ACC GGT ACC ACT GGC CCG CAG TCT TTC GAC AGC AAC TGG ATT CCA CTG TCC ACC CAA CTC GGT TAT ACT CCT TGC TGG ATC TCT CCG CCG CCG TTT ATG CTG AAC GAT ACT CAG GTA AAC ACT GAA TAC ATG GTA AAC GCT ATC ACC GCT CTG TAC GCA GGT TCT GGT AAC AAC AAA CTG CCA GTG CTG ACC TGG TCC CAG GGT GGT CTG GTT GCA CAA TGG GGC CTG ACT TTC TTC CCG TCT ATC CGT TCT AAA GTG GAC CGT CTG ATG GCA TTC GCT CCG GAC TAC AAA GGT ACT GTG CTG GCT GGC CCG CTG GAT GCA CTG GCT GTA TCT GCG CCA TCC GTG TGG CAG CAG ACC ACT GGT TCT GCG CTG ACC ACT GCA CTG CGT AAC GCT GGT GGT CTG ACC CAG ATC GTT CCG ACT ACT AAC CTG TAC AGC GCA ACC GAT GAG ATC GTT CAG CCG CAG GTA TCT AAC TCC CCG CTG GAT TCT TCT TAC CTG TTC AAC GGT AAG AAC GTT CAG GCT CAG GCT GTT TGT GGC CCG CTG TTC GTT ATC GAT CAC GCA GGT TCC CTG ACC TCC CAG TTC AGC TAT GTG GTT GGC CGC TCT GCT CTG CGC TCC ACC ACT GGT CAA GCG CGC TCT GCT GAC TAC GGC ATC ACC GAC TGC AAC CCG CTG CCG GCG AAC GAC TTA ACC CCG GAA CAG AAG GTT GCA GCT GCG GCT CTG CTG GCA CCG GCT GCA GCT GCA ATT GTT GCG GGC CCG AAA CAG AAC TGC GAA CCG GAC CTG ATG CCG TAC GCT CGT CCG TTC GCG GTT GGT AAA CGC ACT TGT TCT GGC ATC GTA ACT CCG

Site directed mutagenesis. Using the synthesized CAL-B (opt2CAL-B) as a template, the mutant gene was created by overlap PCR mutagenesis [17-20] with the mutagenesis primers,

F_Opt2CAL-B_L147D (5′-CC GCTGGATGCAGATGCTGTATCTGCG-3′)
R_Opt 2CAL-B_L147D (5′-CGCAGATACAGCATCTGCA TCCAGCGG-3′)
F_Opt2CAL-B_L199D (5′-GTA TCTAACTCCCCGGATGATTCTTCTTACCTG-3′)
R_Opt2CAL-B_L199D (5′-CAGGTAAGAAGAATC ATCCGGGGAGTTAGATAC-3′)
F_Opt2CAL-B_ L219D (5′-GTTTGTGGCCCGGACTTCGTTATCG AT-3′)
R_Opt2CAL-B_L219D (5′-ATCGATAAC GAAGTCCGGGCCACAAAC-3′)
F_Opt2CAL-B_I255D (5′-GCTGACTACGGCGATACCGACTGCA AC-3′)
R_Opt2CAL-B_I255D (5′-GTTGCAGTC GGTATCGCCGTAGTCAGC-3′)
F_Opt2CAL-B_L261D (5′-GACTGCAACCCGGACCCGGCGAAC GAC-3′)
R_Opt2CAL-B_L261D (5′-GTCGTT CGCCGGGTCCGGGTTGCAGTC-3′)

The mutant gene was digested with *Nco* I and *Sal* I and inserted into pBAD/gIIIa. The plasmid of the mutant was transformed into *E. coli* (Top10).

Expression and purification of CAL-B. Overnight culture (1 ml of *E. coli*) was added to LB medium (100 ml; ampicillin, 100 μg/ml) and incubated at 37℃ and 200 rpm to an OD_{600} of 0.5. Protein expression was induced by adding arabinose (1 ml; 2% w/v) and incubated for 6 h at 25℃ and 200 rpm. When the OD_{600} reached ~1.5, the cells were harvested by centrifugation (10 min, 3,800 g, 4 ℃) and the supernatant was discarded. The cell pellet (~0.8 g) was resuspended in the lysis buffer (5 ml/g wet wt; NaH_2PO_4, 50 mM; NaCl, 300 mM; imidazole, 10 mM; pH 8.0 adjusted with NaOH), and lysozyme was added to 1 mg/ml. Incubation on ice for 45 min was followed by a freeze-thaw cycle at -20 ℃ and room temperature. The viscous lysate was passed several times through a sterile 20-gauge syringe

needle and centrifuged (10 min, 10,000 g, 4 ℃). The supernatant was separated from the cell debris. The cell debris was dissolved in 8 M urea solution (4 ml, containing 1 mM dithiothreitol) for SDS-PAGE analysis. Ni-NTA agarose resin (1 ml, 50% w/v slurry) was added to the supernatant (4 ml) and the mixture was stirred at 25 ℃ for 1 h. The lysate-Ni-NTA mixture was loaded on a Poly-Prep column (Bio-Rad), drained, and then washed three times with the wash buffer (4 ml; NaH_2PO_4, 50 mM; NaCl, 300 mM; imidazole, 20 mM; pH 8.0 adjusted with NaOH). The His_6-CALB enzyme was eluted from the column with four volumes of the elution buffer (0.5 ml; NaH_2PO_4, 50 mM; NaCl, 300 mM; imidazole, 250 mM; pH 8.0 adjusted with NaOH). Eluate (2 ml) from the Ni-NTA column containing the purified CAL-B was exchanged from the elution buffer to BES (5 mM, pH 7.2) using a centrifugal device (Amicon Ultra-15, Millipore).

Determination of the amount of functional enzymes. The functional expression yield was confirmed by measuring the amount of purified enzymes. The amount of purified enzymes was determined by Bio-Rad Protein Assay kit (Bio-Rad) according to the manufacturer's instructions.

Measurement of hydrolytic activity toward hydrolysis of *p*-nitrophenyl acetate of the wild-type CAL-B and the 5D-mutant enzyme. Hydrolytic activity of the enzymes was measured by following the hydrolysis of *p*-nitrophenyl acetate at 404 nm. The assay solution was prepared by mixing *p*-nitrophenyl acetate (20 μl, 200 mM in acetonitrile), acetonitrile (870 μl), and BES buffer (5 mM, pH 7.2, 11,110 μl). The absorbance change

was measured at 404 nm for 5 min after mixing the assay solution (1 ml) with the enzyme solution (50 μl). The final concentrations in the reaction solution were 0.32 mM substrate, 4.65 mM BES, 7% acetonitrile. The activity was calculated according to the method of Janes et al. [20] where $\Delta\varepsilon$ = 17,300 $M^{-1}cm^{-1}$.

Determination of enantioselectivity for hydrolysis of *rac*-1- phenylethyl acetate. The hydrolytic reaction was monitored using a pH-stat. The reaction was started by an addition of the enzyme solution (500 μl, 0.06 mg/ml in 5 mM BES buffer, pH 7.2) to a solution of *rac*-1-phenylethyl acetate (50 μl of 1 M in acetonitrile) and acetonitrile (650 μl) in 1 mM BES buffer (8.9 ml, pH 7.2). The reaction was stopped at around 40% conversion by extraction with ethyl acetate (5 ml). After drying over anhydrous sodium sulfate, the organic layer was analyzed by GC with a chiral capillary column (Cyclosil-B 30 m × 0.25 mm): initial column temperature 80 ℃ for 10 min, ramp up to 120 ℃ at a rate of 2.5 ℃/min, and then held at 120 ℃ for 10 min. Enantioselectivity was determined by enantiomeric ratio (*E*) that was calculated using the method of Chen et al. [22] from the enantiomeric excesses of both the starting ester and the alcohol product.

References

1. Bornscheuer, U.T.; Kazlauskas, R.J. Hydrolases in organic synthesis. 2nd ed.; Wiley-VCH, Weinheim, **1999.**
2. Rotticci, D. Understanding and engineering the enantioselectivity of Candida antarctica lipase B towards secalcohols. Ph.D. Thesis, KTH, Stockholm, Sweden, **2003**.
3. Hoegh, I.; Patkar, S.; Halkier, T.; Hansen, M.T. *Can. J. Bot*. **1995**, *73*, S869-S875.
4. Rotticci-Mulder, J.C.; Gustavsson, M.; Holmquist, M.; Hult, K.; Martinelle, M. *Protein Expr. Purif.* **2001**, *21*, 386-392.
5. Zhang, N.; Suen, W.C.; Windsor, W.; Xiao, L. Madison. V.; Zaks, A. *Protein Eng.* **2003**, *16*, 599-605.
6. Chodorge, M.; Fourage, L.; Ullmann, C.; Duvivier, V.; Masson, J.M.; Lefe`vre, F. *Adv. Synth. Catal*. **2005**, *347*, 1022-1026.
7. Blank, K.; Morfill, J.; Gumpp, H.; Gaub, H.E. *J. Biotechnol*. **2006**, *125,* 474-483.
8. Liu, D.; Schmid, R.D.; Rusnak, M. *Appl. Microbiol. Biotechnol*. **2006**, *72*, 1024-1032.
9. Uppenberg, J.; Hansen, M.T.; Patkar, S.; Jones, T.A. *Structure* **1994**, *2*, 293-308.
10. Quyen, D.T.; Schmidt-Dannert, C.; Schmid, R.D. *Appl. Environ. Microbiol.* **1999**, *65,* 787-794.
11. Kane, J. *Curr. Opinion. Biotechnol.* **1995**, *6*, 494-500.
12. Prodromou, C.; Pearl, L.H. *Protein Eng*. **1992**, *5*, 827-829.

13. Baneyx, F.; Mujacic M. *Nat. Biotechnol*. **2004**, *22*, 1399-1408.
14. Swamy, K.H.; Goldberg, A.L. *J. Bacteriol.* **1982**, *149*, 1027-1033.
15. Park, S.; Morley, K.L.; Horsman, G.P.; Holmquist, M.; Hult, K.; Kazlauskas, R.J. *Chem. Biol.* **2005**, *12*, 45-54.
16. Park, S.; Kazlauskas, R.J. *J. Org. Chem.* **2001**, *66*, 8395-8401.
17. Higuchi, R.; Krummel, B.; Saiki, R.K. *Nucleic Acids Res.* **1988**, *16*, 7351-7367.
18. Ho, S.N.; Hunt, H.D.; Horton, R.M.; Pullen, J.K.; Pease, L.R. *Gene* **1989**, *77,* 51-59.
19. Senanayake, S.D.; Brian, D.A. *Mol. Biotechnol*. **1995**, *4*, 13-15.
20. Urban, A.; Neukirchen, S.; Jaeger, K.E. *Nucleic Acids Res*. **1997**, *25*, 2227-2228.
21. Janes, L.E.; Cimpoia, A.; Kazlauskas, R.J. *J. Org. Chem.* **1999**, *64*, 9019-9029.
22. Chen, C.S.; Fujimoto, Y.; Girdaukas, G.; Sih, C.J. *J. Am. Chem. Soc.* **1982**, *104*, 7294-7299.

3.2. Recyclable Chaperone-Conjugated Magnetic Beads for *in vitro* Refolding of *Burkholderia cepacia* lipase*

Abstract: Polymer-coated magnetic beads have become widely used in biological applications because of their facile recovery and easily modifiable surface. Herein, we report the application of magnetic beads to *in vitro* refolding of *B. cepacia* lipase. Magnetic particles (Fe_3O_4) prepared by co-precipitation of Fe^{2+} and Fe^{3+} ions under basic conditions were subsequently coated with carboxylic acid-containing polystyrene by emulsion polymerization. The polymer-coated magnetic beads were then conjugated with molecular chaperone proteins to assist with refolding. The chaperone-conjugated magnetic beads efficiently refolded *B. cepacia* lipase and were easily reused. The beads showed comparable refolding activity to the soluble chaperone, and retained more than 95% of their refolding activity after ten cycles of refolding *B. cepacia* lipase.

Introduction

Lipases are widely used in academic and industrial research because of their high stability in organic media and high stereo- and regio-selectivity[1]. Overexpression of lipases in *Escherichia coli* (*E. coli*)

Jung, S.; Park, S. "Recyclable chaperone-conjugated magnetic beads for *in vitro* refolding of *Burkholderia cepacia* lipase," *Biotechnol. Lett.* **2009**, *31*, 107-111.

benefits researchers because *E. coli* grows fast and is easy to handle [2, 3]. However, many lipases, including *B. cepacia* lipase (*Burkholderia cepacia* lipase, old name: *Pseudomonas cepacia* lipase), are poorly expressed in *E. coli* and often form inclusion bodies, which need to be refolded *in vitro* by their molecular chaperones [4, 5]. Recently, Quyen *et al.* [6] reported overexpression of *B. cepacia* lipase in *E. coli* and *in vitro* refolding. Surprisingly, a near-stoichiometric amount of a specific molecular chaperone was required to refold *B. cepacia* lipase, despite the fact that chaperones catalyze protein folding [7]. This requires much effort in production of the functional *B. cepacia* lipase because the chaperone must be expressed and then removed after refolding the lipase. Thus, recycling the chaperone may significantly lower the cost of production. For successful chaperone recycling, immobilization on supporting materials may be necessary.

To immobilize chaperones, the choice of supporting material is important because it may strongly affect enzyme function [8, 9]. The supporting material should be stable under refolding conditions and easy to recover from the reaction media. Polymer-coated magnetic beads are excellent candidates because they are stable in an aqueous solution and easily recovered using a magnetic field or simple centrifugation.

In this paper, we report the immobilization of molecular chaperones on polymer-coated magnetic beads and demonstrate their utility in refolding *B. cepacia* lipase. Moreover, the chaperone-conjugated magnetic beads can be reused several times.

Results and Discussion

Synthesis of a BCL gene and expression of the BCL. The genes of *B. cepacia* lipase and its chaperone protein used in this study are similar to those used by Schmid and coworkers [6], sharing 90.9% and 92.4% DNA sequence identity, respectively. Consequently, the *B. cepacia* lipase gene also contains a signal sequence, and the chaperone gene has an initial sequence (210 bp) that encodes seventy hydrophobic amino acids. These sequences have been shown to decrease protein yields in *E. coli* [6], and were therefore removed from each of the lipase and chaperone genes prior to subcloning into the pBADgIIIa vector. Expression of the truncated lipase yielded insoluble inclusion bodies while the truncated chaperone was expressed in the soluble fraction (Fig. 1). The total protein content of the crude inclusion-body solution containing the lipase was 2.6 mg/ml, approximately 60% of which was lipase as estimated by SDS-PAGE (Fig. 1). After being dissolved in a urea solution, the inclusion bodies were used for refolding. The chaperone in the soluble fraction was purified to homogeneity as an N-terminal His_6-tagged fusion protein using NTA-Ni affinity column chromatography by Ni-NTA affinity chromatography to yield 86 mg/l culture (final concentration of 4.3 mg/ml).

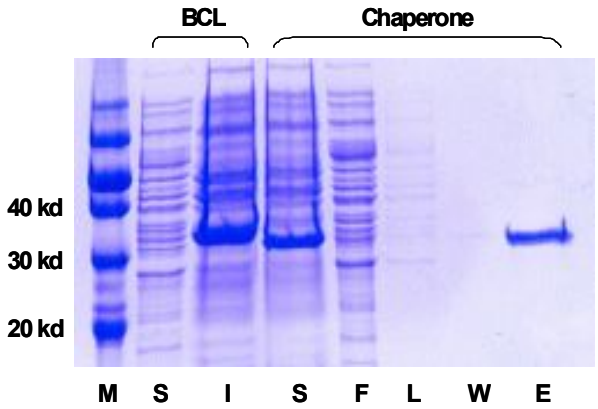

Figure 1. SDS-PAGE analysis of recombinant *B. cepacia* lipase (BCL, M.W. ~38 kDa) and molecular chaperone (M.W. ~ 32 kDa) expressed in *E. coli*. SDS-PAGE was performed on a 12% polyacrylamide gel and stained with Coomassie brilliant blue. Most BCL was present as inclusion bodies while the chaperone was soluble. The chaperone was purified as a His_6-tagged fusion protein using NTA-Ni affinity column chromatography. M, molecular weight marker; I, insoluble fraction; S, soluble fraction; F, flow-through fraction; L, lysis buffer fraction; W, wash buffer fraction; E, elution buffer fraction (for details see the materials and methods section).

Refolding of *B. cepacia* lipase by chaperon-conjugated polymeric beads. In order to test whether the chaperone-conjugated beads can refold the denatured *B. cepacia* lipase, we initially used polymeric beads (LANXESS Korea, Seoul) containing carboxylic acid groups. Carboxylic acid groups in the polymeric beads were activated by EDC and then covalently conjugated to chaperones. The denatured *B. cepacia* lipase was refolded by the chaperone-conjugated polymeric beads with efficiency comparable to that of free chaperone protein, indicating that conjugation to the beads did not affect chaperone activity. However, after five cycles of reuse, the chaperone-conjugated polymeric beads retained only ~60% of their original

refolding activity (Fig. 2), presumably because the polymeric beads are not dense enough to be fully recovered by simple centrifugation. We therefore prepared more dense magnetic beads to increase the recovery yield.

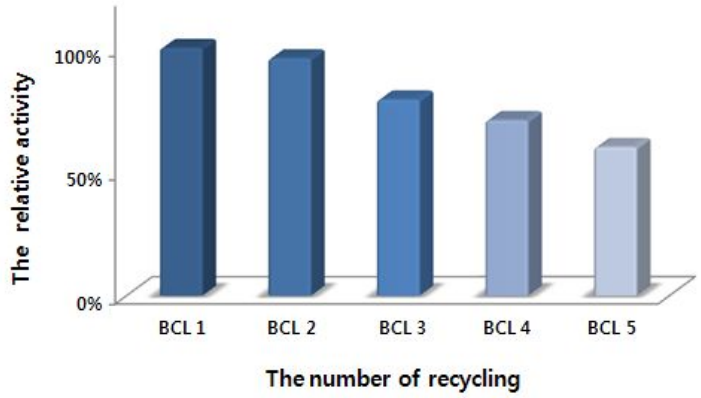

Figure 2. The relative refolding activities of the recycled chaperone-conjugated polymeric beads. The refolding activity was estimated from measurement of the initial reaction rate of the refolded *B. cepacia* lipase toward hydrolysis of *p*-nitrophenylacetate. After five-time reuse, the activity remained above 60%.

Synthesis of polystyrene coated magnetic nanoparticles. Magnetic nanoparticles (Fe_3O_4) prepared from a mixture of Fe^{2+} and Fe^{3+} ions in a basic solution were coated with polystyrene containing acrylic acid. The coating process was achieved by radical-initiated polymerization using styrene and acrylic acid. The average diameter of the prepared beads was estimated to be ~100 nm by scanning electron micrograph (Fig. 3). The chaperones were then conjugated to the polymer-coated magnetic beads in the same manner for polymeric beads.

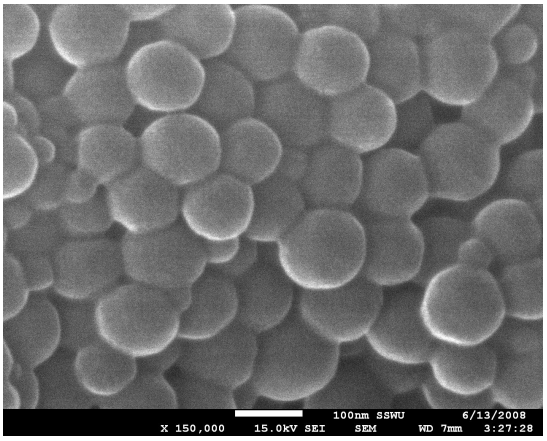

Figure 3. Scanning electron micrographs (SEM) of the polymer-coated magnetic nanobeads. Scale bar = 100 nm.

Refolding *B. cepacia* lipase by chaperon-conjugated magnetic beads and the hydrolytic activity. We refolded the denatured lipase by incubation with the chaperone-conjugated magnetic beads at 4 ºC. The crude inclusion bodies of the lipase were used for refolding experiments. The refolding activity of the beads was estimated from measurement of the initial hydrolysis rate of the refolded lipase toward *p*-nitrophenylacetate (*p*NPAc). After a 24 hours incubation, the supernatant was separated from the beads and concentrated for measuring the hydrolysis rate. A near-stoichiometric amount of chaperone was required to obtain the maximum reaction rate of the lipase (Table 1). Using more than one equivalent of chaperone did not significantly improve the reaction rate, although the refolded enzyme produced from a half equivalent showed only 5% activity. Similarly, a shorter refolding time (12 hr) did not alter the activity of the refolded lipase. The time course for refolding showed that there is no significant increase in lipase activity after 24 hr (Fig. 4).

Table 1. The rates of hydrolysis of *p*-nitrophenyl acetate by *B. cepacia* lipase refolded using varying amounts of chaperone-conjugated magnetic beads[a]

Quantity of chaperone-conjugated magnetic beads (mg)	Refolding time (hr)	Initial reaction rate (μmol/min)	Relative activity (%)
0	24	n.d.[b]	n.d.
250	24	$1.13 \times 10^{-3} \pm 2.0 \times 10^{-7}$[c]	5
500[d]	24	$2.07 \times 10^{-2} \pm 1.7 \times 10^{-4}$	100[e]
750	24	$2.11 \times 10^{-2} \pm 1.1 \times 10^{-5}$	102
1,000	24	$2.71 \times 10^{-2} \pm 4.0 \times 10^{-6}$	105
500	12	1.43×10^{-2}	69
750	12	1.38×10^{-2}	67
1,000	12	1.47×10^{-2}	71

[a] The hydrolysis conditions are identical to those described by Jung and Park (2008).

[b] n.d. = not detected

[c] Errors are standard deviations for at least three measurements; entries without errors are single measurements.

[d] Five hundred milligrams of beads contain 1.85 mg of chaperone. This amount of chaperone represents nearly one stoichiometric equivalent of lipase. See the details in the materials and methods section.

[e] The activity obtained after a 24-h refolding time was regarded as 100%.

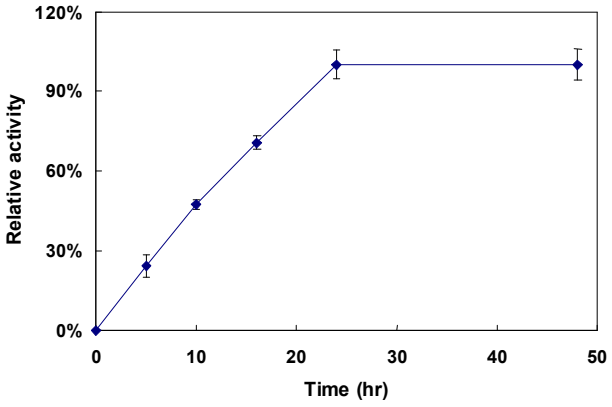

Figure 4 The time course of refolding *B. cepacia* lipase by the chaperone-conjugated magnetic nanobeads. The relative activity was calculated from the initial reaction rate of the refolded *B. cepacia* lipase toward hydrolysis of *p*-nitrophenylacetate. The value for 24-hr refolding time was regarded as 100%. Error bars represent standard deviation for at least three refolding experiments.

Recycling the chaperone conjugated magnetic beads. The chaperone-conjugated magnetic beads were easily recovered by magnetic field or simple centrifugation. We reused the chaperone-conjugated magnetic beads up to ten times and compared the reaction rate using pNPAc of the refolded lipase at each round. The reaction rates at each round were similar to that for the soluble chaperone (Table. 2). The folding activity of the chaperone-conjugated beads still remained above 95% after being recycled ten times.

Table 2. Rates of *p*-nitrophenyl acetate hydrolysis catalyzed by *B. cepacia* lipase refolded by recycled chaperone-conjugated magnetic beads.

Number rounds of recycling of the beads[a]	Initial reaction rate of refolded *B. cepacia* lipase towards *p*NPAc (μmol/min)[b]	Relative activity (%)
1	2.20×10^{-2}	100
2	2.13×10^{-2}	97
3	2.14×10^{-2}	97
4	1.92×10^{-2}	87
5	2.11×10^{-2}	96
10	2.18×10^{-2}	99
B. cepacia lipase refolded by free chaperone[a]	2.26×10^{-2}	103

[a] A stoichiometric amount of immobilized or soluble chaperone (1.85 mg) was used with respect to the lipase. The refolding was performed for 24 hr.

[b] The hydrolysis conditions are identical to those used to obtain data reported in Table 1.

Conclusion

These results indicate that chaperone-conjugated magnetic beads are suitable for refolding denatured *B. cepacia* lipase and may be extensively recycled to dramatically reduce the costs associated with chaperone-mediated expression of soluble lipases. Moreover, because the

expression of soluble protein represents a major bottleneck for the study of many enzymes, particularly many biologically important membrane-bound proteins, this approach provides an important new tool not only for chemists, but for enzymologists and structural biologists.

Experimental Section

DNA manipulation. The *B. cepacia* lipase and chaperone genes were separately subcloned from pHPCE-AB (gene bank number: AY682925), which contains *B. cepacia* lipase and chaperone genes, into pBADgIIIa vector (Invitrogen) using the following primers containing *Nco* I and *Hind* III restriction sites at the 5' and 3' ends, respectively: CHA_F1_Nco I (AGCACCATGGCCCCGCCGTCGCTCGCCGGCTC) and newCHA_R1_Hind III (TAGAAAAGCTTGAACGCGCGCTGCCCGCCCC) for the chaperone, and mBCL_F1_Nco I (AGCACCATGGCCGCTGGCTACGCGGCG) and BCL_R1_ter_Hind III (TAGAAAGCTTCACACGCCCGCCAGCTTCAGC) for the *B. cepacia* lipase. The cloned genes were transformed into *E .coli* (Top 10).

Expression and purification. One milliliter of *E. coli* overnight culture was added to 100 ml of LB medium, and incubated at 37 °C and 200 rpm to an OD_{600} of 0.5. Protein expression was induced by addition of 1 ml of an arabinose solution (2% w/v) and the expression culture was incubated for 6 h at 25 °C and 200 rpm. When the OD_{600} reached ~1.5, the cells were harvested by centrifugation (15 min, 3,800 *g*, 4 °C) and the supernatant was discarded. The cell pellet (~0.8 g) was resuspended in 4 ml of the lysis buffer (NaH_2PO_4, 50 mM; NaCl, 300 mM; imidazole, 10 mM; pH 8.0

adjusted with NaOH) and then sonication (4 kHz, 5 times of 20 sec pulse with 30 sec interval) was applied. After centrifugation (10 min, 10,000 *g*, 4 °C), the cell debris and the supernatant was separated for further experiments.

For the expression of *B. cepacia* lipase, the cell debris was dissolved in 2 ml of 8 M urea and the concentration (2.6 mg/ml) and purity of the resulting protein solution was assessed by the Bradford assay and SDS-PAGE, respectively. This solution of *B. cepacia* lipase was used for refolding experiments without further purification.

The expressed chaperone was purified by affinity chromatography as follows. Briefly, 1 ml of Ni-NTA agarose resin (50% w/v slurry) was added to the supernatant and the mixture was stirred at 4 °C for 1 h. The lysate-Ni-NTA mixture was loaded on a Poly-Prep column (Bio-Rad), drained, and then washed once with 2 ml of the lysis buffer and three times with 4 ml of the wash buffer (NaH_2PO_4, 50 mM; NaCl, 300 mM; imidazole, 20 mM; pH 8.0 adjusted with NaOH). The His_6-chaperone protein was eluted from the column with four volumes of 0.5 ml elution buffer (NaH_2PO_4, 50 mM; NaCl, 300 mM; imidazole, 250 mM; pH 8.0 adjusted with NaOH). The chaperone solution was exchanged into 1 ml of PBS buffer using a centrifugal device. The concentration was determined to be 4.3 mg/ml based on the absorbance at 280 nm ($\varepsilon_{(chaperone)}$ = 32,430 M^{-1} cm^{-1}, calculated with tools at Swiss Prot Expasy, http://ca.expasy.org/tools/protparam.html).

Synthesis of magnetic nanoparticles. The magnetic particles (Fe_3O_4) were synthesized similarly to the method of Faridi-Majidi et al. [10]. Ferric chloride hexahydrate (26 g, 0.096 mol) and ferrous sulfate heptahydrate (18 g, 0.065 mol) were dissolved in 50 ml of Milli-Q water under a nitrogen atmosphere, and the solution was heated to 70 ºC. After addition of 50 ml ammonium hydroxide (28% w/w), oleic acid (5 g) was added to the mixture. The mixture was stirred at 200 rpm for 1 h and then the reaction temperature was increased to 80 ºC to remove ammonia. The suspension was repeatedly centrifuged and resuspended in water until the pH of the suspension was ~7 and the pH of the suspension was adjusted to 4-5 with 0.1 M HCl.

Preparation of polystyrene-coated magnetic beads. One gram of the prepared magnetic nanoparticles was suspended in 48 ml of Milli-Q water containing 0.02 g of SDS and sonicated on ice (6 kHz, 30 times of 20 sec pulse with 30 sec interval). After addition of 20 mg of potassium persulfate, the nanoparticle suspension was shaken for 30 min at 500 rpm under a nitrogen atmosphere. The suspension was then heated to 75 ºC and shaken again at 200 rpm for 30 min. Five milliliters of styrene(washed with 0.1 N NaOH and water before use), 0.1 g of SDS, and 0.08 g of hexadecane were added to 80 ml of Milli-Q water and the mixture was emulsified by vigorous shaking. The styrene emulsion was slowly added into the above nanoparticle suspension. After addition of 1 ml of acrylic acid, the mixture was additionally stirred at 75 ºC for 20 h. The products were washed once with 10 ml of SDS solution (0.1 wt %) and 10 ml of water three times. The yield of the polymer-coated magnetic beads was 1.3 g.

Conjugation of chaperone to the polystyrene-coated magnetic beads. Five hundred milligrams of the prepared magnetic beads were suspended in 5 ml of MES buffer (0.1 M, pH 5.0). After addition of 500 mg of EDC (1-ethyl-3-(3-dimethylaminopropyl) carbodiimide), the suspension was shaken for 20 min at room temperature. The beads were separated and washed three times with 5 ml of PBS buffer. The magnetic beads were resuspended in 1 ml of PBS buffer and then 1 ml of chaperone solution (4.3 mg/ml) was added. The mixture was incubated overnight at 4 ºC, and the chaperone-conjugated magnetic beads were washed three times with 1 ml of PBS buffer. The amount of bound chaperone was determined to be 3.7 mg per g of beads by the difference in absorbance of the supernatant at 280 nm, before and after incubation.

Refolding of *B. cepacia* lipase by the chaperone-conjugated magnetic beads and activity assay. One milliliter of a lipase-containing urea solution (total protein content: 2.6 mg/ml) obtained from solubilization of the inclusion bodies was added to 50 ml of the refolding buffer (2 mM calcium chloride in 5 mM BES, pH 7.2) in the presence of 500 mg of the chaperone-conjugated magnetic beads, and the mixture was incubated for 24 h at 4 ºC. A control without magnetic beads was also performed using 0.43 ml of the soluble chaperone (4.3 mg/ml). After removal of the magnetic beads, the supernatant was concentrated to 1 ml and lipase activity of a 50 μl aliquot was measured by monitoring the hydrolysis of *p*-nitrophenylacetate as previously described [3]. The chaperone-conjugated magnetic beads collected by centrifugation or magnetism were recycled by washing three times with 15 ml of BES buffer (5 mM, pH 7.2).

References

1. Bornscheuer, U. T. *Angew Chem Int Ed*. **2003**, *42*, 3336-3337.
2. Baneyx, F. *Curr Opin Biotechnol*, **1999**, *10*, 411-21.
3. Jung, S.; Park, S. *Biotechnol Lett*. **2008**, *30*, 717-722.
4. Middelberg, A. P. J. *Trends Biotechnol*. **2002**, *20*, 437-443.
5. Hobseon, A. H.; Buckley, C. M.; Aamand, J. L et al. *Proc Natl Acad Sci USA* **1993**, *90*, 5682-5686.
6. Quyen, D. H.; Schmidt-Dannert, C.; Schmid, R. D. *App Environ Microbiol*. **1999**, *65*,787.
7. Fink, A. L. *Physiol Rev*. **1999**, *79*, 425-449.
8. Bornscheuer, U. T.; Kazlauskas, R. J. Hydrolases in organic synthesis: Regio- and stereoselective biotransformations. Weinheim, Germany: Wiley-VCH. 1999; 13 p
9. Cao, L. *Curr Opin Chem Biol*. **2005**, *9*, 217-226.
10. Faridi-Majidi, R.; Sharifi-Sanjani, N.; Agend, F. *Thin Solid Films.* **2006**, *515*, 368-374.

3.3. Facile Preparation of Biocatalyst-Decorated Magnetic Nanobeads

Abstract: Magnetic beads with coated polymethylmethacrylate (PMMA) were investigated for immobilization enzymes. The PMMA-encapsulated magnetic beads were synthesized by emulsion polymerization. The size of magnetic beads was uniform, and the average diameter was about ~81 nm. After prepared PMMA-encapsulated magnetic beads, eight commercial enzymes, Lipase B from *Candida antarctica* (CAL-B), Lipase from *Burkholderia cepacia* (BCL), Lipase from *Candida rugosa* (CRL), Lipase type I from Wheat Germ (WGL), Lipase from *Rhizopus arrhizus* (RAL), Lipase from *Mucor javanicus* (MJL), Lipase from *Thermomyces Lanuginosus* (TLL), and protease S, immobilized by carbodiimide activation. The amounts of immobilized enzymes were about 1 mg/g. The lipase-conjugated magnetic beads showed similar hydrolytic activity to the free enzyme. The recycling experiment showed that the lipase-conjugated magnetic beads can be used several times with maintaining the same activity.

Introduction

Immobilization is a conventional approach for improving stability and recyclability of enzymes [1, 2]. Most techniques for immobilization of enzymes are based on physical adsorption on porous supporting materials, which contain a large surface area. Adsorption of enzymes on such materials can decrease a tendency for aggregation of enzymes and thereby

sustaining the active forms in organic solvents. However, enzymes immobilized by this method are not recyclable when the reaction is performed in aqueous media on account of enzymes' leaching out of the supporting matrix. Covalent immobilization can be one of the alternative approaches for recycling biocatalysts in aqueous media. Nevertheless, covalent linkage of enzymes on the macro-sized porous polymer materials causes mass transport limitation because the interior enzymes in the porous materials may have less or slow contact with substrates. Mass transport limitation results in retardation of reactions as well as decrease of enantioselectivity [3]. Instead, utilizing nano-sized polymer particles as a supporting material can reduce mass transport limitation, but it is often problematic to recover the particles by centrifugation from an aqueous media due to their low density [4]. To overcome these drawbacks, using nano-sized magnetic particles as a supporting material has been proposed.

Protein-decorated magnetic nanoparticles have garnered more attention in biotechnology, such as isolation of proteins, enhancement of magnetic resonance imaging, and immobilization of enzymes [5-15]. Nano-sized magenetic particles possess a greatly enhanced surface area, which affords better contact with substrates without mass transport limitation. In addition, one of the most distinct characteristics of magnetic nanoparticles over polymer nanobeads in bio-applications is that they are conveniently separable from a reaction media by applying an external magnetic field or by simple centrifugation. Although several enzymes, such as hydrolase [16-21], glucose oxidase [22], alcohol dehydrogenase [23], and chloroperoxidase [24], have been directly or indirectely immobilized on magnetic nanoparticles, many cases do not provide sufficient activity or

require a complicated process for manufacturing. For example, direct conjugation of a lipase (*Candida rugosa* lipase) to magnetic nanoparticles showed 236-fold activity decrease compared to the free form of the lipase [16]. Silica- or polymer-entrapped enzymes on magnetic particles showed improved activity and stability, but additional processes after encapsulating are required to protein conjugation [18, 24]. Herein, we describe a facile process of covalent immobilization of biocatalysts on polymer encapsulated magnetic nanoparticles with maintaining comparable activity to the free enzymes in aqueous media.

Results and Discussion

Synthesis of polymer-coated magnetic nanoparticles. The process of manufacturing enzyme-conjugated magnetic nanobeads is straightforward and simple compared to the previously reported methods [16-24] (Fig. 1). The current approach introduces a functional group to be used for enzyme conjugation during the encapsulation step of polymethylmethacrylate (PMMA) on magnetic nanoparticles, whereas the previous methods required additional processes to introduce such functional groups. The magnetic nanoparticles (Fe_3O_4) were prepared by coprecipitation of Fe (II) and Fe (III) ions in a basic solution.

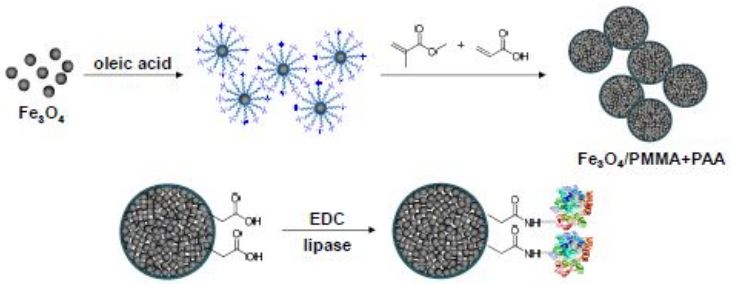

Figure 1. Process for preparation of lipase-conjugated magnetic nanobeads.

The precipitated magnetic particles were then encrusted with oleic acid to enhance interaction with polymers. Initially, we encapsulated the magnetic particles with polystyrene (PS) containing carboxylate groups by emulsion polymerization in an aqueous solution. The PS-coated magnetic beads were uniform, but an average diameter was submicron-sized (~300 nm, Fig. 2).

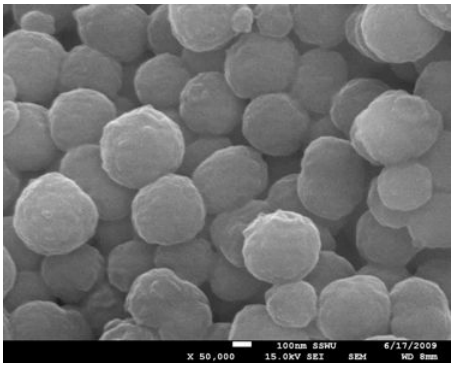

Figure 2. FE-SEM image of PS-coated magnetic beads. An average diameter of the beads is estimated to be ~300 nm. The scale bar = 100 nm.

Presumably, the phenyl groups in PS are strongly amassed and become larger in water. In order to reduce the size of beads and thereby to provide a larger surface area, we used methyl methacrylate, which has lower aggregation propensity in water. The encapsulation process of PMMA was achieved by radical-initiated polymerization using methyl methacrylate and acrylic acid in an aqueous methanolic solution. Powder X-ray diffraction analyses indicate that the polymer encapsulation does not affect the structural integrity of Fe_3O_4 (Fig. 3a), and the nanobeads can be attracted by applying an external magnetic field and thus separable from the reaction media (Fig. 3b). Field-emission scanning electron microscopy (FE-SEM) analyses of the resulting magnetic nanobeads revealed that the magnetic nanobeads are uniformly spherical and an average diameter of the PMMA-coated beads is estimated to be ~81 nm (Fig. 3c and Fig. 4a).

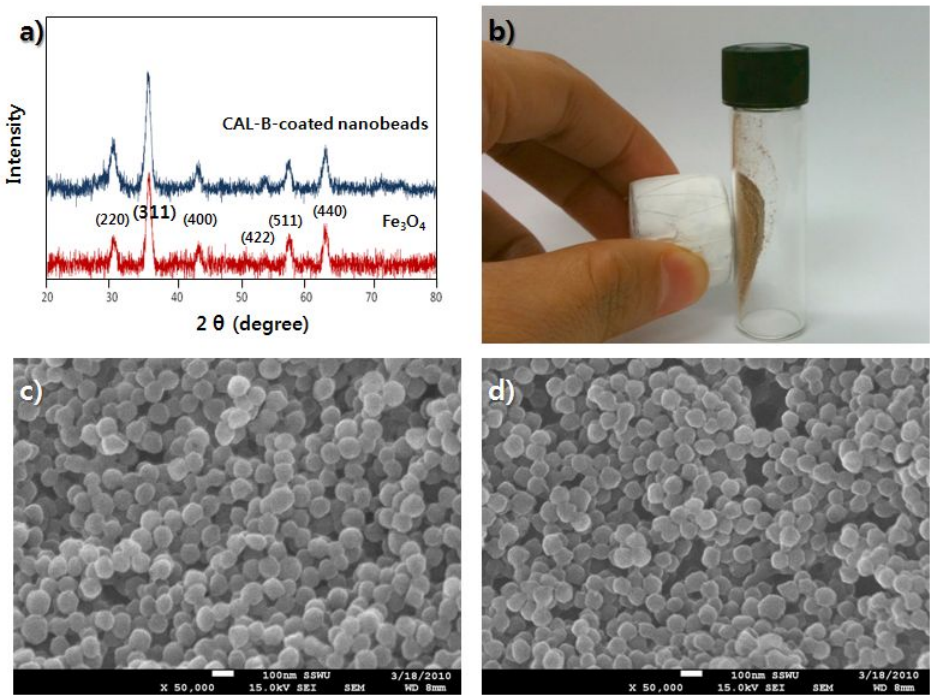

Figure 3. a) PXRD patterns of Fe_3O_4 and PMMA-encapsulated magnetic beads, b) picture showing magnetic attraction. c) FE-SEM image of the polymer-coated magnetic nanobeads, d) FE-SEM image of the CAL-Bconjugated magnetic nanobeads, Scale bar = 100 nm.

Conjugation of enzymes to the polymer-coated magnetic nanoparticles. Commercial seven lipases and one protease (Table 2) were then conjugated to the PMMA-encapsulated magnetic nanobeads after activation of the carboxylate groups on the PMMA-encapsulated magnetic beads by 1-ethyl-3-(3-dimethylaminopropyl) carbodiimide (EDC). The EDC activation of the carboxylate groups on the surface of the PMMA-encapsulated magnetic nanobeads allows formation of an amide bond with the free amino groups

(i.e. the N-terminal or the side chain of lysine) of enzymes.

The morphology of the lipase-conjugated magnetic nanobeads was not altered but the diameter became slightly larger (~84 nm, CAL-B-conjugated beads shown as a representative in Fig. 3d and Fig. 4b). The protein amount in a solution was measured by the Bradford protein assay [25] and the amount of immobilized enzyme was determined to be 0.75-0.91 mg g^{-1} by difference in the protein amount of the supernatant before and after incubation (Table 1).

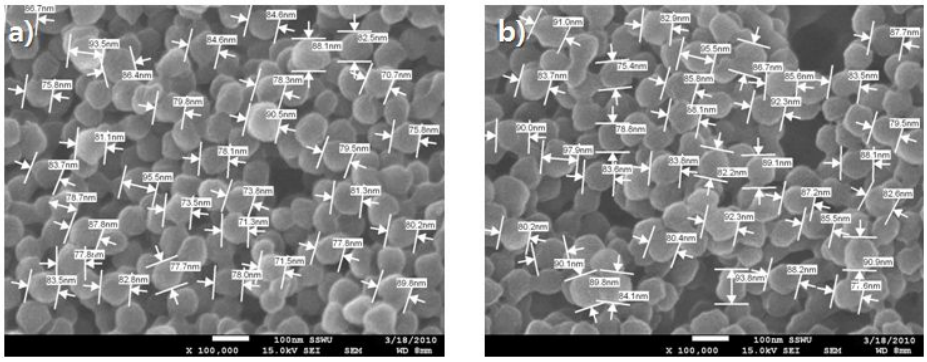

Figure 4. Measuring the diameters of the magnetic beads. a) polymer-coated magnetic nanobeads, b) CAL-B-conjugated magnetic nanobeads. An average diameter was estimated to be 81.0 ± 6.4 nm for polymer-coated magnetic nanobeads and 84.0 ± 11.7 nm for CAL-B-conjugated magnetic nanobeads. The scale bar = 100 nm.

Table 1. The amount of protein bound to the magnetic beads.

entry	enzymes	amount of bound proteins (mg g^{-1})
1	Lipase B from *Candida antarctica* (CAL-B)	0.84
2	Lipase from *Burkholderia cepacia* (BCL)	0.88
3	Lipase from *Candida rugosa* (CRL)	0.83
4	Lipase type I form Wheat Germ (WGL)	0.75
5	Lipase from *Rhizopus arrhizus* (RAL)	0.79
6	Lipase from *Mucor javanicus* (MJL)	0.89
7	Lipase from *Thermomyces Lanuginosus* (TLL)	0.93
8	Protease S	0.91

In order to investigate the detailed morphologies of the surfaces of a single magnetic nanobead, three dimensional atomic force microscopy (AFM) images were obtained (Fig. 5). The surface of a lipase-conjugated nanobead contains fewer valleys and the valleys have longer peak-to-valley distance compared to that of a PMMA-encapsulate magnetic bead, although the separated lipase particles could not be detected.

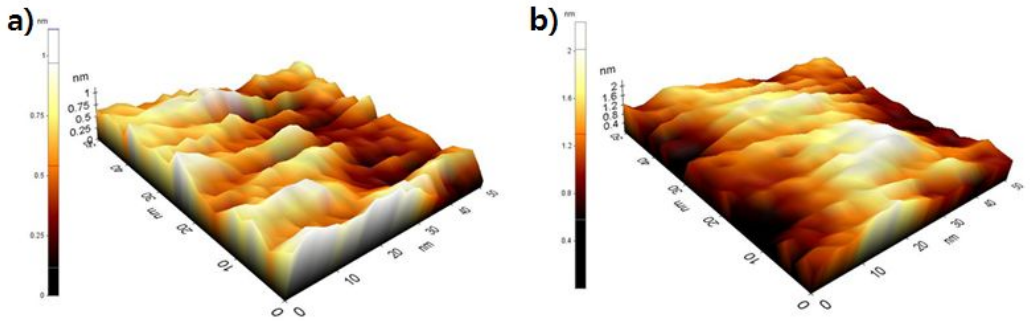

Figure 5. The AFM images of a magnetic nanobeads. a) a PMMA-coated magnetic nanobead, b) a CAL-B-cojugated nanobead.

Comparison of the hydrolytic activity and enantioselectivity between the free enzyme and the enzyme conjugated magnetic nanoparticles. For evaluation of the catalytic efficiency of the immobilized lipases on the magnetic nanobeads, we measured the reaction conversion as well as enantioselectivity towards hydrolysis of rac-1-phenylethyl butanoate in an aqueous solution as a model reaction (Table 2). The kinetic resolution of rac-1-phenylethyl alcohol by lipases has been extensively studied and well documented in the literature [26-32]. The immobilized lipases catalyzed the hydrolysis with 10-75% conversion (entry 1-10) but protease S showed no conversion (entry 11). Presumably, protease S does not accept rac-1-phenylethyl butanoate as a substrate rather than becoming inactive by immobilization. In fact, the reaction of protease-Sconjugated nanobeads with p-nitrophenyl acetate as a substrate showed equivalent activity to that of the free enzyme (Fig. 6)

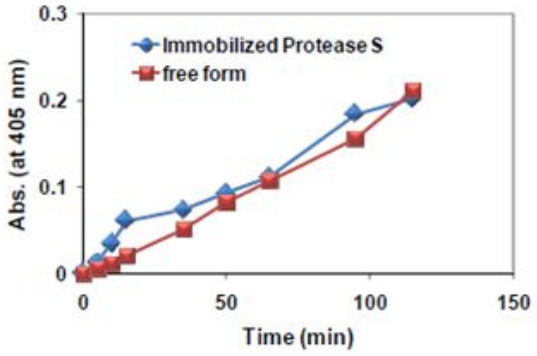

Figure 6. Hydrolysis of p-nitrophenyl acetate by protease S. The reactions were performed as the previously reported method [31] with using 30 mg of protease-S-conjugated magnetic nanobeads and the corresponding amount of free protease S (27 μg). Both immobilized and free protease S showed similar activity.

Among seven lipase-conjugated nanobeads, CAL-B-, BCL-, and CRL-conjugated ones showed high conversion as well as high enantioselectivity (entry 1, 3, and 5, respectively). The reactions by those three free lipases were also carried out in order to determine the varation of enzyme activities by the current immobilization method (entry 2, 4, and 6). Interestingly, the reactions by the lipase-conjugated nanobeads in this study showed comparable conversions to the reactions by the free lipases, although it is generally reported in previous literatures that the activity of covalently immobilized enzyme decreases [16-21, 33].

Table 2. Hydrolysis of lipase-conjugated magnetic nanobeads toward *rac*-1-phenylethyl butanoate.

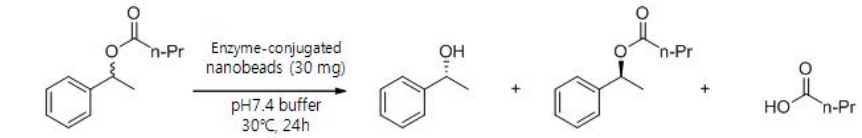

entry	enzymes	ee_s(%)	ee_p(%)	Conversion (%)	E
1	Lipase B from *Candida antarctica* (CAL-B) (20 mg)	>99.9	>99.9	50	>200
2	Lipase B from *Candida antarctica* free form	97.4	>99.9	49	>200
3	Lipase from *Burkholderia cepacia* (BCL)	>99.9	>99.9	50	>200
4	Lipase from *Burkholderia cepacia* free form	53.5	>99.9	35	>200
5	Lipase from *Candida rugosa* (CRL)	80.9	69.8	54	13.7
6	Lipase from *Candida rugosa* free form	59.8	53.2	53	5.9
7	Lipase type I form Wheat Germ (WGL)	3.8	1.3	75	1.1
8	Lipase from *Rhizopus arrhizus* (RAL)	9.5	89.7	10	20.2
9	Lipase from *Mucor javanicus* (MJL)	14.5	80.7	15	10.8
10	Lipase from *Thermomyces Lanuginosus* (TLL)	33.1	98.3	23	156.8
11	Proteaes S	<0.5	<0.5	<1	n.d

Recycling of the enzyme conjugated magnetic nanoparticles. We conducted recycling experiments of the three lipase-conjugated magnetic nanobeads. The lipase conjugated beads were isolated by a magnet for consecutive runs after a reaction completed. As shown in the Fig. 7, the conversion in the reactions by CAL-B- and BCL-conjugated magnetic nanobeads was consistent during six-time recycling with maintaining the same enantioselectivity (E = >200). For the CRL-conjugated magnetic nanobeads, it was observed that the conversion decreased by 5% at each run, but the value is still smaller than the activity loss (~15%) in the previous report [16].

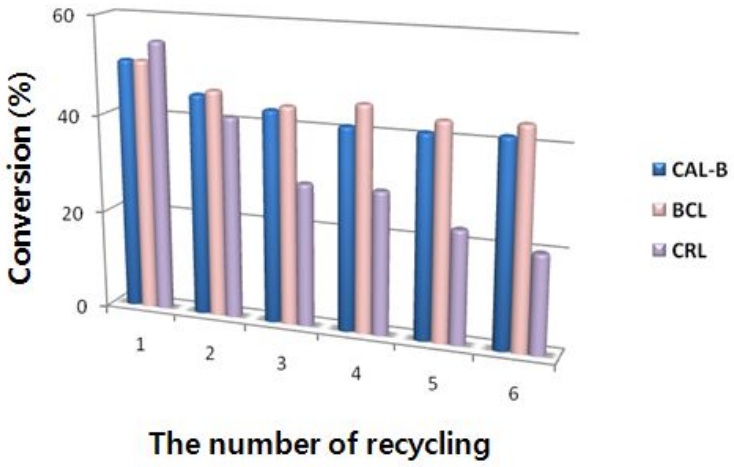

Figure 7. Recycling of th lipase-conjugated nanobeads

Conclusion

The enzyme-conjugated magnetic nanobeads were facilely manufactured in a shorter process in comparison with the methods in the previous literatures. The lipases were covalently anchored onto the surface of the nanobeads after simple treatment by EDC. The immobilized lipases showed no loss of the activity compared to the free enzymes with maintaining identical enantioselectivities. This study also demonstrated that the immobilized lipases by the current method can be easily separable from reaction products and recyclable without significant loss of the activity in aqueous media.

Experimental section

General Methods. Chemicals and buffers were purchased from Sigma-Aldrich. Lipases and protease S were purchased from Sigma-Aldrich or kindly donated from amino enzyme inc. (Japan). The FE-SEM images and were obtained by JSM-7500F (Jeol, Japan). The AFM images were obtained in the non-contact mode by XE-100 (Park system, Korea).

Synthesis of magnetic nanoparticles. The magnetic particles (Fe_3O_4) were synthesized similarly to the method by Faridi-Majidi et al. [34]. Ferric chloride hexahydrate (9.72 g, 35.96 mmol) and ferrous sulfate heptahydrate (6.68 g, 24.03 mmol) were dissolved in 80 ml of Milli-Q water under nitrogen atmosphere. The reaction mixture was heated to 90 °C. After

addition of ammonium hydroxide (28 wt%, 24 ml), oleic acid (5 ml) was added into the reaction mixture. The mixture was stirred at 200 rpm for 3 h at 90 °C. The products were separated by centrifugation and washed with 25 ml of doubly distilled water to neutrality.

Synthesis of polymer coated magnetic beads. Methyl methacrylate (5 ml), Fe_3O_4 (0.5 g), hexadecane (200 μL) and AIBN (2,2′-azobis (2-methylpropionitrile), 125 mg) were mixed and sonicated for 5 min using a bath sonicator. After PVP (polyvinylpyrrolidone, 1.5 g) and acrylic acid (1 ml) were dissolved in an aqueous methanol solution (25% v/v, 100 ml), the methanol solution was heated to 70 °C. Methyl methacrylate suspension was added dropwise to the methanol solution for 5 min. The reaction mixture was stirred at 400 rpm and 70 °C for 16 h under nitrogen atmosphere. The products were washed three times with doubly distilled water (50 ml). The yield was 5.3 g.

Conjugation of enzyme with magnetic beads. The prepared magnetic beads (1 g) were suspended in MES buffer (10 ml, 0.1 M, pH 5.0). After addition of EDC (1-ethyl-3-(3-dimethylaminopropyl) carbodiimide, 100 mg), the suspension was shaken for 20 min at room temperature. The beads were separated and washed three times with PBS buffer (10 ml, pH 7.4). The magnetic beads were resuspended in PBS buffer (2 ml) and an enzyme solution (1 mg ml^{-1}, 2 ml) was added. The mixture was incubated overnight at 4 °C. The enzyme-conjugated magnetic beads were washed three times with PBS buffer (2 ml). The amount of the bound enzymes was determined by the Bradford assay (Table 1).

Hydrolysis of (±)-1-phenylethyl butanoate. To 1 ml of PBS buffer (pH 7.4) containing *rac*-1-phenylethyl butanoate (0.05 mmol) in 7 ml vial was added enzyme-conjugated nanobeads (30 mg) except for CAL-B (20 mg) or same amount (17-27 μg) of free enzymes. The reaction mixture was shaken at 200 rpm and 30 °C for 24 h. The supernatant was separated from the catalyst under a magnetic field, and the catalyst was washed with PBS buffer (3×1 ml). The combined buffer solution was extracted with n-hexane (3×3 ml). The organic layer was dried over $MgSO_4$ and analyzed by GC (Agilent 6890N) equipped with FID detector with a chiral capillary column (CHIRADEXTM-BDM, 30m × 0.25 mm I.D., ASTEC). GC condition: The GC column temperature was initially programmed at 100 °C for 10 min, then gradient to 125 °C at 1 °C/min, and then held at 190 °C for 2 min. (S)-Phenylethyl alcohol and (R)-phenylethyl alcohol were detected at 15.4 min and 16.1 min, respectively. Also (S)-phenylethyl butanoate and (R)-phenylethyl butanoate were detected at 25.7 min and 25.1 min, respectively.

Recycling of the lipase-conjugated magnetic nanobeads. To 1 ml of PBS buffer (pH 7.4) containing *rac*-1-phenylethyl butanoate (0.05 mmol) in 7 ml vial was added enzyme-conjugated nanobeads (30 mg) except for CAL-B (20 mg). The reaction mixture was shaken at 200 rpm and 30 °C for 24 h. The supernatant was separated from the catalyst under magnetic field, and the catalyst under magnetic field was carefully washed with PBS buffer (3×1 ml). Then into the reaction vial with the catalyst was added 1 ml of PBS buffer (pH 7.4) containing 1-phenylethyl butanoate (0.05 mmol) to start the new cycle of the reaction for 24h.

Reference

1. Bornscheuer, U. T. *Angew. Chem. Int. Ed.,* **2003**, *42*, 3336-3337.
2. Cao, L. *Curr. Opin. Chem. Biol.,* **2005**, *9*, 217-226.
3. Rotticci, D.; Norin, T.; Hult, K. *Org. Lett.*, **2000**, *2*, 1373-1376.
4. Jung, S.; Park, S. *Biotechnol. Lett.*, **2009**, *31*, 107-111.
5. Lu, A.-H.; Salabas, E.L.; Schüth, F. *Angew. Chem. Int. Ed.,* **2007**, *46*, 1222-1244.
6. Zhao, M.; Josephson, L.; Tang, Y.; Weissleder, R. *Angew. Chem. Int. Ed.*, **2003**, *42*, 1375-1378.
7. Weissleder, R.; Kelly, K.; Sun, E.Y.; Shtatland, T.; Josephson, L. *Nat. Biotechnol.*, **2005**, *23*, 1418-1423.
8. Bulte, J. W. M.; Kraitchman, D. L. *NMR Biomed.*, **2004**, *17*, 484-499.
9. Gu, H.; Ho, P. L.; Tsang, K. W. T.; Wang, L.; Xu, B. *J. Am. Chem. Soc.*, **2003**, *125*, 15702-15703.
10. Xu, C.; Xu, K.; Gu, H.; Zhong, X.; Guo, Z.; Zheng, R.; Zhang, X.; Xu, B. *J. Am. Chem. Soc.*, **2004**, *126*, 3392-3393.
11. Gu, H. W.; Xu, K. M.; Xu, C. J.; Xu, B. *Chem. Commun.*, **2006**, 941-949.
12. Lee, I. S.; Lee, N.; Park, J.; Kim, B.-H.; Yi, Y.-W.; Kim, T.; Kim, T. K.; Lee, I. H.; Paik, S. R.; Hyeon, T. *J. Am. Chem. Soc.*, **2006**, *128*, 658-662.
13. Lee, J.-H.; Huh, Y.-M.; Jun, Y.-W.; Seo, J.-W.; Jang, J.-T.; Song, H.-T.; Kim, S.; Cho, E.-J.; Yoon, H.-G.; Suh, J.-S.; Cheon, J. *Nat. Med.*, **2007**, *13*, 95-96.

14. Yi, D. K.; Selvan, S. T.; Lee S. S.; Papaefthymiou, G. C.; Kundaliya, D.; Ying, J. Y. *J. Am. Chem. Soc.*, **2005**, *127*, 4990-4991.
15. Stoeva, S. I.; Huo, F.; Lee; J.- S.; Mirkin, C. A. *J. Am. Chem. Soc.*, **2005**, *127*, 15362-15363
16. Dyal, A.; Loos, K.; Noto, M.; Chang, S.; Spagnoli, C.; Shafi, K.; Ulman, A.; Cowman, M.; Gross, R. *J. Am. Chem. Soc.*, **2003**, *125*, 1684-1685.
17. Gardimalla, H. M. R.; Mandal, D.; Stevens, P. D.; Yen, M.; Gao, Y. *Chem. Commun.*, **2005**, 4432-4434.
18. Lee, J.; Lee, Y.; Youn, J.; Na, H.; Yu, T.; Kim, H.; Lee, S.; Koo, Y.; Kwak, J.; Park, H. *Small*, **2008**, *4*, 143-152.
19. Lee, D.; Ponvel, K.; Kim, M.; Hwang, S.; Ahn, I.; Lee, C. *J. Mol. Catal. B: Enzym.*, **2009**, *57*, 62-66.
20. Huang, S.; Liao, M.; Chen, D. *Biotechnol. Prog.*, **2003**, *19*, 1095-1110.
21. Lee, K. S.; Woo, M. H.; Kim, H. S.; Lee, E. Y.; Lee, I. S. *Chem. Commun.*, **2009**, 3780-3782.
22. Rossi, L.; Quach, A.; Rosenzweig, Z. *Anal. Bioanal. Chem.*, **2004**, *380*, 606-613.
23. Liao, M.; Chen, D. *J. Mol. Catal. B: Enzym.*, **2002**, *16*, 283-291.
24. Wang, W.; Xu, Y.; Wang, D. I. C.; Li, Z. *J. Am. Chem. Soc.*, **200**9, *131*, 12892-12893.
25. Bradford, M. M.; *Anal. Biochem.,* **1976**, *72*, 248-254.
26. Park S.; Kazlauskas, R. J. *J. Org. Chem.*, **2001**, *66*, 8395-8401.
27. Schofer, S.H.; Kaftzik, N.; Wasserscheid, P.; Kragl, U. *Chem. Commun.*, **2001**, 425-426.
28. Shah, S.; Gupta, M. N. *Bioorg. Med. Chem. Lett.*, **2007**, *17*, 921-924.
29. Csajagi, C.; Szatzker, G.; Toke, E. R.; Urge, L.; Darvas, F.; Poppe, L.

Tetrahedron: Asymmetry, **2008**, *19*, 237-246.

30. Kourist, R.; de Maria, P. D.; Bornscheuer, U. T. *ChemBioChem*, **2008**, B, 491-498.
31. Jung, S.; Park, S. *Biotechnol. Lett.,* **2008**, *30*, 717-722.
32. Wang, Y. H.; Wang, R.; Zhang, Q. S. LiZ. M.; Feng, Y. *J. Mol. Catal. B: Enzym.*, **2009**, *56*, 142-145.
33. Moreno, J.-M.; Arroyo, M.; Hernáiz, M.-J.; Sinisterra, J.-V. *Enz. Microb. Technol.*, **1997**, *21*, 552-558.
34. Faridi-Majidi, R.; Sharifi-Sanjani, N.; Agend, F. *Thin Solid Films,* **2006,** *515*, 368-374.

3.4. Biofunctionalization of Metal-Organic Frameworks by Covalent Protein Conjugation

Abstract: Metal-Organic Frameworks which are synthesized by solvothermal method were measured by X-ray diffraction (XRD) patterns and Scanning Electron Microscope (SEM). Then proteins such as Enhance green fluorescent protein (EGFP) and *Candida Antarctica* lipase B (CAL-B), was covalently bound to the MOFs by a simple chemical treatment. The EGFP fluorescence on the MOFs was confirmed using a fluorescence microscope and luminescence spectrometer. Furthermore, the X-ray diffraction (XRD) studies were carried out in order to compare the structure of MOFs and conjugated-CAL-B MOFs in order to compare the structure. Finally, we compared the specific activity and the enantiomeric ratio of the commercial CAL-B, conjugated-CAL-B MOFs, and Novozyme 435 in order to determine the effect of the MOFs for immobilized proteins.

Introduction

Metal-organic frameworks (MOFs) are garnering more interest in material science. Thermally and mechanically stable MOFs with large void volumes have been useful in advanced applications such as selective catalysis, sensors, and high-efficiency gas storage [1-14]. Although diverse MOF materials have been prepared by solvothermal reactions between metal ions and organic linker compounds, organic linkers should possess

adequate thermal stability because of their synthetic conditions. To incorporate thermally unstable compounds into MOFs, the "postsynthetic covalent modification" was recently explored by several research groups [15-25]. For instance, Cohen and coworkers used IRMOF-3 (isoreticular metal-organic framework-3) as a starting MOF material for postsynthetic modification. IRMOF-3 is composed of Zn(II) ions and 2-amino-1,4-benzene dicarboxylic acid (NH_2-BDC). The two carboxylate groups of NH_2-BDC link Zn_4O nodes but the amino group is intact during the IRMOF-3 formation. Thus, the amino groups are available for further modification of the framework. Cohen and cowokers have shown that the amino groups can be modified by simple organic reactions and introduced several organic groups [15]. Since then many groups have reported modifications of MOFs using similar approaches, which require a special functional group, such as amino group, for further modification [15-24]. Therefore, these approaches should be limited for the MOFs bearing such functional groups in the original linker molecules.

Results and Discussion

Synthesis of metal-organic frameworks. We have explored to overcome this limitation by using the linking groups of MOFs. In fact, typical organic linkers of the MOFs contain carboxylate groups. For example, a series of IRMOFs are composed of Zn_4O nodes and dicarboxylate organic linkers [6]. A new indium(III)-based one-dimensional (1D) coordination polymer was prepared from the reaction between $In(NO_3)_3$ and 1,4-phenylenediacetic acid

(H_2pda) in *N,N*-diethylformamide (DEF). The crystal structure was shown in Fig. 1 and 2.

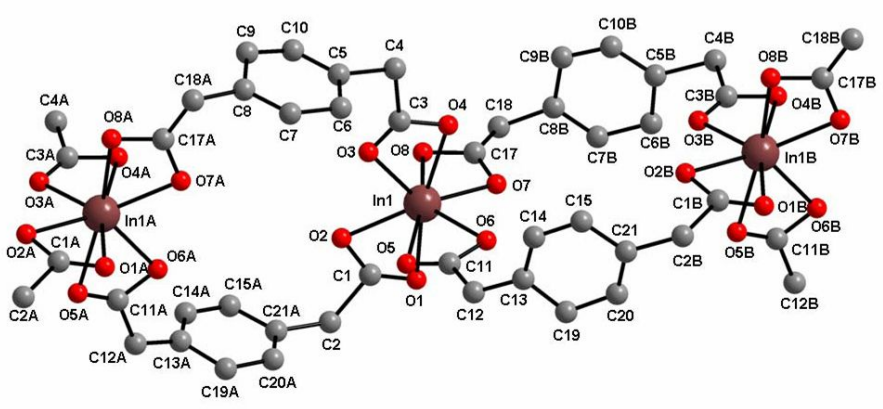

Figure 1. A perspective view of the 1D-MOF (1) indicating the pseudotetrahedral 8-coordinate In(III) centers. The $[H_2NEt_2]^+$ ions and hydrogen atoms are omitted for clarity. Symmetry operations: A (x, -y, 0.5+z) and B (x, -y, -0.5+z).

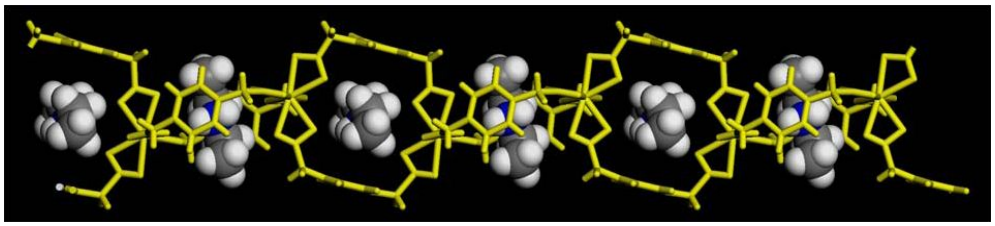

Figure 2. A view of the 1D-MOF (1) with the $[H_2NEt_2]^+$ ions. The $[H_2NEt_2]^+$ ions are shown in a CPK model.

The coordination mode of indium in the 1D-MOF is 8-coordinated by four carboxylates. Overall bonding scheme of the indium ion is very similar to those observed in several previous examples of 3D In-MOFs. The indium ion formed pseudotetraheral structure with four bridging pda ligands chelated

in a bidentate manner. However, the bent geometry of methylene groups of the bridging pda ligands prevented the pseudotetrahedral motifs from expanding into a 3D network. Instead, it formed a 1D coordination polymer bearing a relatively large cavity between two negatively-charged indium ions and two parallel benzene rings from the pda ligands. In fact, the counter cation, diethylammonium ion, is perfectly captured in this cavity. The diethylammonium ions were generated from the decomposition of solvent molecules, DEF, during the reaction. The 2D-MOF, $[Zn(bpydc)(H_2O)\cdot(H_2O)]_n$, is composed of zinc ions and 2,2'-bipyridine 5,5'-dicarboxylate (bpydc) [26]. IRMOF-3 was used as the 3D-MOF [27].

Characters of conjugated prtoeins to the MOFs by EDC or DCC activiation. Either pendent Zn_4O nodes or carboxylate groups should occupy the surface of the frameworks and thereby are exposed on the surface of IRMOFs. If pendent carboxylate groups are present on the surface of MOFs, then they could be activated and modified by simple organic reactions. We assumed that a certain amount of the carboxylate groups are exposed and can be activated by 1-ethyl-3-(3-dimethylaminopropyl) carbodiimide (EDC) or dicyclohexyl carbodiimide (DCC). Then, the activated carboxylates can be conjugated with other compounds or even biomaterials, such as proteins. We exploited this idea of conjugating proteins to coordination polymers or MOFs with different structural architectures, such as one-, two- and three dimensional (3D) structures. To our knowledge, the incorporation of functional proteins to MOFs has not yet been achieved. We first chose enhanced green fluorescence protein (EGFP) as a model protein because its presence and the folding status of EGFP can be easily tracked

by fluorescence microscopy. All organic linkers of the MOFs contain carboxylate groups. We attempted to conjugate MOFs with EGFP by treating EDC to activate the dangling carboxylate groups of MOFs (Fig. 3).

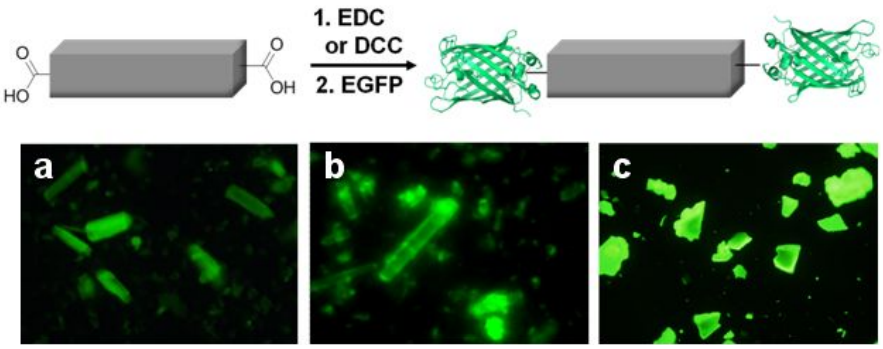

Figure 3. Schematic representation of the bioconjugation of the 1D-polymer, $[(Et_2NH_2)(In(pda)_2)]_n$, with EGFP. Fluorescence microscopic images of EGFP coated MOFs. a) 1D + EGFP. b) 2D + EGFP. c) 3D + EGFP. An Olympus WIB filter set (λ_{ex} = 460–490 nm; λ_{em} > 515 nm) was used for recording the fluorescence

We noticed, however, the 1D-polymer was only activated and conjugated with EGFP. Presumably, pda was rather easily activated in aqueous media because aliphatic carboxylate is more reactive than aromatic one [28]. In addition, this observation implies that no physical adsorption of EGFP to the MOFs occurs. For 2D and 3D-MOFs, we activated the carboxylates by DCC in dichloromethane instead of EDC in an aqueous buffer. This activation step did not alter the crystallinity of the MOFs (Fig. 4).

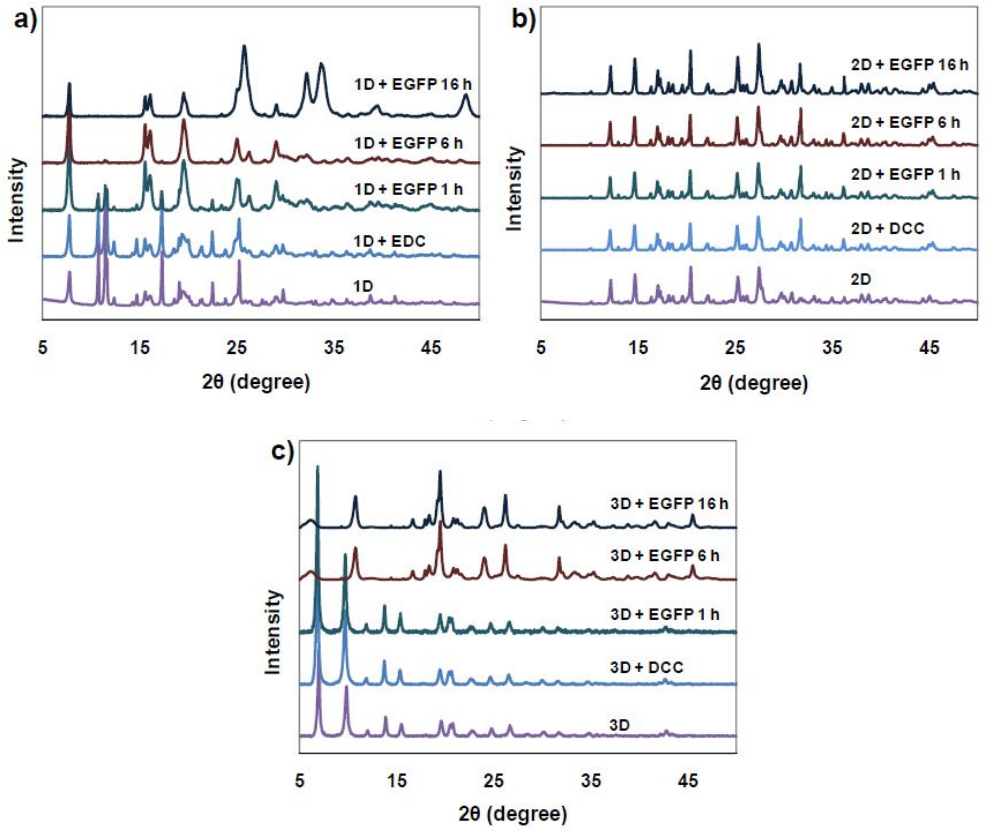

Figure 4. PXRD patterns of the 1D-MOF (a), 2D-MOF (b), and 3D-MOF (c), and the corresponding EGFP-conjugated 1D-, 2D-, and 3D-MOFs. The activation step by EDC or DCC did not alter the PXRD patterns for all MOFs.

For the following protein-conjugation step, we need to use a buffer (PBS, pH 7.3) as a reaction media in order to conjugate proteins because proteins are not soluble in most organic solvents. The use of a buffer could be problematic because MOFs, especially the 3D-MOF (IRMOF-3), may be not stable against water. Therefore, we evaluated the stability of the 3D-MOF in water and PBS buffer by comparing PXRD patterns before and after soaking the 3D-MOF in water or PBS buffer. To our surprise, 1-h

incubation of the 3D-MOF in a PBS buffer did not alter the PXRD pattern of the original phase while longer incubation (for 6 h) in PBS buffer or incubation in water did (Fig. 5).

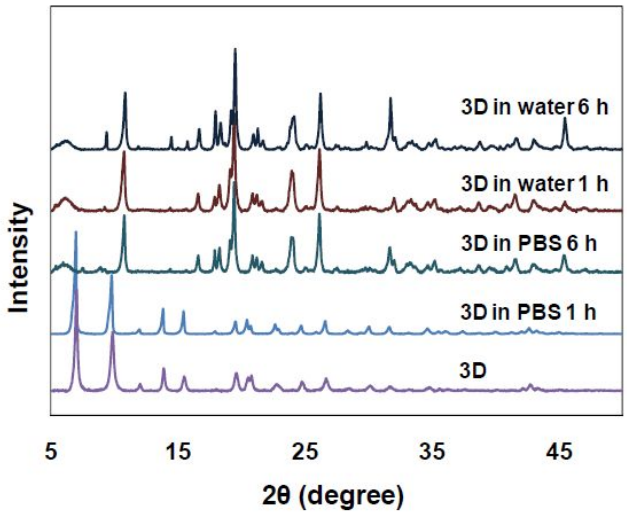

Figure 5. PXRD patterns before and after soaking the 3D-MOF in water and PBS buffer.

We envision that this finding will broaden the scope of IRMOF-3 functionalization in an aqueous buffer solution. After activation of the MOFs, we successfully conjugated EGFP with the MOFs. However, the longer reaction period (> 1 h) for binding EGFP to 1D- and 3D-MOFs altered the structural integrity while the 2D-MOF remained unchanged (Fig. 4). The six-histidine tag attached to the N-terminal of EGFP may coordinate to the metal ions of the 1D- and 3D-MOFs and result in the structural alteration but not for the 2D-MOF. The different coordination environment (N_2O_4) of 2D-MOF is presumably more stable than those of the other MOFs.

The presence of EGFP on the surface of the MOFs was confirmed

by a fluorescence microscope. The EGFP-decorated crystals emitted a uniform green fluorescence (Fig. 3). In addition, the IR spectra of EDC- and EGFP decorated 1D-MOF showed different patterns from that of 1D-MOF (Fig. 6).

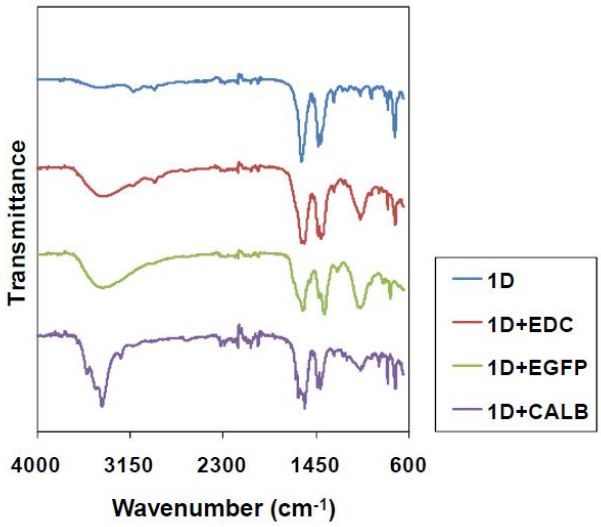

Figure 6. IR spectra of 1D-MOF and the conjugated 1D-MOFs.

Thus, it can be concluded that EGFP was successfully introduced on the surface of the MOFs and the anchored EGFP is still functional. Solid-state luminescence measurements also provided the characteristic spectrum of EGFP (Fig. 7).

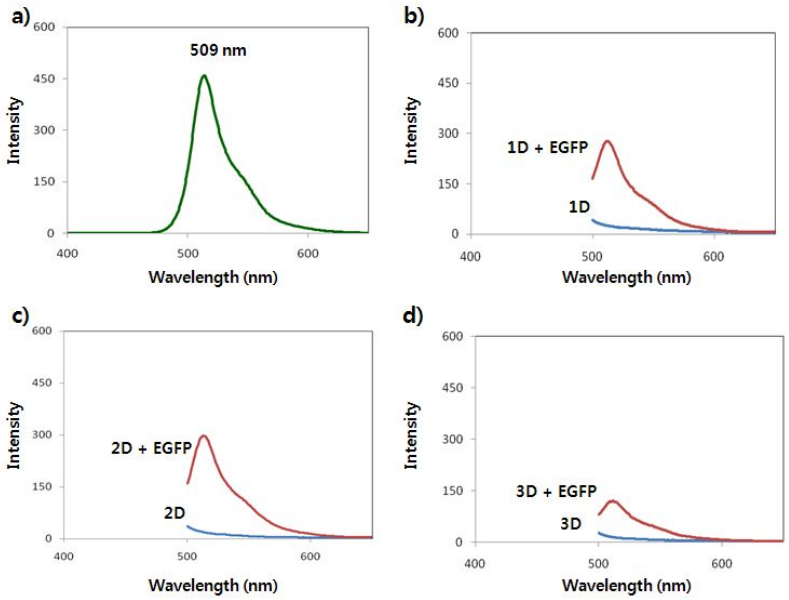

Figure 7. Emission spectrum: EGFP (a), 1D and 1D + EGFP (b), 2D and 2D + EGFP (c), and 3D and 3D + EGFP (d). The emission spectra were recorded under 488-nm excitation at room temperature. The characteristic maximum emission for EGFP is 509 nm.

The surface modification of the MOFs was further confirmed by using a confocal laser scanning microscope (CLSM). Most green emissions from the EGFP-decorated MOFs were observed from the surface of crystals (Fig. 8). The amounts of EGFP coated on the MOFs were determined as 0.048, 0.052, 0.064 mg g^{-1} of the 1D-, 2D-, and 3D-MOFs, respectively. To our knowledge, this is the first direct bioconjugation of coordination polymers or MOFs.

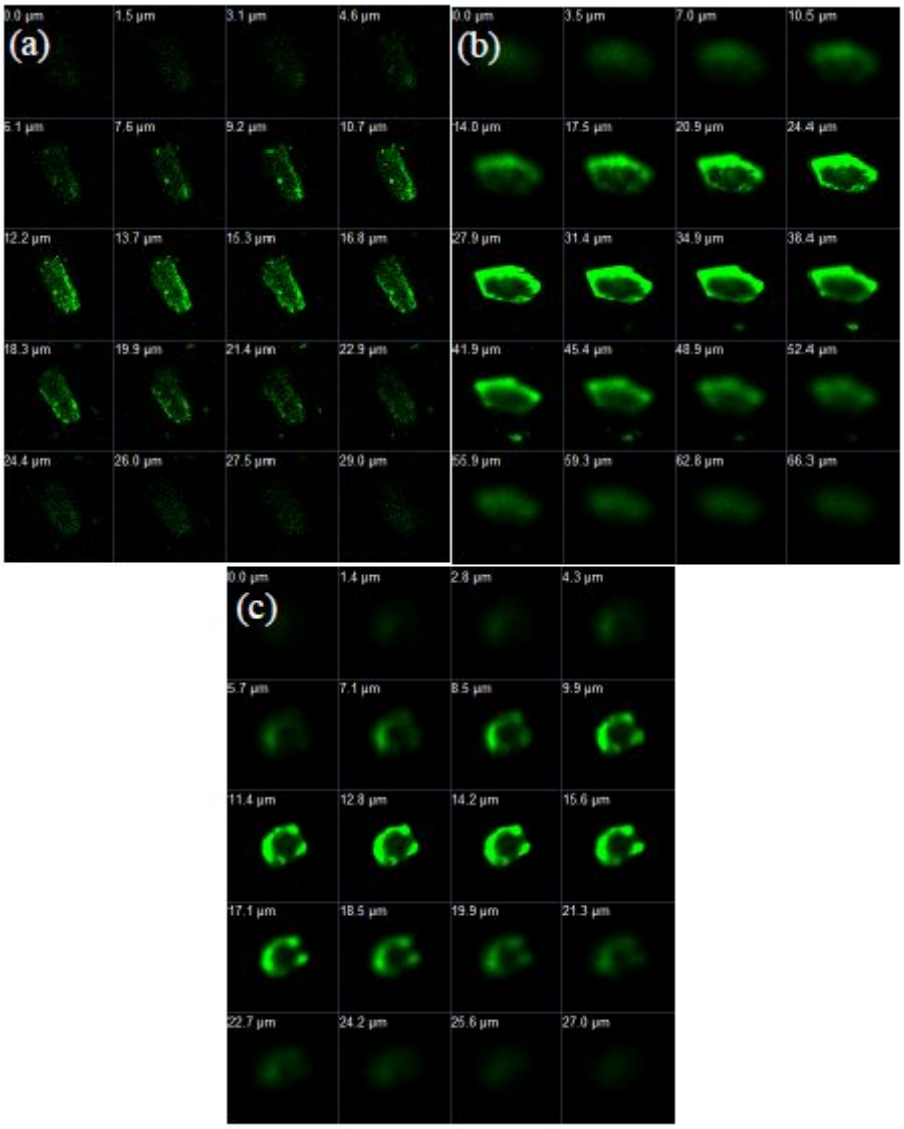

Figure 8. Z-stacked CLSM images of 1D + EGFP (a), 2D + EGFP (b), and 3D + EGFP (c). The excitation wavelength is 488 nm.

The catalytic activity and enantioselectivity of CAL-B conjugated MOFs and recycling experiment. We also applied this strategy to conjugate MOFs with a functional protein, such as an enzyme. We chose CAL-B (*Candida antarctica* lipase B) that catalyzes hydrolysis or formation of an ester. CALB is one of the most widely used enzymes because of its high activity and selectivity [29-30]. CAL-B was conjugated to the three MOFs through the same coupling methods. The amounts of proteins decorated on MOFs were determined as 0.12, 0.17, and 0.18 mg g^{-1} of the 1D-, 2D-, and 3D-MOFs, respectively (Table 1).

Table 1. The catalytic activity and enantioselectivity of CAL-B/MOF conjugates

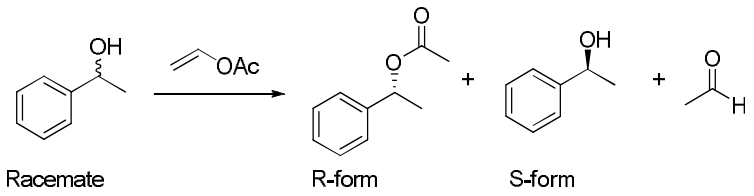

Enzyme	The amount of CAL-B protein decorated (mg g^{-1})	Specific activity (μmol min^{-1} mg^{-1})	Enantiomeric ratio (E)[a]
Free CAL-B	-	0.037 ± 0.013 [b]	>200
1D	-	n.d.[c]	-
1D+CAL-B	0.12	14± 3.7	>200
2D	-	n.d.	-
2D+CAL-B	0.17	23 ± 3.8	>200
3D	-	n.d.	-
3D+CAL-B	0.18	40 ± 3.3	>200

[a] E = enantiomeric ratio as defined by C. S. Chen, Y. Fujimoto, G. Girdaukas, C. J. Sih, *J. Am. Chem. Soc.* **1982**, *104*, 7294-7299. [b] Error are standard deviations for three measurements obtained from recycling experiments. [c] n.d. = not detected.

PXRD patterns showed that the structural integrity of frameworks was intact after CAL-B conjugation (Fig. 9). It is noteworthy to realize that

even the hydrolytically unstable 3D IRMOF-3 maintained its framework structure during the conjugation. For example, nitrogen sorption measurement at 77 K for the EGFP-conjugated 3D-MOF exhibited very low Brunauer-Emmett-Teller (BET) surface area, 15.0 m^2 g^{-1}, compared with the activated native 3D-MOF which showed BET surface area of 1605.1 m^2 g^{-1} (Fig. 10). The pore volume also significantly decreased from 0.78 cm^3 g^{-1} to 0.08 cm^3 g^{-1} after CAL-B-conjugation. These data clearly demonstrate the efficient outer surface functionalization of 3D-MOF by CAL-B.

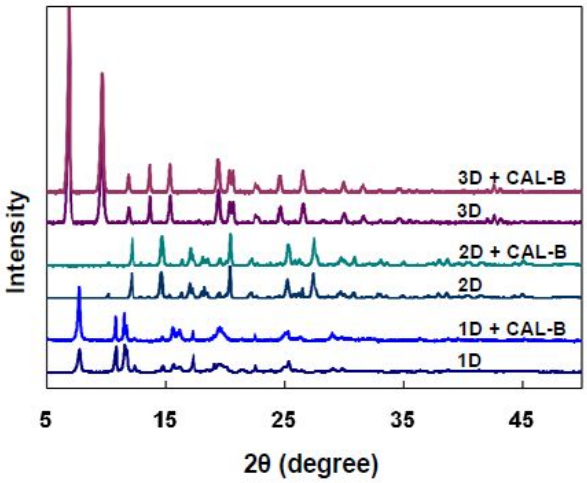

Figure 9. PXRD patterns of the 1D-, 2D- and 3D-MOFs, and CAL-B-conjugated 1D-, 2D- and 3D-MOFs.

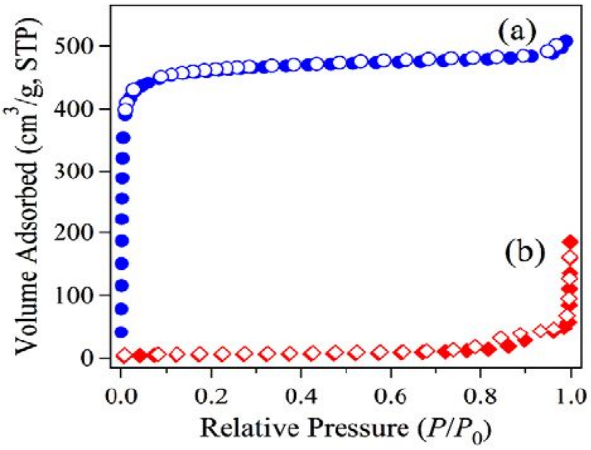

Figure 10. N_2 adsorption/desorption isotherms for the native 3D-MOF (a) and the CAL-B-3D-MOF (b) measured at 77 K. Both samples were activated at 393 K for 2 h.

To evaluate the activity of the immobilized CAL-B, we tested the catalytic activity in the transesterification of (±)-1-phenylethanol as a model reaction (Scheme 1). In addition, CAL-B has high enantioselectivity toward (*R*)-(+)-1-phenylethanol (*E* = >200) [31]. We also measured the enantioselectivity of the immobilized CAL-B and the free CAL-B. We compared the specific activities of the CAL-B coated coordination polymers with free CAL-B enzyme. In general, immobilized enzymes are more active in organic solvents than free enzymes and can be easily separated from the reaction mixture and re-used. We have measured and averaged the specific activities from three-times recycling experiments (Fig. 11, 12 and Table 1).

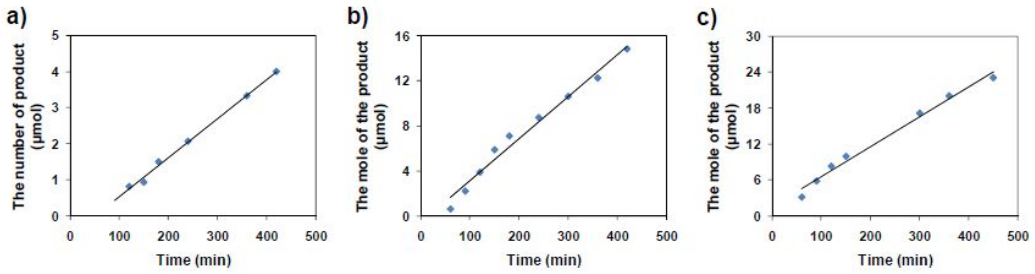

Figure 11. Measurements of the specific activities of CAL-B-conjugated MOFs: 1D-MOF + CAL-B (a), 2D-MOF + CAL-B (b), and 3D-MOF + CAL-B (c). Only a single measurement was shown as a representative example.

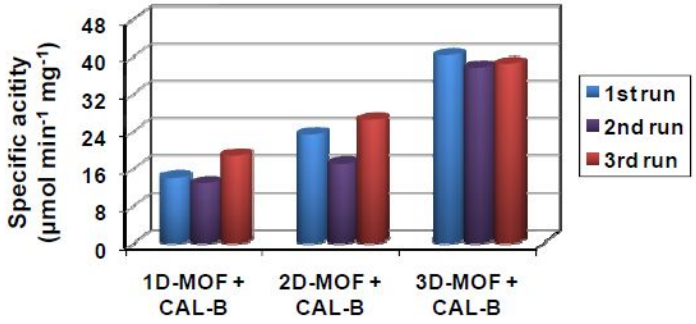

Figure 12. Recycling experiment results for the CAL-B-conjugated MOFs. The averaged values were shown in the Table 1.

The recycling did not cause a significant decrease of the activity CAL-B-coated coordination polymers indeed showed several hundred-fold higher activities and the same enantioselectivity of the product compared to the native CAL-B. Especially, the CAL-B on 3D-MOF showed about 10^3-fold higher activity than free CAL-B. In addition, the enantioselectivity of CAL-B coated on the three MOFs is as high as that of the free CAL-B. Despite the lack of detailed rate enhancement mechanism at the moment, we

speculate that the MOFs might provide confined spaces nearby the surface resided enzymes for substrates to contact enzymes more efficiently. The enhanced rate acceleration of 3D-MOF compared with 1D- and 2D-MOFs could be explained by the same speculation. In addition, the amino groups of IRMOF-3 presumably help to maintain the optimum pH for the enzymatic reaction because an addition of a weak base to an enzymatic reaction media can prevent a decrease of pH caused by formation of a by-product, such as acetic acid which can be generated by hydrolysis of vinyl acetate [28].

Conjugated EGFP to CAL-B decorated 3D-MOF. After CAL-B was incorporated onto 3D-MOF, the CAL-B decorated 3D-MOF is still bearing unmodified amino groups. These amino groups may be served as further modification sites. Thus, the CAL-B-decorated 3D-MOF can be conjugated with another protein. We introduced EGFP (0.063 mg g^{-1}), which was activated by EDC, to the CAL-B-decorated 3D-MOF (Fig. 13) to form dual protein-conjugated MOF. The dual proteinconjugated 3D-MOF showed multi-functionality, *i.e.* fluorescence and transesterification activity (38 μmol min^{-1} mg^{-1}).

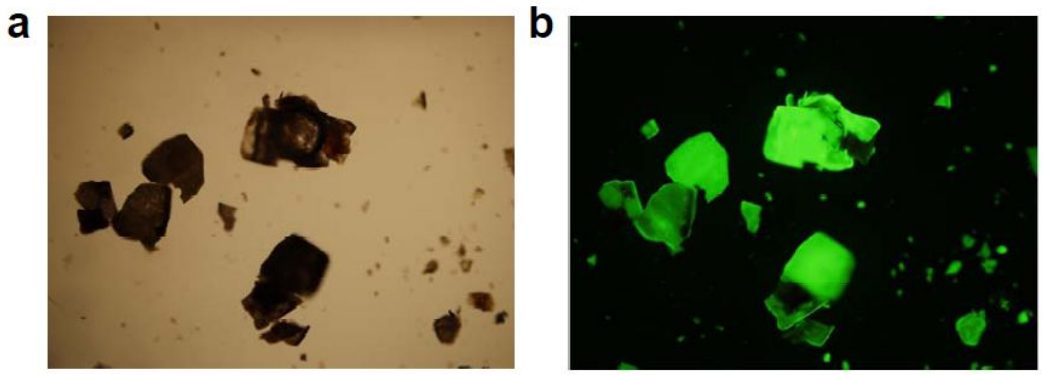

Figure 13. Microscopic images of dual protein decorated 3D-MOF: an optical microscopic image (a) and a fluorescence microscopic image (b).

Conclusion

The protein, Enhance Green Fluorescent Protein and *Candida antarctica* lipase B, was covalently bound to the MOFs after simple treatment by EDC. The immobilized enzyme with MOFs has the high specific activity compared free enzyme in organic solvent. These results clearly indicate that functional proteins can be decorated on MOFs without losing their functions and recyclable without significant loss of the activity. media. This study also This approach therefore is an important step towards the functional modification of MOFs.

Experimental section

General Methods. Chemicals, buffers, and CAL-B were purchased from TCI or Sigma-Aldrich. The Ni-NTA agarose resin was purchased from QIAGEN.

Synthesis of the compound 1D. A mixture of $In(NO_3)_3 \cdot xH_2O$ (0.301 g, 1.0 mmol) and 1,4-phenylenediacetic acid (0.388 g, 2.0 mmol) in 20 ml *N*,*N*-diethylformamide (DEF) was heated in a Teflon-lined high pressure bomb at 150 ºC for 72 h. Colorless needles were separated by filtration and washed with DEF and ethanol. The crystals were air-dried at ambient conditions. X-ray quality needles were chosen from the mother liquor.

Single-Crystal Structural Analysis of 1D-MOF (1). Data were collected on a Bruker SMART APX diffractometer using Mo-Kα radiation (λ = 0.71073 Å). The data were obtained at 150-170 (2) K and refined by full-matrix least-squares refinements on *F* 2 using all data with SHELXTL programs. The crystallographic data are listed in Table 2. Selected bond lengths and angles are listed in Table 3.

Table 2. Crystal data and structure refinement for 1.

Empirical formula	C_{24} H_{28} In N O_8
Frormula weight	573.29
Temperature	293(2) K
Wavelength	0.71073 Å
Crystal system	Monoclinic
Space group	Cc
Unit cell dimensions	a = 19.192(4) Å α = 90.00°
	b = 8.7720(18) Å β = 120.71(3) °
	c = 16.666(3) Å γ = 90.00°
Volume	2412.3(8) $Å^3$
Z	4
Density (calcuated)	1.579 Mg/m^3
Absorption coefficient	1.029 mm^{-1}
F(000)	1168
Crystal size	0.15 x 0.05 x 0.05 mm^3
Theta range for data collection	2.47 to 25.995.
Index ranges	-17 ≤ h ≤ 23, -10 ≤ k ≤ 9, -20 ≤ l ≤ 20
Reflections collected	6523
Independent reflection	3280 [R(int) = 0.0358]
Completeness to theta =25.99	99.7 %
Absorption correction	None
Refinement method	Full-matrix least-squares on F^2
Data / restraints / parameters	3280 / 2 / 309
Goodness-of-fit on F_2	0.991
Final R indices [I>2sigma(I)]	R1 = 0.0382, wR_2 = 0.0764
R indices (all data)	R1 = 0.0650, wR_2 = 0.0847
Absolute structure parameter	0.00
Largest diff. peak and hole	0.474 and -0.365 $e.Å^{-3}$

Table 3. Selected bond lengths [Å] and angles [°] for **1**.

In(1)-O(7)	2.250(11)	O(5)-C(11)	1.15(2)	O(5)-In(1)-O(6)	54.5(5)
In(1)-O(3)	2.251(13)	O(6)-C(11)	1.303(19)	O(8)-In(1)-O(6)	135.6(5)
In(1)-O(1)	2.278(14)	O(4)-C(3)	1.28(2)	O(2)-In(1)-O(6)	129.6(5)
In(1)-O(5)	2.285(14)	C(15)-C(21)	1.38(2)	O(7)-In(1)-O(4)	81.5(5)
In(1)-O(8)	2.291(12)	C(3)-O(3)	1.15(2)	O(3)-In(1)-O(4)	54.3(4)
In(1)-O(2)	2.304(11)	C(18)-C(8)#2	1.52(3)	O(1)-In(1)-O(4)	167.7(5)
In(1)-O(6)	2.306(14)	C(21)-C(20)	1.32(3)	O(5)-In(1)-O(4)	103.6(3)
In(1)-O(4)	2.373(13)	C(21)-C(2)#2	1.50(3)	O(8)-In(1)-O(4)	86.6(6)
In(1)-C(1)	2.524(16)	C(20)-C(19)	1.42(3)	O(2)-In(1)-O(4)	133.8(4)
In(1)-C(3)	2.66(2)	N(1S)-C(2S)	1.379(17)	O(6)-In(1)-O(4)	81.4(5)
In(1)-C(11)	2.660(10)	N(1S)-C(3S)	1.40(2)	O(7)-In(1)-C(1)	109.2(5)
O(1)-C(1)	1.17(2)	C(2S)-C(1S)	1.499(12)	O(3)-In(1)-C(1)	111.2(6)
O(8)-C(17)	1.30(2)	C(4S)-C(3S)	1.62(3)	O(1)-In(1)-C(1)	27.5(6)
C(12)-C(13)	1.42(3)			O(5)-In(1)-C(1)	78.4(5)
C(12)-C(11)	1.50(2)	O(7)-In(1)-O(3)	131.5(4)	O(8)-In(1)-C(1)	89.8(5)
C(14)-C(15)	1.32(2)	O(7)-In(1)-O(1)	87.1(5)	O(2)-In(1)-C(1)	30.4(5)
C(14)-C(13)	1.33(2)	O(3)-In(1)-O(1)	138.0(5)	O(6)-In(1)-C(1)	111.5(6)
C(17)-O(7)	1.268(18)	O(7)-In(1)-O(5)	131.8(4)	O(4)-In(1)-C(1)	164.1(5)
C(17)-C(18)	1.40(2)	O(3)-In(1)-O(5)	82.4(4)	O(7)-In(1)-C(3)	108.4(5)
C(1)-O(2)	1.286(19)	O(1)-In(1)-O(5)	80.7(5)	O(3)-In(1)-C(3)	25.4(5)
C(1)-C(2)	1.65(2)	O(7)-In(1)-O(8)	56.1(4)	O(1)-In(1)-C(3)	163.4(5)
C(4)-C(3)	1.60(3)	O(3)-In(1)-O(8)	98.3(5)	O(5)-In(1)-C(3)	92.8(5)
C(4)-C(5)	1.61(2)	O(1)-In(1)-O(8)	90.80(19)	O(8)-In(1)-C(3)	93.0(5)
C(5)-C(10)	1.34(2)	O(5)-In(1)-O(8)	167.5(5)	O(2)-In(1)-C(3)	106.0(5)
C(5)-C(6)	1.43(2)	O(7)-In(1)-O(2)	130.87(16)	O(6)-In(1)-C(3)	96.4(6)
C(13)-C(19)	1.40(2)	O(3)-In(1)-O(2)	81.3(5)	O(4)-In(1)-C(3)	28.9(5)
C(8)-C(7)	1.37(2)	O(1)-In(1)-O(2)	58.0(5)	C(1)-In(1)-C(3)	136.2(6)
C(8)-C(9)	1.44(2)	O(5)-In(1)-O(2)	79.4(5)	O(7)-In(1)-C(11)	108.8(4)
C(8)-C(18)#1	1.52(3)	O(8)-In(1)-O(2)	88.3(5)	O(3)-In(1)-C(11)	92.2(5)
C(6)-C(7)	1.45(2)	O(7)-In(1)-O(6)	79.9(5)	O(1)-In(1)-C(11)	88.6(5)
C(2)-C(21)#1	1.50(3)	O(3)-In(1)-O(6)	108.4(2)	O(5)-In(1)-C(11)	25.5(5)
C(10)-C(9)	1.33(2)	O(1)-In(1)-O(6)	92.2(5)	O(8)-In(1)-C(11)	164.8(5)

O(2)-In(1)-C(11)	104.1(5)	C(3)-C(4)-C(5)	105.4(13)	O(6)-C(11)-In(1)	60.1(7)
O(6)-In(1)-C(11)	29.3(5)	C(10)-C(5)-C(6)	119.7(16)	C(12)-C(11)-In(1)	170.2(12)
O(4)-In(1)-C(11)	90.7(5)	C(10)-C(5)-C(4)	125.7(14)	C(3)-O(4)-In(1)	88.0(12)
C(1)-In(1)-C(11)	96.6(5)	C(6)-C(5)-C(4)	114.6(15)	C(14)-C(15)-C(21)	119.4(16)
C(3)-In(1)-C(11)	91.9(2)	C(14)-C(13)-C(19)	116.1(17)	O(3)-C(3)-O(4)	120.3(19)
C(1)-O(1)-In(1)	88.1(11)	C(14)-C(13)-C(12)	127.8(17)	O(3)-C(3)-C(4)	131.3(17)
C(17)-O(8)-In(1)	94.0(10)	C(19)-C(13)-C(12)	116.0(18)	O(4)-C(3)-C(4)	108.5(17)
C(13)-C(12)-C(11)	124.8(16)	C(7)-C(8)-C(9)	118.1(17)	O(3)-C(3)-In(1)	57.1(11)
C(15)-C(14)-C(13)	127.2(16)	C(7)-C(8)-C(18)#1	118.2(17)	O(4)-C(3)-In(1)	63.2(10)
O(7)-C(17)-O(8)	112.3(16)	C(9)-C(8)-C(18)#1	123.5(15)	C(4)-C(3)-In(1)	171.6(12)
O(7)-C(17)-C(18)	127.3(14)	C(5)-C(6)-C(7)	114.6(16)	C(8)-C(7)-C(6)	123.2(16)
O(8)-C(17)-C(18)	119.6(15)	C(21)#1-C(2)-C(1)	121.2(15)	C(17)-C(18)-C(8)#2	108.4(15)
O(1)-C(1)-O(2)	129.6(17)	C(9)-C(10)-C(5)	126.2(17)	C(20)-C(21)-C(15)	115.3(17)
O(1)-C(1)-C(2)	121.7(17)	C(11)-O(5)-In(1)	95.8(10)	C(20)-C(21)-C(2)#2	119.1(17)
O(2)-C(1)-C(2)	108.2(15)	C(10)-C(9)-C(8)	117.5(16)	C(15)-C(21)-C(2)#2	125.1(18)
O(1)-C(1)-In(1)	64.4(11)	C(11)-O(6)-In(1)	90.6(10)	C(21)-C(20)-C(19)	126.1(18)
O(2)-C(1)-In(1)	65.3(8)	O(5)-C(11)-O(6)	117.8(12)	C(13)-C(19)-C(20)	115.5(17)
C(2)-C(1)-In(1)	169.8(12)	O(5)-C(11)-C(12)	131.0(15)	C(2S)-N(1S)-C(3S)	108.1(10)
C(1)-O(2)-In(1)	84.3(10)	O(6)-C(11)-C(12)	110.6(15)	N(1S)-C(2S)-C(1S)	111.1(11)
C(17)-O(7)-In(1)	97.0(10)	O(5)-C(11)-In(1)	58.7(8)	N(1S)-C(3S)-C(4S)	113.2(11)

Symmetry transformations used to generate equivalent atoms:
#1 x,-y,z+1/2 #2 x,-y,z-1/2

Expression and purification of the EGFP. The EGFP proteins were expressed and purified according to the literature [32].

Activation of 1D-MOF. The 1D-compound (100 mg) was suspended in MES buffer (5 ml, 0.1 M, pH 5.0) and EDC (100 mg) was added. The mixture was then shaken for 20 min and centrifuged. After the supernatant being decanted, the activated 1D was washed three times with PBS buffer (5 ml, 0.1 M, pH 7.3) and resuspended in PBS buffer (1 ml).

Activation of 2D- and 3D-MOF. The 2D- and 3D-MOFs (100 mg) were suspended in a solution (10 ml) of 1% w/v hexanediamine and 1% w/v DCC in dichloromethane and shaken for 4 hr at 10 ºC. The activated compounds were washed with dichloromethane (10 ml), acetone (10 ml), and ice-cold water (10 ml), and resuspended in PBS buffer (1 ml).

Conjugation of proteins with the activated 1D-, 2D-, and 3D-MOF. The above suspension in PBS buffer (100 μL) and protein solution (100 μL, 1 mg ml^{-1}) were mixed and incubated at 4 ºC for 1 h (in the cases of 1D- and 3D-MOFs) or 16 h (in the case of 2D-MOF). The protein- conjugated 1D-, 2D- and 3D-MOFs were washed three times with PBS buffer (1 ml) and air-dried. The amount of the proteins in the solution was determined by Bio-Rad Protein Assay kit (Bio-Rad) according to the manufacturer instructions. The amount of the conjugated proteins to MOFs was estimated by the difference of the amount of protein in the supernatant before and after incubation.

Conjugation of EGFP with the CAL-B-conjugated 3D-MOF. EDC (10 mg) was added to an EGFP solution (100 μL, 3.4 mg ml^{-1} in 10 mM of PBS buffer, pH 7.3). The solution was incubated overnight at 4 ºC. The CAL-B-conjugated IRMOF-3 was added to the activated EGFP solution. The mixture was incubated at 4 °C for 16 h. The CAL-B and EGFP-conjugated 3D-MOF was washed three times with PBS buffer (1 ml, 10 mM, pH 7.3).

Spectroscopic Techniques. The emission spectra with set of λ_{ex} = 488 nm were recorded in the wavelength range of 450–50 nm with an LS 55 Luminescence Spectrometer. The slit width for excitation and emission was 5.0 nm and the scan speed was 100 nm min^{-1}.

Confocal Laser Scanning Microscope (CLSM). CLSM images of the EGFP-coated MOFs were obtained by using a Zeiss LSM 700 system. Green channel images were obtained with an excitation wavelength of 488 nm.

X-ray Powder Diffraction (PXRD). PXRD patterns were obtained by using a Bruker D8 Focus with an X-ray tube with a Cu target.

Nitrogen Sorption Analysis. The N_2 sorption analysis was performed on a Belsorp-miniII (BEL Japan) at 77 K. The fresh as-prepared 3D-MOF (IRMOF-3) crystals immediately soaked in $CHCl_3$ in a screw-capped vial were shaken for two days. The $CHCl_3$-exchanged sample was dried at 393 K under high vacuum for 2 h before measurements. The CAL-B-3D-MOF was also dried at 393 K under the same condition.

Measurement of catalytic activities of the CAL-B-conjugated MOFs toward the transesterification of (±)-1-phenylethanol. The CAL-B-conjugated MOFs or free CAL-B powders were mixed with (±)-1-phenylethanol (1 mmol) and vinyl acetate (1 mmol) in isopropylether (5 ml). The samples (100 μL) were retrieved with 30-min intervals for 420 min and analyzed by a GC with a chiral column (Cyclosil-B 30 m × 90.25 mm). The reactions were finished

before 5% conversion reached in order to obtain the initial reaction rates. After the reaction was completed, the CAL-B-conjugated MOFs were recovered by centrifugation and washed three times with isopropylether. The recovered CAL-B conjugated MOFs were used for the next run under the same reaction condition. The reactions were carried out three times. The GC condition: initial column temperature 80 ºC for 10 min, ramp up to 120 ºC at a rate of 2.5 ºC min^{-1} and then held at 120 ºC for 10 min.

References

1. Kitagawa, S.; Kitaura, R.; Noro, S.-I. *Angew. Chem. Int. Ed.* **2004**, *43*, 2334–2375.
2. Rosi, N. L.; Eckert, J.; Eddaoudi, M.; Vodak, D. T.; Kim, J.; Keeffe, M. O''; Yaghi, O. M. *Science* **2003**, *300,* 1127–1129.
3. Frey, G.; Latroche, M.; Serre, C.; Millange, F.; Loiseau, T.; Percheron-Gugan, A. *Chem. Commun*. **2003**, 2976–2977.
4. Rowsell, J. L. C.; Millward, A. R.; Park, K. S.; Yaghi, O. M. *J. Am. Chem. Soc.* **2004**, *126,* 5666–5667.
5. Rowsell, J. L.; Yaghi, C. O. M. *Angew. Chem. Int. Ed.* **2005**, *44,* 4670–4679.
6. Eddaoudi, M.; Kim, J.; Rosi, N.; Vodak, D.; Wachter, J.; O''Keeffe, M.; Yaghi, O. M. *Science* **2002**, *295,* 469–472.
7. Ma, S.; Sun, D.; Simmons, J. M.; Collier, C. D.; Yuan, D.; Zhou, H.-C. *J. Am. Chem. Soc.* **2008**, *130,* 1012–1016.
8. Matsuda, R.; Kitaura, R.; Kitagawa, S.; Kubota, Y.; Belosludov, R. V.; Kobayashi, T. C.; Sakamoto, H.; Chiba, T.; Takata, M.; Kawazoe,

Y.;Mita, Y. *Nature* **2005**, *436*, 238–241.

9. Millward, A. R.; Yaghi, O. M. *J. Am. Chem. Soc*. **2005**, *127,* 17998–17999.
10. Banerjee, R.; Phan, A.; Wang, B.; Knobler, C.; Furukawa, H.; O"Keeffe, M.; Yaghi, O. M. *Science* **2008**, *319,* 939–943.
11. Fujita, M.; Kwon, Y. J.; Washizu, S.; Ogura, K. *J. Am. Chem. Soc.* **1994**, *116,* 1151–1152.
12. Li, H.; Eddaoudi, M.; O"Keeffe, M.; Yaghi, O. M. *Nature* **1999**, *402,* 276–279.
13. Huh, S.; Kwon, T.-H.; Park, N.; Kim, S.-J.; Kim, Y. *Chem. Commun.*, **2009**, 4953-4955.
14. Gu, J.-M.; Kwon, T.-H.; Park, J.-H.; Huh, S. *Dalton Trans*. **2010**, *39*, 5608-5610.
15. Wang, Z.; Cohen, S. M. *J. Am. Chem. Soc.* **2007**, *129*, 12368–.12369.
16. Seo, J.; Whang, S.D.; Lee, H.; Jun, S. I.; Oh, J.; Jeon, Y. J.; Kim, K. *Nature* **2000**, *404*, 982–986.
17. Wang, Z.; Cohem, S. M. *Angew. Chem. Int. Ed.* **2008**, *47*, 4699–4702. 18. Tanabe, K. K.; Wang, Z.; Cohen, S. M. *J. Am. Chem. Soc.* **2008**, *130*, 8508–8517.
19. Ingelson, M. J.; Barrio, J. P.; Guilbaud, J.-B;. Khimyak, Y. Z.; Rosseinsky, M. J. *Chem. Commun*. **2008**, 2680–2682.
20. Costa, J. S.; Gamez, P.; Black, C. A.; Roubeau, O.; Teat, S.; Reedijk, J. *Eur. J. Inorg. Chem.* **2008**, 1551–1554.
21. Burrows, A. D.; Frost, C. G.; Mahon, M. F.; Richardson, C. *Angew. Chem. Int. Ed.* **2008**, *47*, 8482–8486.
22. Gadzikwa, T.; Lu, G.; Stern, C. L.; Wilson, S. R.; Hupp, J. T.; Nguyen,

S. T. *Chem. Commun*. **2008**, 5493-5495.

23. Wang, Z.; Tanabe,;K. K.; Cohen, S. M. *Inorg. Chem*. **2009**, *48*, 296–306.
24. Teppei, Y.; Kitagawa, H. *J. Am. Chem. Soc.* **2009**, *131*, 6312–6313.
25. Taylor-Pashow, K. M. L.; Rocca, J. D.; Xie, Z.; Tran, S.; Lin, W. *J. Am. Chem. Soc.* **2009**, *131*, 14261–14263.
26. Huh, S.; Jung, S.; Kim, Y.; Kim, S.; Park, S. *Dalton Trans*. **2010**, *39*, 1261-1265.
27. Roswell, J. L. C.; Yaghi, O. M. *J. Am. Chem. Soc.* **2006**, *128*, 1304–1315.
28. Dhimitruka, I.; SantaLucia, J. Jr. *Org. Lett*. **2006**, *8*, 47–50.
29. Park, S.; Kazlauskas, R. J. *J. Org. Chem*. **2001**, *66*, 8395–8401.
30. Kirk, O.; Christensen, M. W. *Org. Proc. Res. Dev*. **2002**, *6*, 446-451.
31. Jung, S.; Park, S. *Biotechnol. Lett*. **2008**, *30*, 717–722.
32. Jung, S.; Huh, S.; Cheon, Y.-P.; Park, S. *Chem. Commun.* **2009**, 5003-5005.

Chapter 3. Appendix

Two-dimensional metal–organic frameworks with blue luminescence†

Seong Huh,[a] Suhyun Jung,[b] Youngmee Kim,[c] Sung-Jin Kim[c] and Seongsoon Park*[b]

Received 5th August 2009, Accepted 19th October 2009
First published as an Advance Article on the web 23rd November 2009
DOI: 10.1039/b916176g

Three new isostructural two-dimensional metal–organic frameworks (MOFs), $[M(bpydc)(H_2O)\cdot H_2O]_n$ where M = Zn (**1**); Co (**2**); Ni (**3**) and the bpydc is 2,2′-bipyridine-5,5′-dicarboxylate), were prepared by various methods such as hydrothermal, ultrasonic and microwave-assisted synthetic methods. Microcrystalline **1** could be obtained by using ultrasonification or microwave irradiation in a short time. Their solid-state structures were revealed by X-ray crystallography. The coordination environment of the metal ions is distorted octahedral geometry. The metal ions are coordinated by two nitrogen atoms from the bipyridyl moiety, two oxygen atoms from one carboxylate in a bidentate manner, one oxygen atom from another carboxylate in a monodentate manner, and one oxygen atom from the aqua ligand. The multiple coordination modes of the bpydc ligand led to a novel topologically interesting two-dimensional sheet structure; a 6-connected uninodal net with Schläfli symbol of $3^3\cdot4^4\cdot5^5\cdot6^2\cdot7$. Thermal and luminescence properties of the three MOFs were also investigated. The weight maintained constant in the range 290–342 °C for **1**, 250–470 °C for **2**, and 275–470 °C for **3** after the initial weight loss related to the dehydration steps. In particular, $[Zn(bpydc)(H_2O)\cdot H_2O]_n$ (**1**) displays strong solid state blue luminescence.

Introduction

Nanoporous metal–organic frameworks (MOFs) are interesting materials in the material research area because of their large void spaces and unique geometrical structures.[1,2] These zeotype materials often maintain thermally robust crystalline frameworks with a permanent porosity. This nanoporosity makes MOFs potentially useful in catalysis, separation, nonlinear optics, and gas storage.[3] Luminescent MOFs can be prepared by combining metal ions with fluorescent ligands. For example, Li *et al.* reported a luminescent Zn-MOF containing both 4,4′-biphenyldicarboxylate and 1,2-bipyridylethene.[4] Luminescent MOFs are garnering more interest because of their potential applications as fluorescent sensors or in light-emitting devices (LEDs).[4,5]

Typically, luminescent aromatic organic molecules and conjugated organic polymers have been employed for LED applications.[6] Although high solubility of organic LED materials in solvents makes easier processing into thin films (*e.g.* from solution), organic LED materials lack enough thermal and chemical stabilities. In addition, the preparation of blue (~450–470 nm) emitter, one of the important color components in LEDs, remains challenging because of the large energy requirement for excitation.[7] Pure inorganic blue LED materials, such as GaN and some doped (Ba, Sr)$MgAl_{10}O_{17}$ phases and some nitrides, can be used for improvement of chemical and thermal stability. Nevertheless, the disadvantage of these inorganic materials is difficulties in processing, although many of these are easily produced in nanoparticle form.[8]

MOFs are alternative candidates for LED applications owing to their better thermal stability and solvent resistance than pure organic compounds.[9] Besides, the processing temperatures and conditions for LEDs are probably amenable to deposition of MOFs for applications such as organic LEDs.

Multidentate ligands are usually chosen for preparing MOFs.[3b] Most MOFs are constructed by a unit of a symmetric molecule, which can bridge neighboring metal ions, such as 1,4-benzenedicarboxylate[10] and 1,3,5-benzenetricarboxylate.[11] Choosing a suitable ligand is of significant importance towards multifunctional MOFs because the structural characteristics and physicochemical properties of MOFs primarily depend on the nature of bridging ligands.

The multidentate ligand 2,2′-bipyridine-5,5′-dicarboxylate (bpydc) contains a bipyridyl moiety and two carboxylate groups, which can multiply coordinate to several metal ions.[12] The bipyridyl group can chelate a metal ion and the two carboxylates, which are positioned at each end of the bipyridyl ring, can further connect two metal ions in three distinct coordination modes (Scheme 1). These multiple coordination modes of bpydc may lead to MOFs with topologically interesting structures. Furthermore, the inherent weak luminescence of the bpydc molecule can be enhanced by coordination to a metal ion.[13] Despite the potential usefulness of the bpydc ligand for functional MOFs, MOFs containing bpydc have been less explored to date.[12]

[a]*Department of Chemistry and Protein Research Center for Bio-Industry, Hankuk University of Foreign Studies, Yongin, 449-791, Korea*
[b]*Department of Chemistry, Center for NanoBio Applied Technology, and Institute of Basic Sciences, Sungshin Women's University, Seoul, 136-742, Korea. E-mail: spark@sungshin.ac.kr; Fax: 82 2 920 2047; Tel: 82 2 920 7646*
[c]*Department of Chemistry and Nano Science, Ewha Womans University, Seoul, 120-750, Korea*

† Electronic supplementary information (ESI) available: X-ray crystallographic data, XRD patterns for ultrasonic synthesis of **1**, microscopic images of **1**, and Tables S1–S4. CCDC reference numbers 679395 (**1**), 727193 (**2**) and 727194 (**3**). For ESI and crystallographic data in CIF or other electronic format see DOI: 10.1039/b916176g

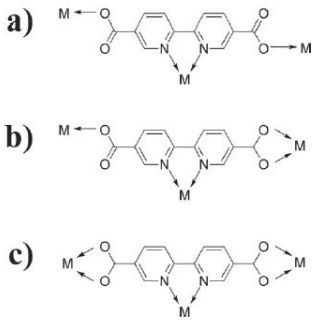

Scheme 1 The possible binding modes of 2,2′-bipyridine-5,5′-dicarboxylate to metal ions.

Experimental section

Materials and physical measurements

The ligand 2,2′-bipyridine-5,5′-dicarboxylic acid (bpydc) was purchased from Sigma-Aldrich and used as received. The metal salts and solvents were reagent grade commercial products. Thermogravimetric analyses were carried out on a TGA Q5000 (TA Instruments) under constant flow of nitrogen. The excitation and emission spectra were recorded in the wavelength range of 350–650 nm with an LS 55 Luminescence Spectrometer. The slit width for excitation and emission was 8.0 nm and the scan speed was 20 nm min^{-1}. X-ray powder diffraction (PXRD) experiments were performed by using a Bruker D8 Focus with an X-ray tube with a Cu target.

Hydrothermal syntheses of 1-3

Metal nitrates (0.4 mmol), bpydc (24.4 mg, 0.1 mmol), and distilled water (10 mL) were mixed in a teflon-lined high pressure bomb (50 mL capacity). The product compounds were prepared hydrothermally at 150 °C for 48 h. Rod shape crystals were retrieved by a filtration and washed with hot water. The crystals were air-dried for 24 h. $[Zn(bpydc)(H_2O)\cdot H_2O]_n$ (**1**): IR data (KBr pellet, cm^{-1}): 3743(w, br), 1652(s), 1558(s), 1085(s, br), 775(w), 667(w); analytically calcd (%) for $C_{12}H_{10}N_2O_6Zn$: C 41.94, H 2.93, N 8.15; found C 42.09, H 2.95, N 7.98. $[Co(bpydc)(H_2O)\cdot H_2O]_n$ (**2**): IR data (KBr pellet, cm^{-1}): 3599(w, br), 3518(w, br), 3373(s, br), 3047(s, br), 1614(s), 1541(w), 1433(m), 1377(s), 1163(m), 1034(m), 874(w), 850(m), 775(s), 710(m), 573(w). 422(m, br); analytically calcd (%) for $C_{12}H_{10}CoN_2O_6$: C 42.73, H 2.99, N 8.31; found C 42.66, H 3.03, N 8.59. $[Ni(bpydc)(H_2O)\cdot H_2O]_n$ (**3**): IR data (KBr pellet, cm^{-1}): 3599(w, br), 3508(w, br), 3392(s, br), 3003(s, br), 1616(s), 1541(w), 1437(m), 1377(s), 1163(m), 1140(w), 1036(m), 876(w), 850(m), 775(s), 710(m), 575(w). 430(m, br); analytically calcd (%) for $C_{12}H_{10}N_2NiO_6$: C 42.78, H 2.99, N 8.31; found C 41.92, H 3.04, N 8.19.

Ultrasonication- or microwave-assisted synthesis of 1

$Zn(NO_3)_2\cdot 6H_2O$ (118.8 mg, 0.4 mmol), bpydc (24.4 mg, 0.1 mmol), and with or without $LiOH\cdot H_2O$ (8.39 mg, 0.2 mmol) were added in distilled water (10 mL). For ultrasonic method, the reaction mixture was sonicated for 90, 120, and 180 min using an ultrasonic bath (Bransonic 2510*R*-DTH, 100 W, 42 kHz) at room temperature. For microwave-assisted synthesis, the reaction mixture was heated at 95 °C for 9 min with setting at maximum 300 W using a microwave reactor (Discover S-class system) and then cooled to room temperature. The products were washed with hot water and ethanol, and air-dried.

Crystallographic studies

Data were collected on a Bruker SMART APEX diffractometer or a Nonius Kappa CCD diffractometer using Mo-Kα radiation (λ = 0.71073 Å). The data were obtained at 150-170(2) K and refined by full-matrix least-squares refinements on F^2 using all data with SHELXTL programs. The crystallographic data for compounds **1**, **2**, and **3** are listed in Table 1. Selected bond lengths and angles are listed in Table S1 in the ESI. CCDC reference numbers 679395 (**1**), 727193 (**2**) and 727194 (**3**).†

Results and discussion

Syntheses and crystal structures

The bpydc ligand was allowed to react with Zn(II), Co(II), and Ni(II) ions to form **1**, **2**, and **3**, respectively. All three compounds were hydrothermally synthesized in a teflon-lined high pressure bomb. The bpydc ligand was mixed with four equivalent metal ions in distilled water and then the reaction mixture was heated at 150 °C for 48 h. The crystalline products were obtained after cooling to room temperature.

All three compounds (**1–3**) are isostructural (Table 1), and the crystal structure showed that bpydc binds to metal ions through both bipyridine and carboxylates in mode (b) (Scheme 1). The coordination geometry around metal ions are distorted octahedral constructed by two nitrogen atoms from the bipyridyl group, two oxygen atoms from one carboxylate, one oxygen atom from the other carboxylate, and one oxygen atom from the aqua ligand (Fig. 1). This N_2O_4 coordination around the metal ion has *mer*-arrangement (two N atoms and one O atom from water, and three O atoms from two carboxylates in two perpendicular planes).

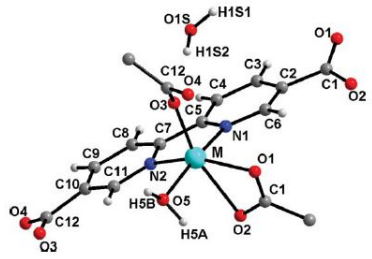

Fig. 1 The coordination environment of the metal center for the compounds **1–3** (M = Zn for **1**, Co for **2**, and Ni for **3**). Compounds **1–3** are isostructural. One water molecule per metal ion occupies the internal cavity.

Table 1 Crystal data and collection parameters for **1–3**

Compounds	1	2	3
Empirical formula	$C_{12}H_{10}N_2O_6Zn$	$C_{12}H_{10}CoN_2O_6$	$C_{12}H_{10}N_2NiO_6$
M/g mol^{-1}	343.59	337.15	336.93
Crystal system	Monoclinic	Monoclinic	Monoclinic
Space group	$P2_1/n$	$P2_1/n$	$P2_1/n$
a/Å	11.9962(13)	11.9696(6)	11.9640(9)
b/Å	8.2565(9)	8.1857(5)	8.2127(7)
c/Å	12.6200(13)	12.6795(8)	12.5386(6)
β(°)	98.823(2)	97.507(4))	97.170(4)
U/Å^3	1235.2(2)	1231.68(12)	1222.37(15) Å^3
Z	4	4	4
T/K	170(2)	150(2)	150(2)
Density (calculated)/Mg m^{-3}	1.848	1.818	1.831
μ/mm^{-1}	2.020	1.425	1.619
F(000)	696	684	688
Crystal size/mm	0.25 × 0.20 × 0.20	0.15 × 0.10 × 0.07	0.12 × 0.09 × 0.04
Data/restraints/parameters	2058/4/206	2795/0/198	2791/0/190
Goodness-of-fit on F^2	1.099	1.058	1.029
Final R indices [$I > 2\sigma(I)$]	R_1 [a] = 0.0468	R_1 [a] = 0.0496	R_1 [a] = 0.0516
R indices (all data)	wR_2 [b] = 0.1220	wR_2 [b] = 0.1189	wR_2 [b] = 0.1016
Largest diff. peak and hole/e Å^{-3}	R_1 [a] = 0.0873	R_1 [a] = 0.0780	R_1 [a] = 0.1120
	wR_2 [b] = 0.1418	wR_2 [b] = 0.1381	wR_2 [b] = 0.1266
	1.699 and –2.451	0.621 and –0.726	1.118 and –0.668

[a] $R_1 = \sum(|F_o| - |F_c|)/\sum|F_o|$. [b] $wR_2 = \{\sum[w(|F_o|^2 - |F_c|^2)^2]/\sum[w(|F_o|^2)^2]\}^{1/2}$.

The bpydc ligand links two adjacent metal centers to form an infinite two-dimensional (2D) network (Fig. 2). In addition, two water molecules were found around the metal center. One water molecule directly binds to the metal ion with the distance of 2.076(3), 2.074(3), and 2.038(3) Å for **1**, **2**, and **3** (Table S1†), respectively, and the other occupies the cavities. The solvate water molecules are hydrogen bonded to the carboxylate groups (Table S2†). The cavity volume was calculated as 7.1% by PLATON. However, no significant adsorption of nitrogen was observed at 77 K after the samples were dried at 250 °C under high vacuum (data not shown).

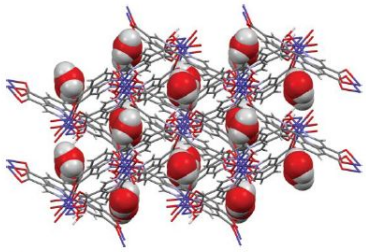

Fig. 2 The 2D structure of **1** along the *c*-axis. The solvate water molecules occupying 1D channels are represented in a CPK model. The volume without water solvates was calculated as 7.1% by PLATON.

The topology of the network assuming a metal atom as a central node is calculated as a new 6-connected uninodal net with Schläfli symbol $3^3{\cdot}4^4{\cdot}5^5{\cdot}6^2{\cdot}7$ (Fig. 3 and Table S3†). The central metal ion links by bridging ligands and has common vertex with six other metal atoms.

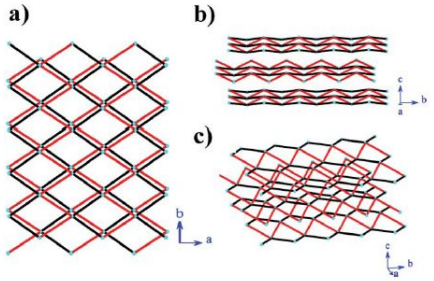

Fig. 3 a) A diagram of the 2D network along the *c*-axis. b) A view of the same network down the *a*-axis with a slight tilting. c) Angled view of the same network.

Thermal properties

The thermogravimetric analyses (TGA) of the MOFs **1**, **2**, and **3** were performed in the temperature range of 30–800 °C under constant N_2 flow (Fig. 4). The TG profiles indicated that all three compounds were thermally stable up to 200 °C without any loss of the weight. However, the compounds showed different thermal stability above 342 °C. The TGA profiles for all frameworks showed stepwise decrease of the weight until around 600 °C. For all three compounds, the first weight decrease in the range from 200 to around 270 °C was 10.2–11.3%, corresponding to the loss of two water molecules, a solvate water and an aqua ligand. The weight maintained constant in the range 290–342 °C for **1**, 250–470 °C for **2**, and 275–470 °C for **3**. The second weight loss for **1** was observed 342–570 °C for complete loss of the bpydc ligand. For **2** and **3** compounds, the second sharp weight loss from 470 °C

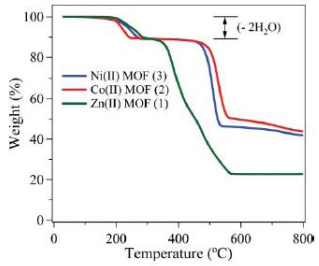

Fig. 4 The TGA profiles of **1**–**3**.

to 570 °C and to 540 °C, respectively, may be the result of partial loss of the bpydc ligand.

Photoluminescence properties of the compound 1

Photoluminescence measurements were performed through collecting both emission and excitation spectra for the control bpydc ligand and the compound **1** in the solid state (Fig. 5). The bpydc ligand exhibited a weak emission (Fig. 5a). It was excited at 395 nm and emitted at 445 nm presumably due to π–π^* transitions. Upon complexation of the bpydc ligand to zinc ions, the fluorescence was enhanced and the emission color was shifted to 452 nm with excitation at 372.5 nm (Fig. 5b). The blue fluorescent emission of **1** probably originates from the metal-perturbed intraligand fluorescent emission.[9] Interestingly, the blue fluorescence emission of **1** fits into the wavelength required (~450–470 nm) as a material for blue-light emitting diode devices.[7]

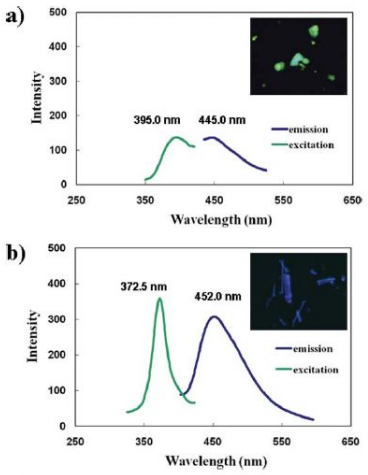

Fig. 5 Solid-state excitation and emission spectra of the bpydc ligand (a) and the MOF **1** (b) at room temperature. The insets are fluorescence microscopic images.

Ultrasonication- or microwave-assisted synthesis of the compound 1

Rapid and bulk synthesis of functional MOFs is economically important. However, solvothermal synthesis for **1** required 48 h. Recently ultrasonication- or microwave-assisted synthesis of MOF have been reported.[5a,14] Ultrasonication- or microwave-assisted synthesis significantly reduces the reaction time compared to the solvothermal synthesis, although these methods produce smaller MOF particles. We applied ultrasonication and microwave to the synthesis of **1** to reduce the reaction time. In the ultrasonication-assisted synthesis, we varied the reaction time from 90 min to 180 min with 30-min intervals. The PXRD analyses showed that the sample prepared by an irradiation of ultrasonic wave for 120 min provided a similar diffraction pattern to that of the sample from the solvothermal method (Fig. S1†). For the microwave-assisted synthesis, the initial attempt, 9-min irradiation of microwave, did not give a similar diffraction pattern as observed in the case of 120-min irradiation of ultrasonic wave (Fig. S1†). This is presumably due to the poor solubility of bpydc in water. However, the poor solubility may not be problematic for a long-period synthesis, such as solvothermal synthesis and ultrasonication method. To overcome the low solubility of bpydc, we added two equivalent of LiOH to produce the bpydc salt and thereby increasing the solubility. Indeed the addition of LiOH helped the formation of **1** for 9 min by an irradiation of microwave (Fig. 6). The SEM images indicated that the MOF **1** synthesized by irradiation of ultrasonic wave or microwave is rod-shaped particles (Fig. 7). The microwave-assisted synthesis provided rather uniform particles compared to those by ultrasonication (Fig. 7). The product obtained by the microwave irradiation also showed blue luminescence (Fig. S2†).

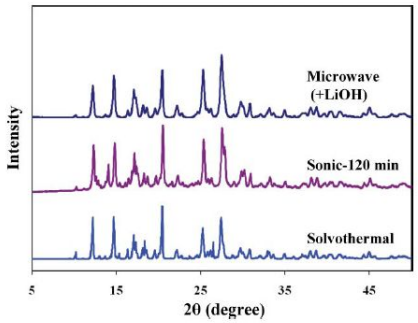

Fig. 6 PXRD patterns of **1** synthesized by several methods. Solvothermal: hydrothermal synthesis; Sonic-120 min: ultrasonication for 120 min; microwave: microwave irradiation with an addition of LiOH for 9 min.

Conclusions

We present preparations and crystal structures of three new MOFs of Zn(II), Co(II), and Ni(II) with the bridging bpydc ligand. The resulting MOFs provided an infinite 2D architecture with a topologically interesting geometry. Co(II) and Ni(II) MOFs, **2** and **3**, are thermally stable up to 470 °C. We also showed that **1**

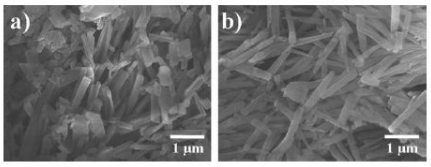

Fig. 7 SEM images of **1** synthesized by ultrasonication for 120 min (a) and microwave irradiation in the presence of LiOH for 9 min (b).

could be synthesized by ultrasonification- or microwave in a short time, although smaller particles were obtained. The Zn(II) MOF, **1**, showed decent blue luminescence and thermal stability up to 200 °C. The thermally stable and solvent-resistant blue luminescent material is potentially amenable for LED applications.

Acknowledgements

This work was supported by the Sungshin Women's University Research Grant of 2007-1-21-002.

Notes and references

1 M. Eddaoudi, H. Li and O. M. Yaghi, *J. Am. Chem. Soc.*, 2000, **122**, 1391.
2 (*a*) J. C. MacDonald, P. C. Dorrestein, M. M. Pilley, M. M. Foote, J. L. Lundburg, R. W. Henning, A. J. Schultz and J. L. Manson, *J. Am. Chem. Soc.*, 2000, **122**, 1169; (*b*) P. K. Thallapally, J. Tian, M. R. Kishan, C. A. Fernandez, S. J. Dalgarno, P. B. McGrail, J. E. Warren and J. L. Atwood, *J. Am. Chem. Soc.*, 2008, **130**, 16842; (*c*) K. K. Tanabe, Z. Wang and S. M. Cohen, *J. Am. Chem. Soc.*, 2008, **130**, 8508.
3 (*a*) S. Kitagawa, R. Kitaura and S.-I. Noro, *Angew. Chem., Int. Ed.*, 2004, **43**, 2334; (*b*) M. Eddaoudi, D. B. Moler, H. Li, B. Chen, T. M. Reineke, M. O'Keeffe and O. M. Yaghi, *Acc. Chem. Res.*, 2001, **34**, 319; (*c*) L. Zhang, Y.-Y. Qin, Z.-J. Li, Q.-P. Lin, J.-K. Cheng, J. Zhang and Y.-G. Yao, *Inorg. Chem.*, 2008, **47**, 8286; (*d*) Y. K. Park, S. B. Choi, H. Kim, K. Kim, B.-H. Won, K. Choi, J.-S. Choi, W.-S. Ahn, N. Won, S. Kim, D. H. Jung, S.-H. Choi, G.-H. Kim, S.-S. Cha, Y. H. Jhon, J. K. Yang and J. Kim, *Angew. Chem., Int. Ed.*, 2007, **46**, 8230; (*e*) S. Huh, T.-H. Kwon, N. Park, S.-J. Kim and Y. Kim, *Chem. Commun.*, 2009, 4953; (*f*) T. Gadzikwa, G. Lu, C. L. Stern, S. R. Wilson, J. T. Hupp and S. T. Nguyen, *Chem. Commun.*, 2008, 5493.
4 A. Lan, K. Li, H. Wu, D. H. Olson, T. J. Emge, W. Ki, M. Hong and J. Li, *Angew. Chem., Int. Ed.*, 2009, **48**, 2334.
5 (*a*) L.-G. Qiu, Z.-Q. Li, Y. Wu, W. Wang, T. Xu and X. Jiang, *Chem. Commun.*, 2008, 3642; (*b*) L.-G. Qiu, Z.-Q. Li, Y. Wu, W. Wang, T. Xu and X. Jiang, *Inorg. Chem. Commun.*, 2008, **11**, 727; (*c*) B. Chen, L. Wang, F. Zapata, G. Qian and E. B. Lobkovsky, *J. Am. Chem. Soc.*, 2008, **130**, 6718.
6 (*a*) A. Kraft, A. C. Grimsdale and A. B. Holmes, *Angew. Chem., Int. Ed.*, 1998, **37**, 402; (*b*) Review:U. H. F. Bunz, *Chem. Rev.*, 2000, **100**, 1605.
7 R. C. Evans, P. Douglas and C. J. Winscom, *Coord. Chem. Rev.*, 2006, **250**, 2093.
8 L. Kim, P. O. Anikeeva, S. A. Coe-Sullivan, J. S. Steckel, M. G. Bawendi and V. Bulović, *Nano Lett.*, 2008, **8**, 4513.
9 A. Y. Robin and K. M. Fromm, *Coord. Chem. Rev.*, 2006, **250**, 2127.
10 T. M. Reineke, M. Eddaoudi, M. O'Keeffe and O. M. Yaghi, *Angew. Chem., Int. Ed.*, 1999, **38**, 2590.
11 O. M. Yaghi, Hailian Li and T. L. Groy, *J. Am. Chem. Soc.*, 1996, **118**, 9096.
12 (*a*) K. C. Szeto, K. O. Kongshaug, S. Jakobsen, M. Tilset and K. P. Lillerud, *Dalton Trans.*, 2008, 2054; (*b*) G.-L. Law, K.-L. Wong, Y.-Y. Yang, Q.-Y. Yi, G. Jia, W.-T. Wong and P. A. Tanner, *Inorg. Chem.*, 2007, **46**, 9754; (*c*) E. Y. Lee and M. P. Suh, *Angew. Chem., Int. Ed.*, 2004, **43**, 2798.
13 B. Chen, Y. Yang, F. Zapata, G. Lin, G. Qian and E. B. Lobkovsky, *Adv. Mater.*, 2007, **19**, 1693.
14 (*a*) W.-J. Son, J. Kim, J. Kim and W.-S. Ahn, *Chem. Commun.*, 2008, 6336; (*b*) Z. Ni and R. I. Masel, *J. Am. Chem. Soc.*, 2006, **128**, 12394.

Conclusion and Summary

The most widely approach for protein delivery system has been to link the cargo protein with carrier. Liposome, cell permeable peptides, polymer and particles are very useful for efficient protein delivery into cells. Enzymes are highly efficient catalyst with extraordinary enantio- and regioselectivity, and they can accept a wide range of substrates. However, one of the major problems in use of enzymes is their inactivation. To improve catalytic stability of enzymes, enzymes have been immobilized to solid supports. The immobilization has many advantages such as cost reduce and reuse. In this thesis, biofunctional materials based on are cell permeable peptides, nanoparticles, and metal-organic frameworks were synthesized and applied for protein delivery, immobilization of recombinant lipase .

In the cellular delivery system for protein studies, I investigated the glucose-coated beads and CPPs for protein delivery. The glucose-coated polymeric beads were synthesized by dispersion polymerization. The result showed the EFGP as a model protein were delivered inside mouse embryonic stem cell and HeLa cell by the glucose-coated beads. In addition, I performed the transfection efficiency of cell permeable peptides (CPPs) in mouse embryonic stem cell under the various conditions. The efficiency of transfection of CPPs-EGFP depends on the sequence of CPPs but the culture time is not a key factor in transfection for the mouse embryonic stem cell. The result showed CPPs would be very useful

vesicles to induce the embryonic stem cells.

In the immobilization of recombinant lipase studies, I first investigated the mutational effect on expression yield of *Candida antarctica* lipase B in *E. coli.* The mutant was created by introduction of hydrophilic resides on surface of CAL-B. The mutant increased expression yield three times compared to the wild type. The mutant resulted in producing more functional enzyme without change of the catalytic machinery of CAL-B. And I employed the polymer-coated magnetic beads as protein immobilized support. *B. cepacia* lipase expressed *E. coli* requires assistance of chaperone to be properly refolded. The chaperone conjugated polymeric magnetic beads efficiently refolded *B. cepacia* lipase and were easily reused by simple methods. The beads showed comparable refolding activity to the soluble chaperone, and retained more than 95% of activity after ten-times recycling. Magnetic nanoparticles and MOFs were investigated for covalent -immobilized supporting materials. The magnetic beads with coated polymethylmethacrylate (PMMA) were synthesized by emulsion polymerization. The lipase-conjugated magnetic beads were showed similar hydrolytic activity to the free enzyme and retained activity after six times recycling. In addition, I used the metal-organic frameworks as enzyme immobilized supporters. The immobilized enzyme with MOFs has higher specific activity compared free enzyme in organic solvent. These results clearly indicate that functional proteins can be decorated on MOFs without losing their functions and recyclable without significant loss of the activity.

ABSTRACT

Preparation of Cellular Delivery System for Protein and Immobilization of Recombinant Lipase

Suhyun Jung
Department of chemistry
Graduate School of
Sungshin Women's University

This thesis deals with preparation of cellular delivery system for protein, and biofuctionalization of nanoparticles and metal-organic frameworks for immobilization of recombinant lipase. In protein delivery, use of therapeutic proteins has been limited by their inability by pass the plasma membrane. To protein delivery into the cell, the carriers are needed. Liposome, cell permeable peptides, and polymer have been used. Recently, delivery carriers synthesis and applications have gained more attention due to increase of the demand for systems of drug delivery or stabilizer.

Enzymes are very useful biocatalyst, and they can catalyze various and have highly enantio- and regioselectivitys and accept a wide range of substrate. However, enzymes are often easily inactivated. There are several stabilization strategies to improve catalytic stability of enzymes, for example,

enzyme modification, genetic modification, and enzyme immobilization strategies. Among these methods, immobilization strategy using solid supports has been most extensively researched due to the specific advantages such as reduce costs by enabling the efficient separation and reuse.

First, the protein delivery system studies were investigated based on the delivery carriers such as nanoparticles and several known cell permeable peptides (CPPs). I prepared glucose-coated polymeric nanobeads by dispersion polymerization. The EGFP (enhanced green fluorescent protein) as a model protein for protein delivery was attached to the beads, and translocated into mouse embryonic stem cells and HeLa cells. The glucose-coated beads delivered the EGFP inside the cells whereas non-glucose-coated beads or the EGFP alone did not. In addition, I examined the transfection efficiency of several known CPPs into mouse embryonic stem cells under various conditions. The transfection of CPPs was independent on its concentration.

Second, immobilization of recombinant lipase were investigated. I achieved increase of the expression yield of CAL-B (lipase B from *Candida antarctica*) by using a codon-optimized synthetic gene and mutagenesis to introduce five aspartates on the surface of CAL-B. The 5D-CAL-B mutant showed three-fold higher expression yield (3.3 mg/L of culture) compared to the wild type. And I employed magnetic beads in refolding *B. cepacia* lipase. The chaperone-conjugated magnetic polystyrene beads efficiently refolded *B. cepacia* lipase and were easily reused. The beads showed

comparable refolding activity to the soluble chaperone, and retained more than 95% of their refolding activity after ten cycles of refolding *B. cepacia* lipase.

In addition, biofuntionalization of nanoparticles and metal-organic frameworks was studied. The eight commercial enzymes were immobilized to the magnetic polymethylmethacrylate (PMMA) beads by carbodiimide activation. The lipase-conjugated magnetic beads were showed similar hydrolytic activity to the free enzyme. The recycling experiment showed that the lipase-conjugated magnetic beads can be used several times with maintaining the same activity. In addition, the Enhance green fluorescent protein (EGFP) and *Candida antarctica* lipase B (CAL-B) were covalently bound to the metal-organic frameworks (MOFs). The immobilized enzyme on MOFs has the higher specific activity compared to the free enzyme in organic solvent. It can be concluded that the functional proteins can be decorated on MOFs without losing their functions and they are recyclable without significant loss of the activity.